28

NASA CR-66397

VOLUME I EXPERIMENT FEASIBILITY

14 APRIL 1967

PRELIMINARY DESIGN STUDY OF SLAMAST SCOUT-LAUNCHED ADVANCED MATERIALS AND STRUCTURES TEST-BED

VOLUME I EXPERIMENT FEASIBILITY

CONTRACT NO. NAS 1-7014

GPO PRICE $ _____

CFSTI PRICE(S) $ _____

Hard copy (HC) 3.00

Microfiche (MF) .65

ff 653 July 65

GENERAL ELECTRIC

RE-ENTRY SYSTEMS DEPARTMENT

NASA CR-66397

VOLUME I EXPERIMENT FEASIBILITY

14 APRIL 1967

PRELIMINARY DESIGN STUDY OF SLAMAST SCOUT-LAUNCHED ADVANCED MATERIALS AND STRUCTURES TEST-BED

VOLUME I EXPERIMENT FEASIBILITY

CONTRACT NO. NAS 1-7014

Prepared for

National Aeronautics and Space Administration
Langley Research Center
Langley Station
Hampton, Virginia

GENERAL ELECTRIC

RE-ENTRY SYSTEMS DEPARTMENT
A Department Of The Missile and Space Division
3198 Chestnut Street, Philadelphia 4, Penna.

ABSTRACT

This report presents the results of a feasibility study of a small, lifting re-entry vehicle test-bed capable of being launched by a Scout launch vehicle and capable of being recovered. The purpose of the study was to determine if it was possible to conduct meaningful, sub-scale, thermostructural experiments involving panels of interest of representative full scale, manned, lifting re-entry vehicles. The study was based upon the HL-10 vehicle concept.

PRECEDING PAGE BLANK NOT FILMED.

CONTENTS

ILLUSTRATIONS

ILLUSTRATIONS (CONTINUED)

TABLES

1. SUMMARY

1. SUMMARY

This section of the report describes an approach to thermostructural similitude for lifting re-entry vehicles in general with specific emphasis on the HL-10 vehicle. Analysis to date shows that an application of margin of safety philosophy combined with a utilization of traditional similarity parameters, test panel designs, and trajectory shaping holds promise of resulting in useful and valid simulation of full scale MLRV thermostructural systems with an economical sub scale vehicle. In addition it is shown that in the process of flying a thermostructural similitude mission valuable data can be simultaneously obtained concerning aerodynamics, thermodynamics, heat shield materials performance, flow transition and overall structural response.

An approach to the simulation process is presented which permits more flexibility than the usual method involving the duplication of a large number of dimensionless parameters related to an idealized thermostructural situation. This approach is discussed in detail along with its application to the HL-10. Also presented is the numerical substantiation generated during the study period as well as consideration of the limitations of the simulation technique and a comparison of ground test capabilities versus flight test.

It is believed that the approach developed is both sound and workable. The work done during the study period has not yielded any information to the contrary. The great flexibility in environment generation potentially available with the SLAMAST vehicle tends to reinforce the judgment. However, the numerical analyses which could be generated during the span of this study are not extensive enough nor complete enough to permit an unequivocal statement of feasibility.

2. INTRODUCTION

2. INTRODUCTION

The primary purpose of the SLAMAST study was to demonstrate the feasibility of flying experiments on a sub-scale vehicle that would provide meaningful information applicable to the design of manned lifting re-entry vehicles. The class of MLRV which has been considered is that having L/D's on the order of 1.4. Specifically, the study was related to the HL-10 vehicle developed by NASA/LRC.

The basic approach to experiment feasibility has been the investigation of similarity parameters which could be used to correlate the sub-scale and prototype vehicles. By NASA direction, primary emphasis was placed on the area of thermostructural design; therefore, the majority of this section of the report is associated with thermostructural similitude.

The flexibility of a maneuvering vehicle such as SLAMAST, however, provides precise environmental control and thereby allows a number of experiments to be conducted over discrete portions of the flight. The flexibility of the SLAMAST system provides for additonal experiments in the areas of material performance, flow transition, and aerodynamic performance, which can be conducted simultaneously with the thermostructural flight evaluations.

It is in this vein that the SLAMAST system is most useful, that of a flying test facility to evaluate and qualify MLRV designs through multiple experiment usage. Therefore, this volume also discusses alternate experiments that can be flown on SLAMAST.

3. APPROACH TO THERMOSTRUCTURAL SIMILITUDE

3. APPROACH TO THERMOSTRUCTURAL SIMILITUDE

3.1 INTRODUCTION

The design of a structure, whether it be a flight structure, a civil structure, or any other type of structure, involves three basic elements:

(1) the environment to which the structure will be exposed during its useful life,

(2) the characteristics of the materials being employed in the design (i.e., the material properties), and

(3) the analysis techniques used to predict the structure's performance, behavior, or response.

The main concern is flight structures. The primary items which contribute to each of the three elements for flight structures are shown in Figure 3-1.

The next point in the development of the simulation approach is testing. Tests are performed primarily for the purpose of proving that the structure will not fail in its anticipated environment, or that it does not have excessive strength in its environment. In other words, it should be neither overdesigned or underdesigned.

In the development of manned lifting re-entry vehicles, there are questions in all three areas of concern, i.e., environment, material characteristics, and analysis techniques; hence, the need for testing. While the primary purpose of SLAMAST is thermostructural response simulation, it is impossible to completely isolate this from the environmental and the material characteristic considerations. The similitude philosophy developed here will take advantage of this fact, and it will be shown that with the use of the SLAMAST flying laboratory some verification of environment and material characteristics will be obtained as part of the thermostructural similitude.

Let us return to considerations of structural design. The specification of structural sizes, thicknesses, stiffnesses, etc. depends on a knowledge of all three of the basic elements. A deficiency in any one of these areas could result in a structure which is incapable of withstanding the environment or one that is overdesigned and, hence, overweight. Testing with proper instrumentation will reveal these deficiencies if they indeed exist. So testing becomes a job of demonstrating the accuracy with which environments (pressures, temperature distributions, loads) can be predicted, material behavior in the presence of that environment is known, and structural response in the presence of both these can be predicted.

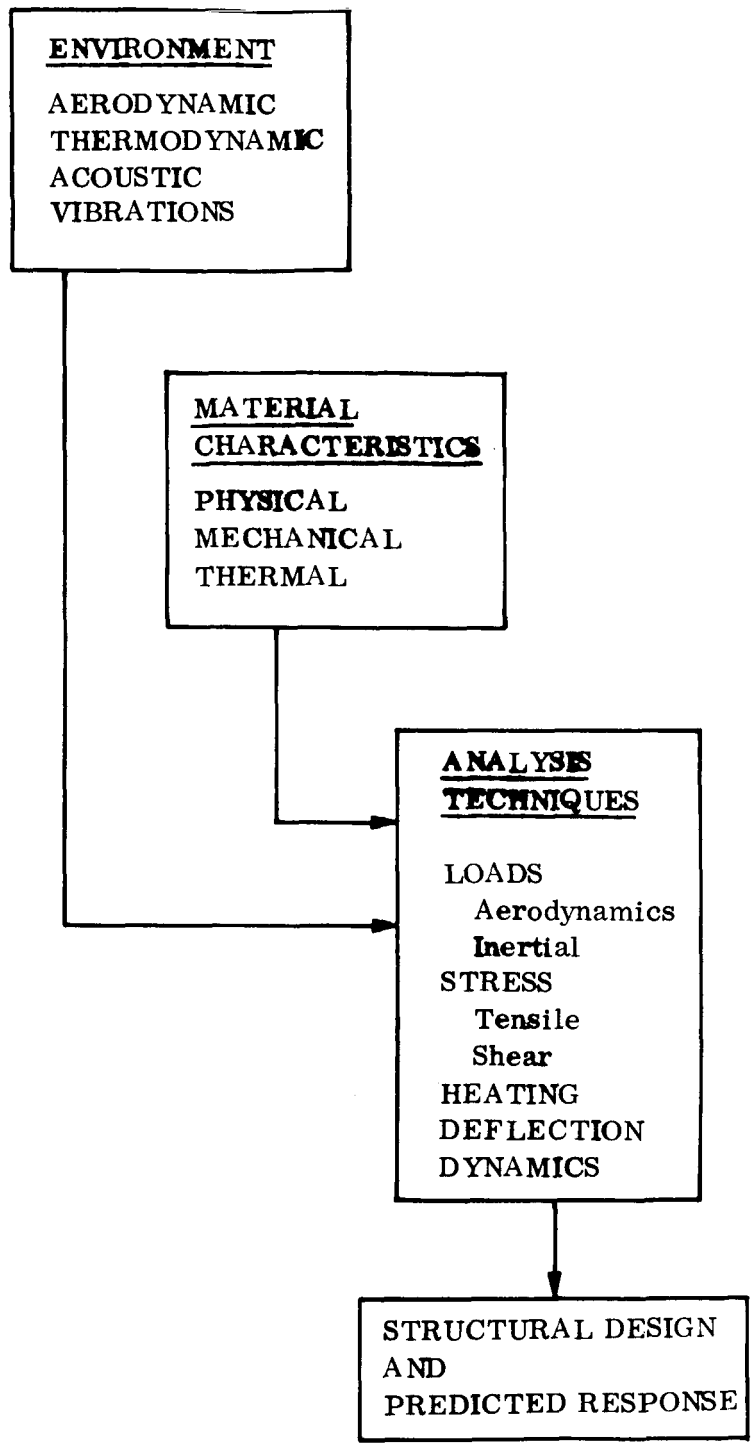

Figure 3-1. - Elements of Structural Design

The final design of a structure is specified in terms of detail drawings of the structure and a structural analysis of the design. This structural analysis includes a consideration of many or several types of potential failure modes such as:

(1) Buckling

(2) Thermal stress

(3) Mechanical stress

(4) Excessive deflection or strain

These various structural behaviors need investigation in all the possible flight regimes including:

(1) Launch

(2) Abort

(3) Space flight

(4) Re-entry

  (a) Nominal

  (b) Overshoot

  (c) Undershoot

(5) Approach to touchdown

Once the structure has been designed its capability can, and usually is, presented in terms of margins of safety. A margin of safety is given for each potential mode of failure. The margin of safety is defined as

$$MS = \frac{\text{Allowable stress (or strain, etc.)}}{\text{(Actual expected stress) x F.S.}} - 1$$

The factor of safety is a number which the expected stress (or load or strain, etc.) is multiplied by to account for variations in material quality and manufacturing variancies. There is a factor of safety for yield (usually 1.0) and an ultimate factor of safety (usually 1.4 or 1.5 for manned vehicles). Design criteria essentially says that no yielding shall exist at yield load and no failures (breaking or buckling) shall exist at ultimate load.

If the margin of safety for each potential mode of failure is plotted as a function of time, a curve similar to the one shown in Figure 3-2 would result. If the curves correspond to the modes discussed above, it is seen that the minimum margin of safety (the critical mode of failure) or the "weak link" in the structure is buckling (point 1) at time t_1. This is a prediction based on analytical or empirical techniques. It tells us that based on our knowledge of the environment, material properties, and structural response, the structure is closer to buckling than to any other mode of failure. However, since the margin is positive no failure should occur.

3.2 SIMULATION PHILOSOPHY

With these thoughts in mind, a simulation philosophy, or approach, was formulated. This approach consists essentially of reproducing, in an experimental panel on a sub-scale maneuvering vehicle, the minimum margins of safety of the full scale prototype at a particular time, which will be called the experiment time. This is to be done in a flight environment sufficiently similar to the prototype environment that the same phenomena are encountered. It is most significant to note that the primary difference between this approach and the traditional one is that this is similitude from a practical engineering viewpoint rather than a completely theoretical viewpoint. The latter approach to the problem tends to lead to the conclusion that anything short of one-to-one matching is unacceptable or at least highly questionable.

It is important to realize that exact similitude between the SLAMAST and the HL-10 (or between any flight test model and a prototype lifting re-entry vehicle) is impossible because:

(1) Aerodynamic modelling, thermal modelling, and structural modelling do not have the same scaling laws, and there are conflicts which cannot be satisfied exactly.

(2) There are factors which are extremely difficult or impossible to scale physically such as thermal contact resistance, boundary layer transition between laminar and turbulent flow and structural details such as initial eccentricities, attachment details, and honeycomb core to face bonding considerations, all of which affect the structural design.

(3) The structural concepts being considered for the HL-10 are very involved (ring-pressure vessel-honeycomb sandwich - rings - insulation - outer honeycomb sandwich shell - bond line - ablation material) such that the comparatively simple thermal and structural dimensionless parameters previously developed by many authors for a simple plate or shell element are inadequate.

(4) Even if perfect similitude were obtained by a one to one correspondence of all parameters, the distortions arising in an actual structure caused by attachments (resulting in thermal shorts or leaks and structural edge effects and differences in edge fixity) would negate the identical similitude calculated analytically in any physical structure of this type.

However, this in no way negates the utilization of a test bed (such as the SLAMAST vehicle) to obtain valuable information for the HL-10 and other lifting re-entry vehicles of this class. SLAMAST can be used to confirm or correlate the the three basic elements of design; i.e., the environment, the material characteristics, and the analytical and design tools. In particular it can:

(1) Provide additional knowledge about the aerodynamic environment associated with lifting re-entry vehicles.

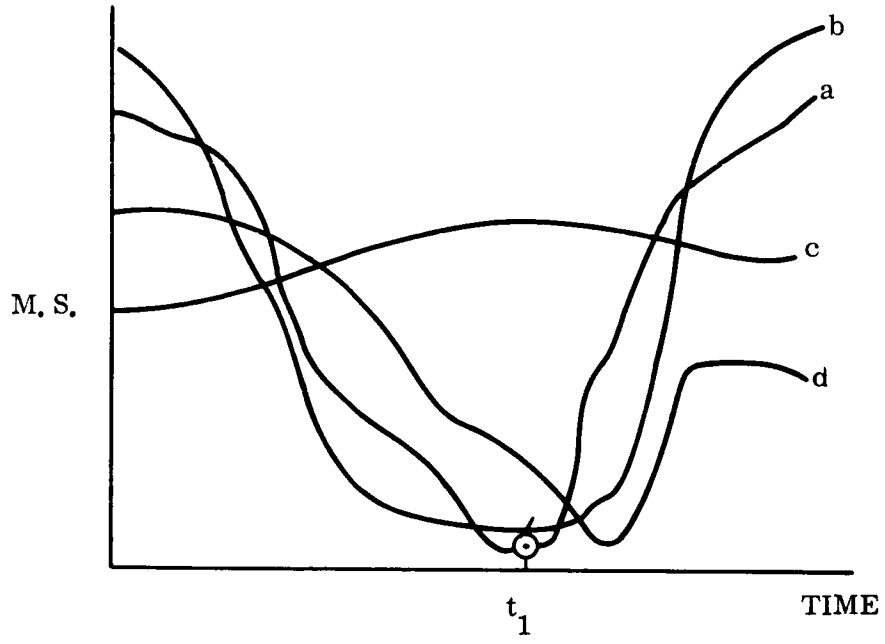

Figure 3-2. - Margin of Safety as a Function of Time

(2) Provide a means to check the adequacy of present analytical and empirical methods of analysis for pressures, transition points, flow separation, and effectiveness of control surfaces.

(3) Provide additional knowledge about the thermal environment and the heat transfer to and through the vehicles, including ablation rates.

(4) Provide a means to check the adequacy of present analytical and empirical methods of thermal analysis for convective heat transfer, ablation, conduction through complex structures including honeycomb sandwich, and multilayer insulation.

(5) Provide a means of checking structural methods of analysis and design procedures for complex structures of this type subjected to thermal loads, in-plane loads, and lateral pressure loads.

(6) Provide a means of checking the actual performance of material systems under actual flight conditions, and comparing them with data obtained by laboratory tests, including the ablation materials, bonding materials, insulations, as well as the load bearing structural materials.

What then is necessary for SLAMAST to include to insure that valuable information is produced which is applicable to prototype lifting re-entry vehicles?

(1) It is necessary that SLAMAST have a sufficiently similar environment to include all phenomena that will exist in the flight of a prototype lifting re-entry vehicle. This means that there must be sufficient heating that ablation will occur in SLAMAST, if it occurs on the prototype vehicle. There must also be sufficient aerodynamic loading such that

(a) if there are portions of the prototype vehicle that are designed by aerodynamic pressure, there must be sufficient aerodynamic pressure during the SLAMAST trajectory to design the corresponding structural element to be critical under aerodynamic pressures, and

(b) if there are portions of the prototype vehicle designed by in-plane loads caused by g-loads, the environment of the SLAMAST must have sufficient g-loads to design the corresponding structural element to be critical in this mode.

(2) It is most desirable for the structural test elements of the SLAMAST to use the same materials as the prototype elements on the full scale vehicle. In order to further insure identity of material, the temperatures should be close to those experienced in the prototype.

(3) It is necessary for the SLAMAST test components to employ the same structural concepts as the corresponding prototype subsystems. If the prototype structural section utilizes a filled honeycomb ablator bonded to a honeycomb sandwich shell or plate, the SLAMAST test section must also utilize the same concept.

(4) It is necessary that the test elements represent the same thermo-structural response characteristics. For example, if the prototype is a rectangular fixed panel, the test panel should be a rectangular fixed panel.

In addition, the following dimensionless parameters must be matched. Previous investigations have omitted these, but they are felt to be very important.

(1) Factor of Safety. - The identical factors of safety used in the design of the prototype should be used in the design of the model test elements.

(2) Mode of Failure. - The SLAMAST test section must be designed to have the same critical mode of failure as the prototype section.

(3) Margin of Safety. - The margin of safety for the critical loading condition of the prototype section should identical to the margin of safety of the test element under the same loading condition. The higher margins of safety should be reproduced in the same proportions as in the prototype to a degree dependent on their closeness to the minimum margin, to accommodate interaction effects.

This final requirement needs some additional discussion since it is an important key to the whole approach. If the minimum margin of safety is .01, for example, and the next lowest one is .5, this clearly indicates that the mode of failure represented by the .01 is certainly the weak link with all other potential failure modes far removed from possibility. This would be the case unless there are major inaccuracies in the environment, material property, or structural response predictions. If, on the other hand, the minimum margin is .01 and the next lowest is .015 it could be most important to reproduce both these margins in the test panel. The reason for this is that even though the mode of failure represented by the .01 margin is predicted to be critical, in reality the mode represented by .015 could be the critical one due to tolerances on all factors going into the prediction process. This is shown in Figure 3-3. It is seen that the tolerances could act in a way to make mode "a" the actual critical mode, whereas mode "b" was predicted to be the weak link. Therefore, the goal in trajectory and test panel design will always be to reproduce, at SLAMAST experiment time, all the HL-10 margins of safety. But, since this is an extreme condition to insist upon, it will be sufficient to reproduce only the minimum margin and others sufficiently close to the minimum as to represent potential critical modes of failure.

Another important item which must be considered in the test design is that the margin of safety for the critical mode in the test panel reaches its minimum value at the experiment time, and that no other margin reaches a value at other flight times which could possibly fail the test panel prematurely.

This philosophy will derive the greatest value from SLAMAST and insure that the prototype vehicle will accomplish its mission. By this procedure, the SLAMAST will uncover by suitable instrumentation any unsatisfactory knowledge of the environment; any deficiencies in analysis, design, or material behavior; and any unforeseen phenomena. With the SLAMAST flight profile simulating as nearly as possible the critical aspects of the prototype flight profile, by using the same materials and the

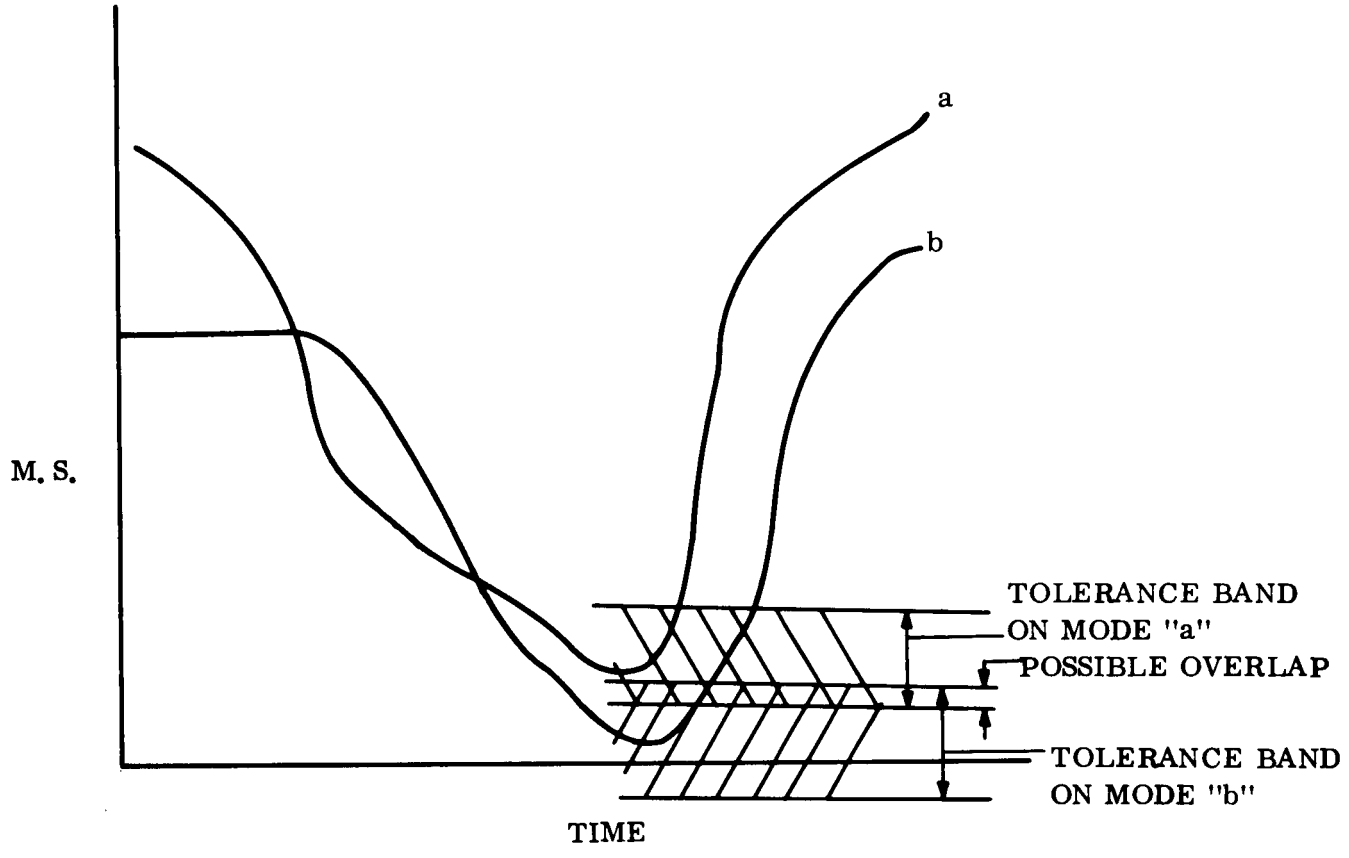

Figure 3-3. - Margin of Safety - Critical Failure Modes

same structural concepts, and by forcing the model structural element to have the same critical mode of failure, with the same factors of safety and the same margin of safety, the most important elements of thermostructural simulation are achieved without the complications of less important considerations.

The test panel designed with this philosophy will be equally close to failure as the full scale prototype. This is perhaps a unique feature of this approach since many models are designed such that failure thresholds are far removed from expected loading levels.

Even though a large number of the critical conditions for the HL-10 structure occur at touchdown, or abort, through the use of the philosophy stated above, the SLAMAST can study these critical conditions although it has no abort or touchdown considerations itself.

It is felt that this philosophy is both theoretically sound and provides a basis for a program that is physically practical. In addition, it reduces the need for flying an expensive full scale prototype to obtain meaningful and valuable data. It can also be seen that relatively simple flights with the subscale SLAMAST vehicle are acceptable provided the right conditions are present at the experiment time. This means that precise matching at many or all scaled flight times is not necessary.

3.3 TEST PANEL DESIGN AND TRAJECTORY SHAPING

As discussed above, the goal in the test panel and the shaping of the trajectory is to arrive at an environment at a specific SLAMAST flight time (the "experiment time"), such that the margins of safety for the various modes of failure are all the same as the margins in the HL-10 or in whatever prototype is being simulated. It is not expected that this can be completely accomplished since this would be perfect similitude, which is most difficult, if not impossible, to achieve. It is necessary only that the minimum one, or ones, be matched.

The margins of safety depend on external pressure and temperature distributions, their resulting imposed loads, and properties of the test panel. It follows therefore, that in order to achieve acceptable simulation at the experiment time a specific combination of pressures, temperatures, and panel design must be present at that time. The use of a manuevering vehicle with its broad flexibility in trajectories appears to make this feasible. In order to determine the right combination of the above items, an iteration process is required where the variables are the trajectory and the test panel (thickness of individual elements of the composite and overall size). In order to make this iteration process a manageable tool and to assist later in defining ground test limitations, use is made of the classical "similarity parameters". The similarity parameters used in this study are germain to rectangular panels undergoing small deflection. This was considered representative, in the gross sense, of HL-10 external wall behavior. These similarity parameters are developed in Section 6, and are given below, together with the type structural behavior or characteristic they represent.

$\frac{N_o L^2}{D_o}$	Buckling Yielding Fracture
N_T/N_o	Thermal and Mechanical Stress
B/B_o	Stiffness, Extensional
D/D_o	Stiffness, Flexural
N_T/N_{T_o}	Thermal stress and strain
M_T/M_{T_o}	Thermal stress and strain
$\Delta P_A/(\Delta P_A)_o$	Aerodynamic load stress

where

N = inplane load or stress resultant, lb/in

N_T = thermal force = $\int_{-h/2}^{h/2} E\alpha T \, dz$, lb/in

M_T = Thermal moment = $\int_{-h/2}^{h/2} E\alpha Tz \, dz$, in lb/in

B = extensional stiffness = $\int_{-h/2}^{h/2} \frac{E}{1-\nu^2} \, dz$, lb/in

D = flexural stiffness = $\int_{-h/2}^{h/2} \frac{Ez^2}{1-\nu^2} \, dz$, in/lb

ΔP_A = Net pressure, lb/in^2

L = characteristic length, in

Z = through the thickness coordinate

The zero subscript represents reference values. The use of these parameters for trajectory shaping is described below.

Figure 3-4 is used to describe this procedure. In (a) one of the structural parameters, ϕ, is plotted as a function of time for HL-10 based on a specific trajectory and panel location. (All parameters must be plotted, but only one is shown here for brevity.) On the same curve the parameter is shown for SLAMAST, again based on a particular SLAMAST trajectory, panel location, and panel design. A reference time is selected for HL-10, t_o, which is arbitrary and could be the time corresponding to minimum margin of safety. In (b) the curve is replotted with both scales normalized

(ϕ/ϕ_o then represents the similarity parameters, M_T/M_{T_o}, for example). The same thing is done for SLAMAST, taking care that the reference time selected is the same percentage of total time as it was in the selected HL-10 reference time (i.e., time to max. temp.). This has nothing to do with experiment time on SLAMAST, but consistency must be maintained in order to insure valid results. The same thing is done for all the similarity parameters. From here, an iteration process is carried out varying the trajectory, ablator thickness, structure thickness, etc. until the optimum or best combination is achieved. If a combination is found which makes each curve for SLAMAST fall directly upon the corresponding curve for HL-10, similitude is perfectly achieved (except for effects of non-scalable parameters as discussed previously). This would also mean that all the margins of safety are reproduced, provided the panel equations used to develop the similarity parameters are exactly representative of the behavior of the panel being simulated, which in general is not the case.

The parameter $N_o L^2/D_o$ is not time dependent. It is indicative, however, of size scaling requirements. That is, if N_o/D_o for the model is constrained to be the same as for the prototype, this parameter would indicate that the size must also be the same. On the other hand, since the size for SLAMAST is less than full scale, this parameter can be used as a guide to determine the required N_o/D_o for SLAMAST.

In general, the iteration process will end with a trajectory and panel combination which best satisfies the matching of all similarity parameters. At this point, the job must be completed by final margin of safety matching. This is a significant innovation to the approach developed and in use here. That is, in view of a lack of perfect matching of all parameters over the complete time scale, one might conclude that simulation cannot be accomplished. However, by injecting practical engineering aspects into the problem, one can evaluate how close to perfect matching he has to come to have meaningful and valid simulation.

It is significant to point out that the HL-10 panel designs from reference 3-1 have local areas at supports and in secondary structure as the weak links and, in fact, have negative margins of safety. No general set of similarity parameters can be developed which would be appropriate to all possible detail design considerations, but the ones used here are representative of general panel behavior and are useful in showing the trends and "zeroing in" on trajectory shaping and final panel design.

The primary "similitude parameters" are margins of safety, factor of safety, and mode of failure. Similarity parameters indicative of gross panel behavior are used to assist in proper trajectory and proper panel design. Final specification of trajectory and panel are arrived at by the margin of safety matching.

It is conceivable that one flight of the SLAMAST vehicle would contain more than one experiment time. By properly designing the trajectory, it is possible that one critical load condition for the prototype can be simulated at one time in the SLAMAST flight, while other conditions are being simulated at other times. The feasibility of achieving this is further enhanced by the fact that there are two experiment locations on SLAMAST, namely, a windward and a leeward panel.

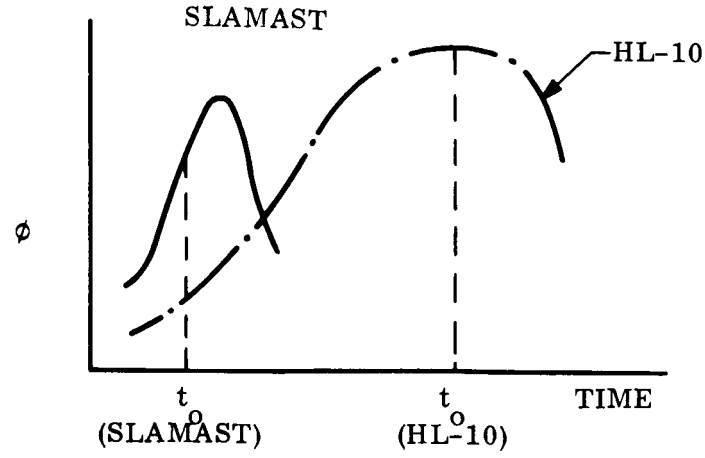

(a)

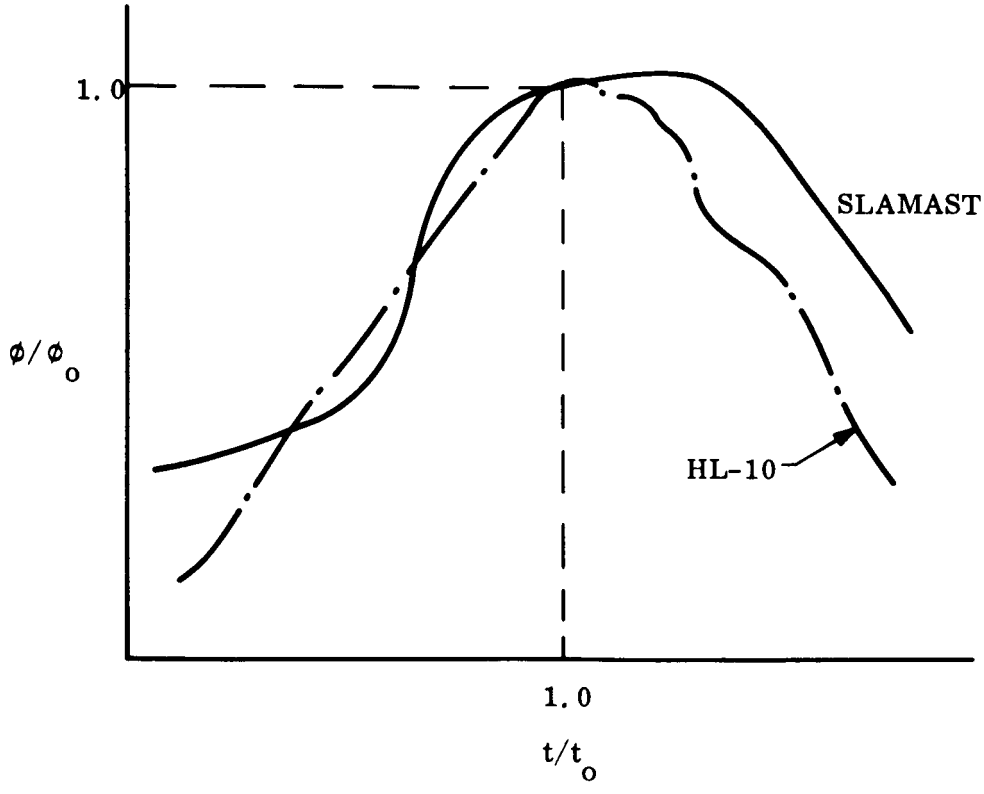

(b)

Figure 3-4. - Similarity Parameters for Trajectory Shaping

Another advantage of having discrete thermostructural experiment times is that other times can be used for aerodynamic or thermodynamic data gathering, thus increasing the cost efficiency of each flight. These other experiments are described in Section 7.

3.4 ENVIRONMENTAL REQUIREMENTS

Simulation of the prototype entry environment with the SLAMAST vehicle must include operating the SLAMAST vehicle in an entry corridor that results in heat transfer rates comparable to those anticipated for the prototype. Figure 3-5 summarizes the peak heat transfer rate distribution predicted for the HL-10 vehicle for the various design trajectories. Superimposed upon Figure 3-5 is the predicted SLAMAST environment for entry velocities of 20,000 and 25,000 fps and re-entry path angles of 1 and 10^{o} DFH. Note that the environment of the SLAMAST vehicle is comparable to the HL-10 environment ranges for the complete range of path angles at V_E = 20,000 fps. However, at an entry velocity of 25,000 fps, the SLAMAST environment is well above that of the HL-10 and well outside the efficient operating range of typical low density ablators. Hence, it appears that an entry velocity of 25,000 fps provides much too severe an environment at the steeper path angles. In addition, note that for an entry velocity of 25,000 fps, the SLAMAST heat transfer environment falls well above the HL-10 environment, in a regime where most low density ablators exhibit relatively poor performance.

In addition, the effect of guidance errors must be considered. A nominal tolerance of ±3/4 degree on entry path angle exists. Figure 3-6 illustrates the effect of re-entry path angle and velocity on maximum stagnation beating rate. Since the local heating distribution is proportional to the stagnation heating, similar trends with path angle will exist for both the stagnation and local body points. Note that the variation of maximum heat transfer rate with entry path angle is much smaller for the 20,000 fps entry velocity than for the 25,000 fps case. Hence, guidance errors would introduce less variation in local heat transfer for the 20,000 fps case than for the 25,000 fps case and thus make the 20,000 fps re-entry case a more desirable one for experimental purposes.

The environmental simulation technique for trajectory definition requires two major inputs:

(1) Histories of those environmental parameters which must be matched to satisfy a particular experiment.

(2) Closed form expressions for the instantaneous local values of the environmental parameters.

The histories of requirement 1 may be a function of velocity or time. Although two or more parameters may be treated simultaneously, solution time increases exponentially with the number of simultaneous parameters. When multiple parameters are considered, weights reflecting the relative importance of each must be assigned to the parameters. The closed form solutions of requirement 2 may, in general, contain terms which are tabular functions of other variables. With these

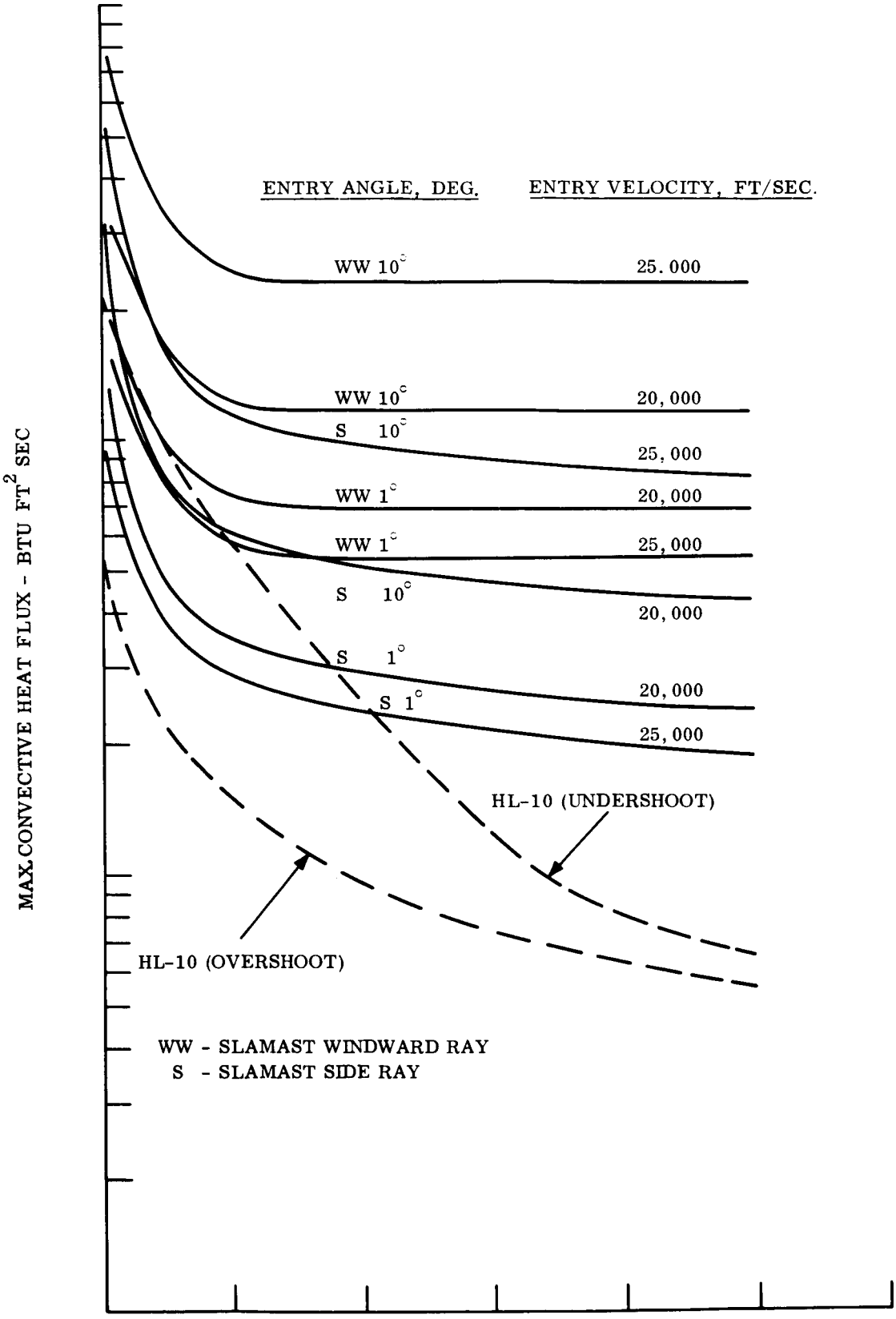

Figure 3-5. - Comparison of Maximum Convective Heat Flux Rates for HL - 10 and SLAMAST Vehicles

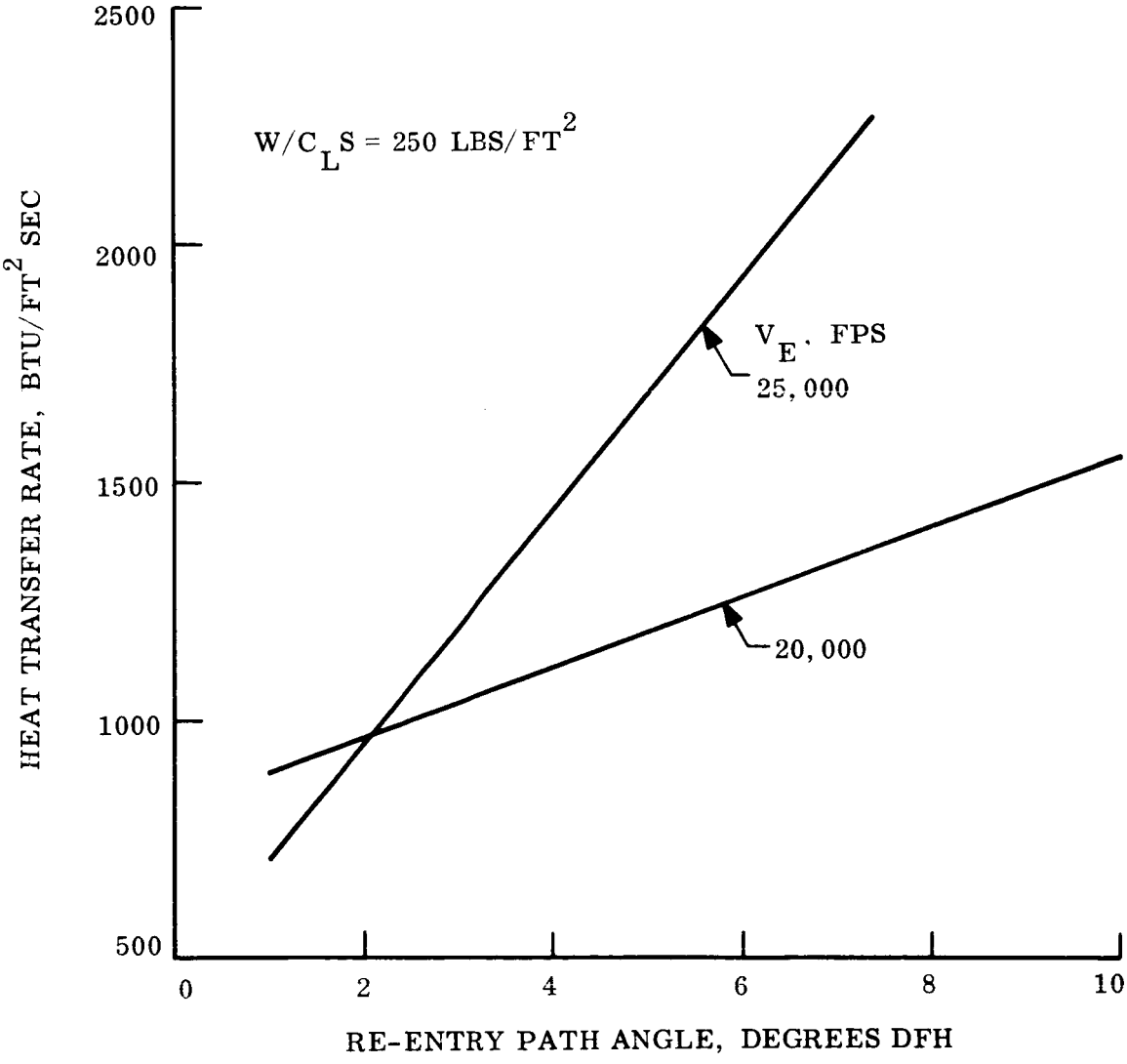

Figure 3-6. - Maximum SLAMAST Stagnation Heat Transfer Rates

inputs plus an initial trajectory to start the iteration, the Optimum Discrete Control (ODC) digital program can be used to generate the SLAMAST trajectory which optimizes the weighted match with the experiment parameters. The computation time required to iterate to a solution is a function of the initial trajectory and can be reduced by using parametric studies to provide a judicious initial trajectory profile. One important environmental parameter which is useful in simulation studies is heat rate. Figure 3-7 shows integrated stagnation heat rate for the initial SLAMAST trajectory and the 11th iteration made by the ODC program in attempting to match the desired stagnation heat history indicated. Further iterations could be made to improve the match, if necessary, since the program was still converging on the desired heating history at the 11th iteration.

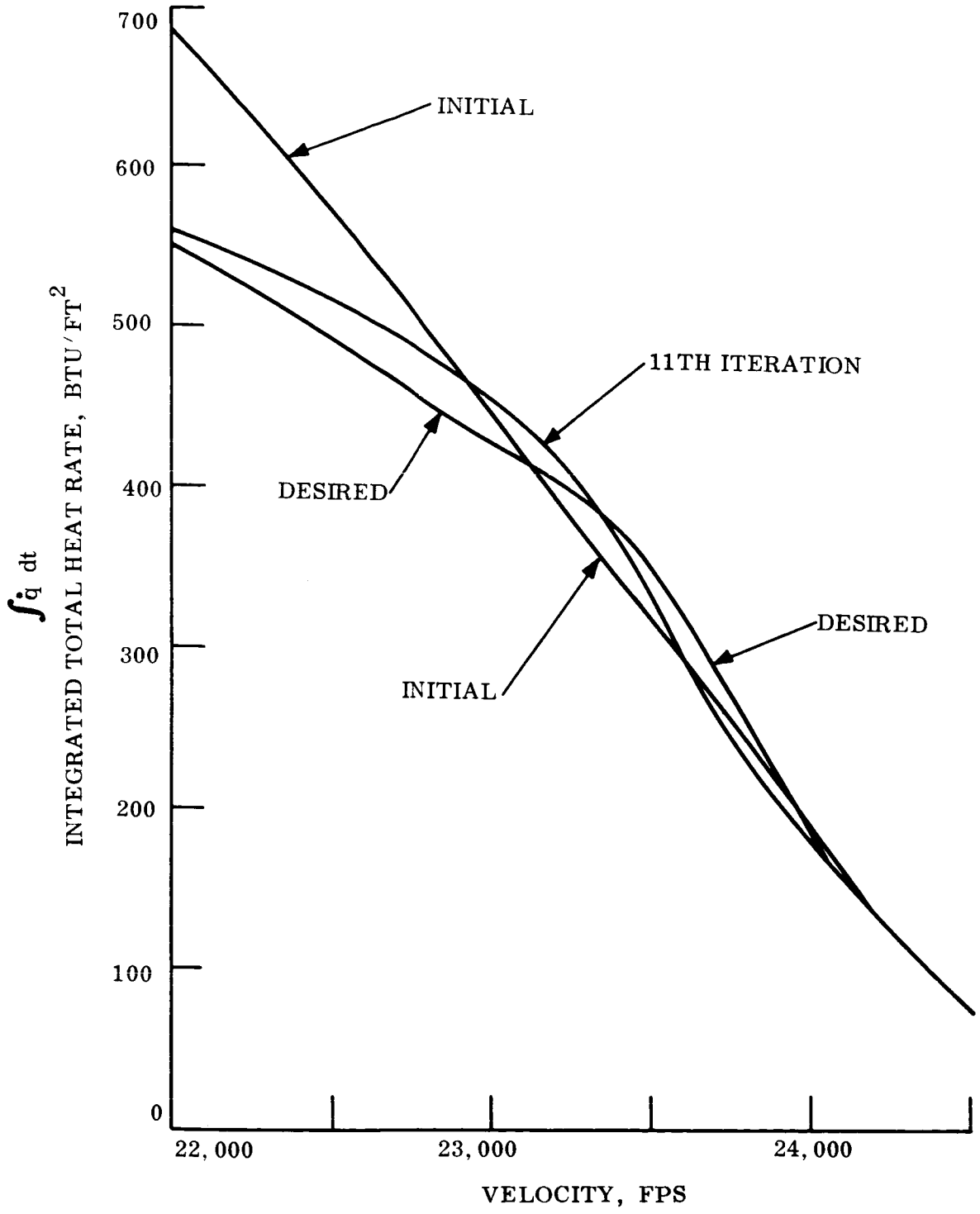

Figure 3-7. - SLAMAST Integrated Stagnation History Versus Velocity

4. APPLICATION OF APPROACH TO HL-10

4.1 DISCUSSION OF HL-10 DESIGN CONSIDERATIONS

In order to apply the simulation approach described in the previous section to the HL-10 vehicle, it would be necessary first to determine the various types of failure modes which can occur on the HL-10 and which in fact actually design the structure.

From previous studies (refs. 4-1, 4-2 and 4-3), it is apparent that the critical modes of failure on the HL-10 are: buckling; bending and subsequent cracking of the ablator; substructure bending failure; and local stress concentrations over isolated supports. A brief description of the type of construction follows.

4.2 GENERAL DESCRIPTION

The basic structural design considered in all the studies was a double wall type of construction in which there is an outer metallic or non-metallic shell surrounding but, in general, separated from an inner pressurized shell, which houses cargo and/or crew. An ablator is bonded to the outer surface of the outer shell. In the study of an "integrated" double wall construction, the load carrying ability of the ablator was incorporated in calculations involving the outer wall. The two shells are separated, but are joined discretely by rings or isolated conical standoffs.

The thermal design of the heatshield was based upon a maximum ablator-outer wall structure interface temperature of 700°F for the double wall construction, which is the limit of available bonding materials. Insulation is placed on the inner side of the outer shell and the inner surface of the insulation is limited to 200°F. The reason for this is that in all double-wall concept comparisons there are identical aluminum inner shell pressure vessels, and this low temperature does not result in significant material property degradation of the aluminum shell.

Each concept was designed to survive the following environments: ascent, space flight, re-entry, and approach to touchdown. In all designs, care was taken to prevent cracking of the ablator during ascent or re-entry.

The details of the double wall construction are given in Figure 1, page 8 of reference 1. The two ablators considered were filled honeycomb and laminated types. The outer shells were honeycomb sandwich of fiberglass or stainless steel. The inner shell is aluminum honeycomb sandwich construction. The insulation is either Q-felt or Micro-Quartz.

4.3 DESIGN CONDITIONS AND FAILURE MODES

The critical design conditions and failure modes determined in ref. 4-1 are summarized in Table 4-1 which was taken directly from ref. 4-1, page 86.

TABLE 4-1. - DOUBLE WALL-FIBERGLASS SHELL
STRUCTURAL SIZES AND WEIGHTS*

Body Location		Ablator	Structure		Weight	Design condition
Nose cap		Lam., F. H. C.	t = 0.11 in.		1.008 lb/ft^2	3(a)
Nose cone		Lam., F. H. C.	t = 0.17		1.558	3(a)
			h_c (in)	$t_{F.S.}$ (in)		
	1st cone (upper)	Lam., F. H. C.	0.145	0.02	0.620	3(a)
	2nd cone (upper)	Lam., F. H. C.	0.220	0.02	0.647	3(a)
	3rd cone (upper)	Lam., F. H. C.	0.300	0.02	0.677	3(a)
	X/C = 0.375 (lower)	Lam.	0.417	0.02	0.720	3(c)
		F. H. C.	1.530	0.03	1.308	3(b)
	X/C = 0.500 (upper)	Lam., F. H. C.	0.480	0.02	0.743	1, 3(a)
	X/C = 0.500 (lower)	Lam.	0.628	0.02	0.797	1
		F. H. C.	1.900	0.03	1.447	3(b)
	S/C = 0.750 (upper)	Lam., F. H. C.	1.040	0.020	0.948	1
	X/C = 0.750 (lower)	Lam.	0.715	0.020	0.829	1
		F. H. C.	1.320	0.030	1.234	3(b)
	Lower	Lam., F. H. C.	0.300	0.020	0.677	3(a)
	Elevons	Lam.	0.580	0.020	1.230	3(c)
		F. H. C.	2.080	0.020	1.230	3(b)
	Fins	Lam.	0.402	0.020	0.747	4(b)
		F. H. C.	1.580	0.020	1.147	3(b)
FRAMES			Height(in)	Area(in^2)		
	X/C = 0.164(upper)	Lam.	1.250	0.287	0.075	3(c)
		F. H. C.	1.250	0.287	0.075	3(c)
	X/C = 0.164(lower)	Lam.	2.500	0.726	0.190	3(c)
		F. H. C.	2.500	0.648	0.169	3(b)
	X/C = 0.375 (upper)	Lam.	2.000	0.434	0.166	3(c)
		F. H. C.	2.000	0.434	0.166	3(c)
	X/C = 0.375 (lower)	Lam.	2.750	1.189	0.454	3(c)
		F. H. C.	3.500	0.642	0.245	3(c)
	X/C = 0.750	Lam.	2.500	0.642	0.245	3(c)
		F. H. C.	2.750	0.906	0.346	3(b)

Legend: Design Condition

1. Buckling at Ascent
2. Space Flight
   a. Buckling due to shell interactions
   b. Bending, cracking of the ablator
   c. Bending, Substructure failure
3. Re-entry
   a. Buckling
   b. Bending, cracking of the ablator
   c. Bending, failure of the substructure
4. Approach to Touchdown
   a. Buckling
   b. Bending

*Taken from NASA-CR-240, Table III, page 86

For the upper surface of the vehicle, the design criteria were buckling under ascent in-plane compressive loads, and bending under touchdown pressure. For the buckling, the plate was assumed to have four sides simply supported. For the bending analysis the plate was assumed to be clamped at the two ends at frame locations to simulate bending over the frames.

Ascent buckling was the critical design condition. For the touchdown condition this resulted in M.S. = 3.7 and 2.8 for the filled H/C and the laminated ablator design, respectively.

For the lower surface of the vehicle, at touchdown, a lateral pressure of 1.15 psi exists. The same plate boundary conditions assumptions were used as for the upper surface.

The performance of the two designs differed considerably at this location due to the large differences in strength and brittleness of the two ablators. The critical condition for the laminated ablator design was the touchdown condition of bending under external pressure when the ablator was not effective structurally. The re-entry M. S. = 2.07. The ablator ultimate strain of 1.2% provided a high M.S. during re-entry.

In the filled H/C ablator the critical design conditions was re-entry. Due to the ablators ultimate strain of 0.4% cracking of the ablator was the critical consideration.

From the latest available studies, the most promising thermostructural panel which would form the outer refurbishable wall of an HL-10 double wall structure is comprised of NASA 602 ablator bonded to a phenolic glass honeycomb substrate panel. This type panel was used as the reference test panel on SLAMAST and has been shown in reference 4-3, page 55.

If identical materials and type of construction can be used in the simulation experiment, the derivation of the parameters and the determination of the margins of safety become simpler. Assume for the initial design that the same materials can be used and that the selection will not create an impossible constraint.

Essentially, these refurbishable thermostructural panels fulfill two basic functions. First, they provide a reliable structural path for thermal, aerodynamic, and inertia induced loads, and, secondly, they provide a given amount of thermal protection for the vehicle. The panel may be supported on the vehicle structure by local standoff members or they may be continuously supported along their edges. The ablator is bonded to the outer face of the structural substrate panel.

Three typical HL-10 panel locations are considered for determining representative heating and loading environments. These are shown in Figure 4-1 as leading edge, bottom, and crown panels. The detail structural design of a given panel will depend on the relationship between temperature and pressure for a given trajectory.

4.4 TRAJECTORY DESIGNATION AND PANEL DESIGN

The procedure for designating the SLAMAST trajectory and panel design to

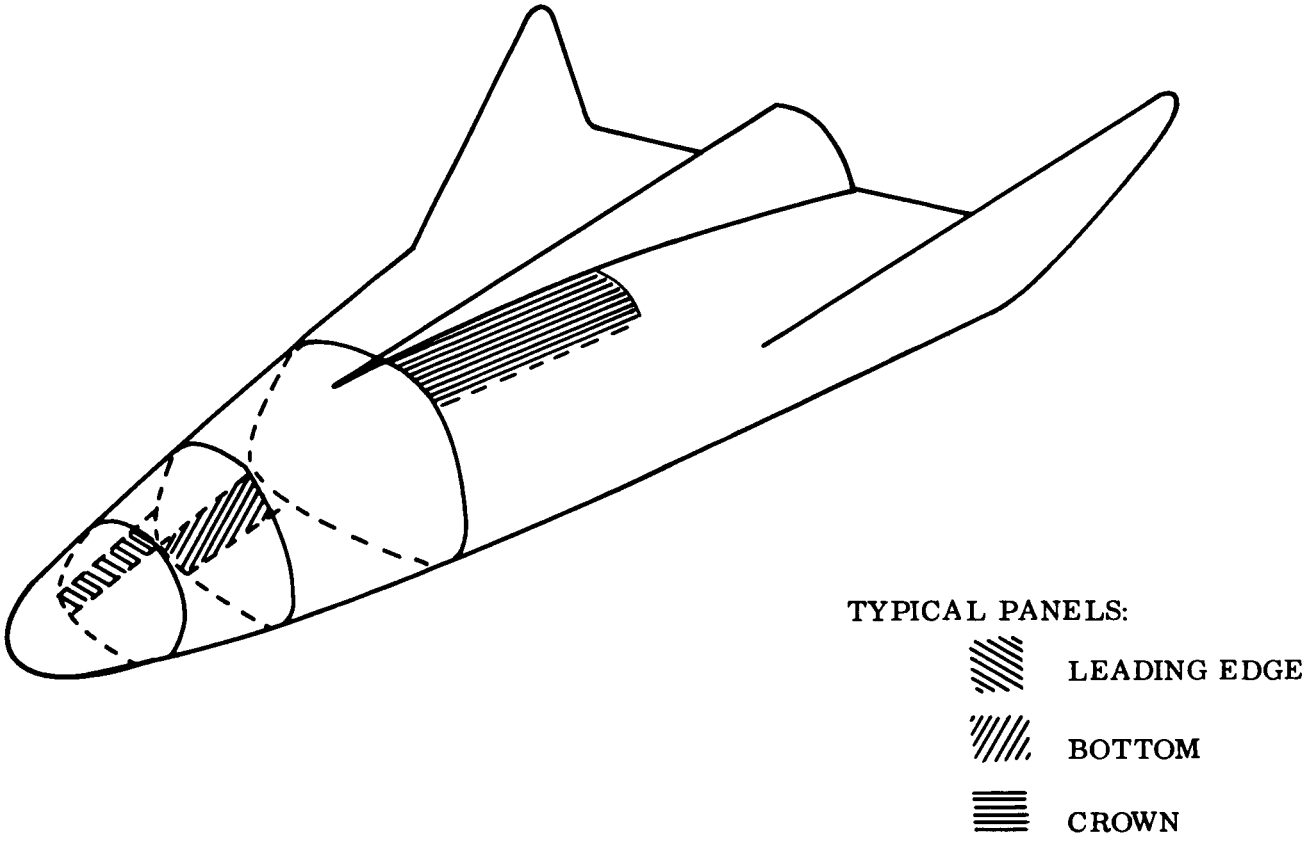

Figure 4-1. - Typical HL-10 Panels

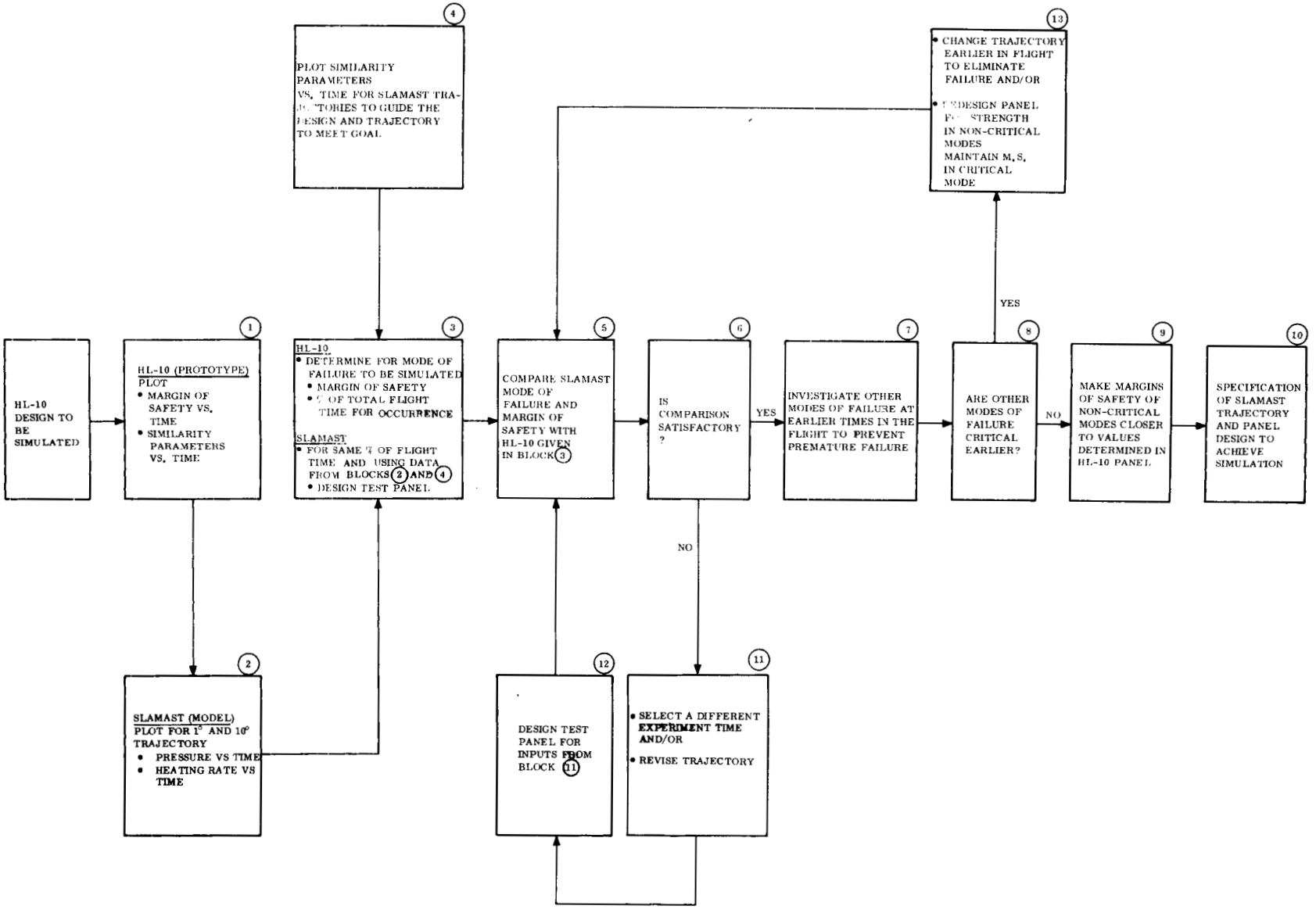

Figure 4-2. - Flow Chart Demonstrating Procedure for Selecting Trajectory and Panel Design for HL-10 Simulation

simulate the HL-10 panel design is illustrated in the flow chart appearing in Figure 4-2.

From the study (ref. 4-3) in which the phenolic/glass honeycomb substrate panel was supported off the primary vehicle by phenolic glass tapered cylindrical cups, the maximum stresses occurred at the support points for all cases, pressure loading, thermal loading and deflection limiations. The margins of safety determined at the support points were always minimum and in many cases were negative. Various methods were suggested to eliminate these local problem areas such as densifying the core or using facing doublers in the immediate area of the supports, reshaping the support cup, etc. The critical design conditions are summarized in Table 4-2 which has been taken directly from page 7 of ref. 4-3.

4.5 DISCUSSION OF REFERENCE PANEL SELECTION (PROTOTYPE)

In order to demonstrate the approach for experimental simulation described above, a reference thermostructural panel for the SLAMAST vehicle has been selected.

TABLE 4-2. SUMMARY PRELIMINARY OF CRITICAL PANEL DESIGN CONDITIONS*

Vehicle panel location	Overpressure		Temperature		Trajectory
	psi	kN/m^2	^oR	^oK	
Leading edge	8.5	58.5	585	325	Maximum load factor abort
	6.64	45.7	740	410	Undershoot
	2.60	17.9	1260	700	Nominal
Bottom	5.85	40.3	585	325	Maximum load factor abort
	4.64	32.0	740	410	Undershoot
	1.82	12.5	1260	700	Nominal
Crown	1.15	7.9	585	325	Maximum dynamic pressure abort
	0.44	3.03	740	410	Undershoot
	0.23	1.58	1260	700	Nominal
	-0.44	-3.03	1080	600	Overshoot

*NASA - CR - 640, page 7, Table 2.

The following is the actual procedure to shape a trajectory and design a panel to simulate a condition in a prototype lifting re-entry vehicle. A sample case is shown to demonstrate how the simulation approach is implemented. Because of lack of complete definition of the detailed design and analysis predictions, assumptions will be made as required to complete the procedure.

The most important items to duplicate in the test panel are the margins of safety in the critical modes of failure that were determined in the HL-10 design. From reference 4-1, the lower surface flat plate design criteria was bending under re-entry and touchdown pressure. Although the specific margins of safety were not indicated, the following values are assumed for illustrative purposes.

HL-10

Mode of failure	Margin of safety
Strength Bending	. 02
Buckling	. 12
Ablator Cracking	. 70
Deflection	3. 4

These modes of failure are typical of normal design procedures. Included in the bending mode of failure for sandwich panels with honeycomb cores under lateral loading are wrinkling of the face in compression, monocell buckling of the face in compression, ultimate shearing strength of the honeycomb core and tension failure of the honeycomb foil material at tension interface of facing and core, (ref. 4-4).

For ease of reference, these margins are assumed to occur during a nominal HL-10 trajectory. The pressure on the panel being considered is plotted as a function of time. This is shown in Figure 4-3 (a). The other important thermostructural parameters for the HL-10 are plotted as a function of time. N (in-plane loading) is shown in Figure 4-3 (b). B (Extensional stiffness) appears in Figure 4-4; D (Flexural stiffness) in Figure 4-5; N_T (thermal thrust) in Figure 4-6; and M_t (thermal moment) in Figure 4-7. The time at which the pressure is maximum will be assumed to be the time at which the margin of safety in bending is minimum. From Figure 4-3 (a), this time is 1800 seconds.

The information generated for SLAMAST at this time is limited to the pressure history and heating rates for 1^o and 10^o trajectories. The external pressures for the 1^o and 10^o trajectories are plotted as a function of time in Figures 4-8 and 4-9. This step is shown as Block 1 in the flow chart in Figure 4-2. As a start, it would be desirable but not a necessity if this condition could be attained at approximately the same proportion of time of the total flight period. This will allow closer simulation to occur. If ablation has occurred at 1800 seconds in the HL-10, a time should be selected on SLAMAST where ablation has also occurred. Assume that the maximum pressure and minimum margin of safety has occurred in the HL-10 at 1800 seconds of a total flight time of 2500 seconds or at 72% of the total flight time. It would be desirable but not essential if the same condition could be attained on SLAMAST at 72% of 700 seconds or 504 seconds. This step is indicated in Block 2 in Figure 4-2. The external pressure at 504 seconds from Figures 4-8 and 4-9 is on the order of 0.1 psi. The idea here is to design the test panel on the SLAMAST to be critical in a bending failure mode with a margin of safety of .02 at this time in the flight trajectory. A trial test panel is first designed. To aid in approaching the correct margin of safety values, identical thermostructural similarity parameters to those plotted for the HL-10 are plotted for SLAMAST for the limiting re-entry path angle trajectories of 1^o and 10^o. These parameters are superimposed over the HL-10 values in Figures 4-4, 4-5, 4-6, and 4-7 on a real time basis. These parameters are non-dimensionalized for both the HL-10 and SLAMAST and replotted in Figures 4-10, 4-11, 4-12, 4-13 and 4-14. The mode of failure must be a bending failure in the sandwich panel with a margin of safety of 0.02. These steps are shown in Blocks 3 and 4 in Figure 4-2. From these figures

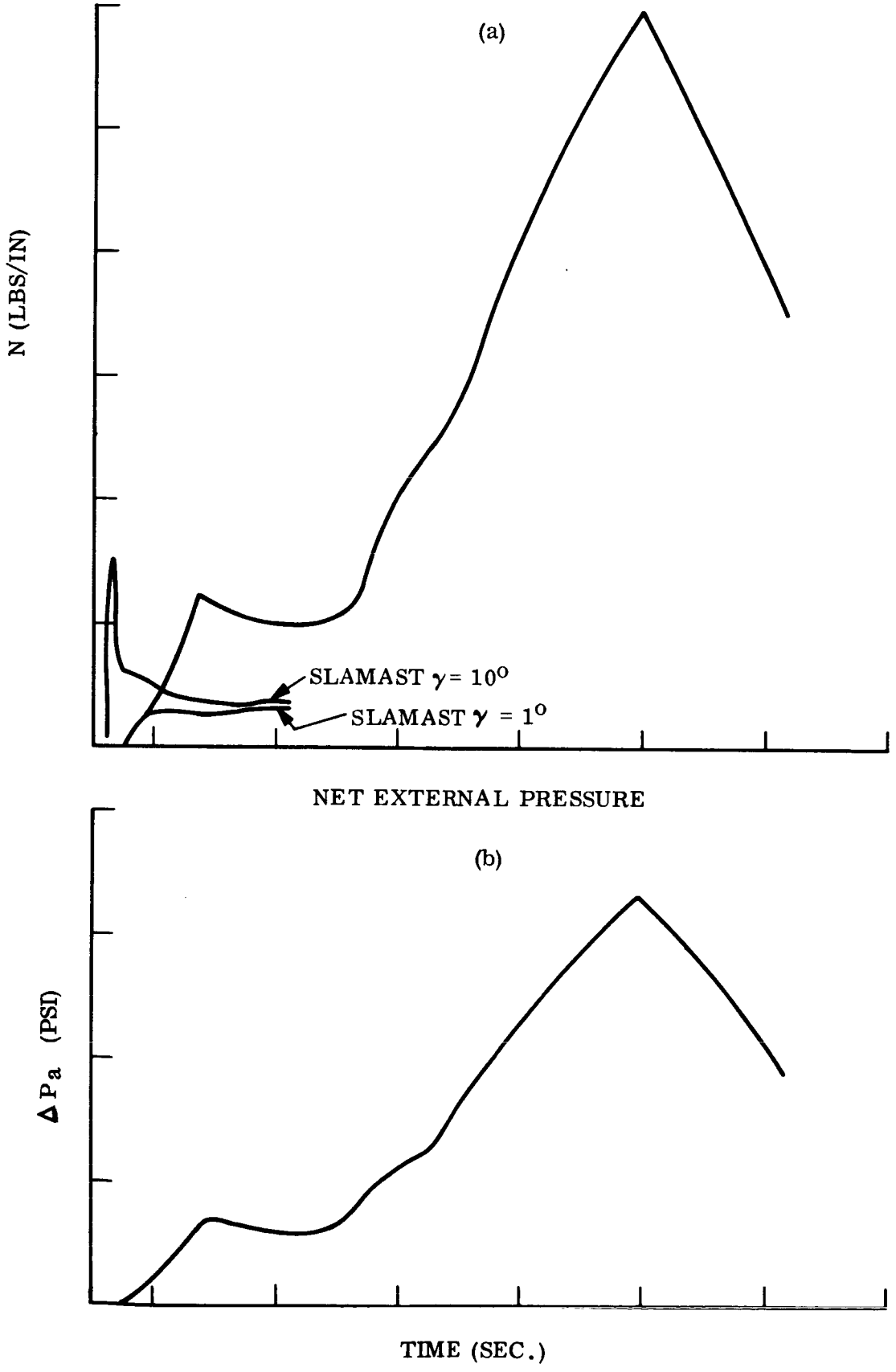

Figure 4-3. - HL-10 Nominal Trajectory, N (In Phase Load) Versus Time

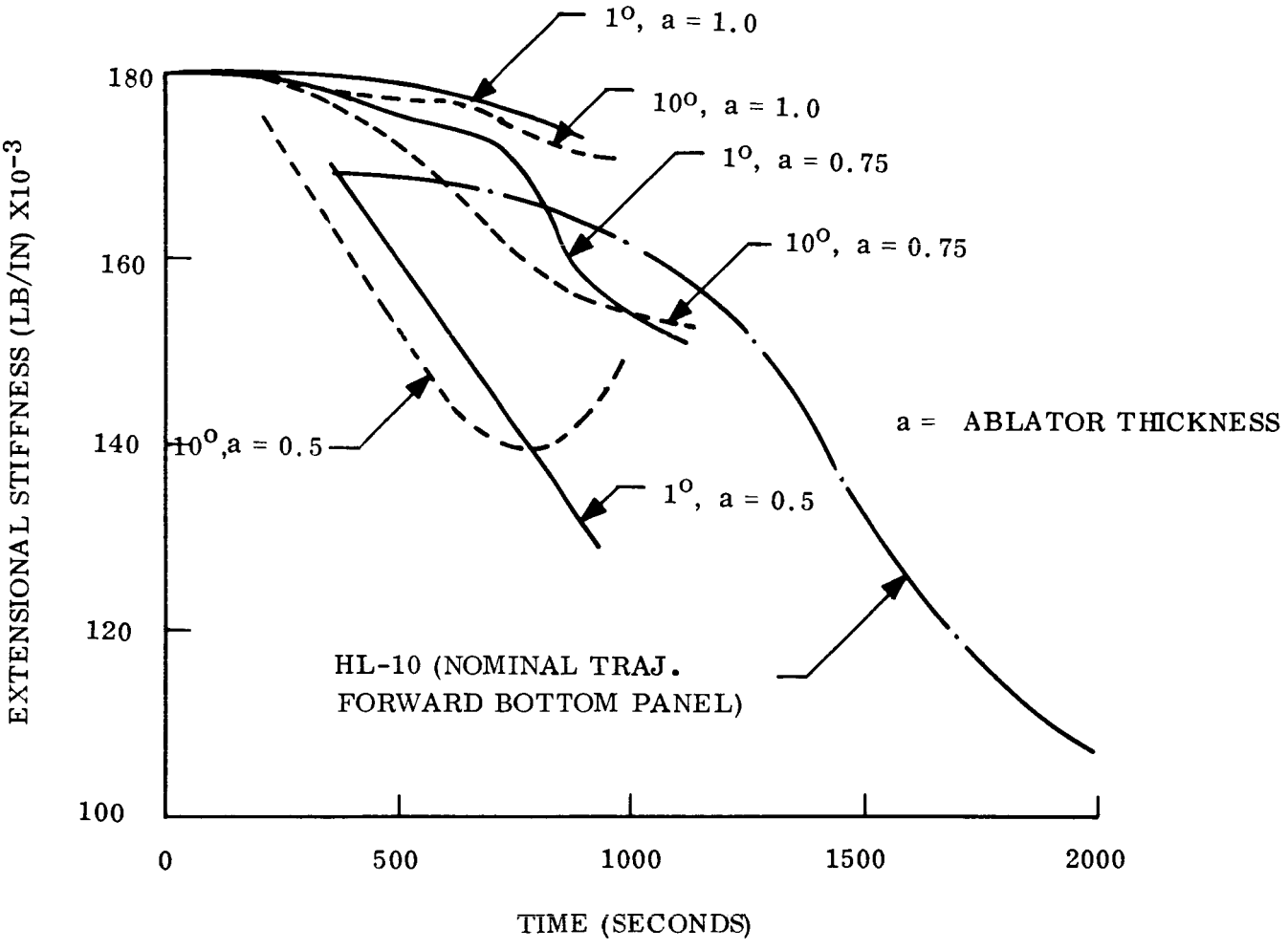

Figure 4-4. - Extensional Stiffness Versus Time,
HL-10 and SLAMAST Trajectories

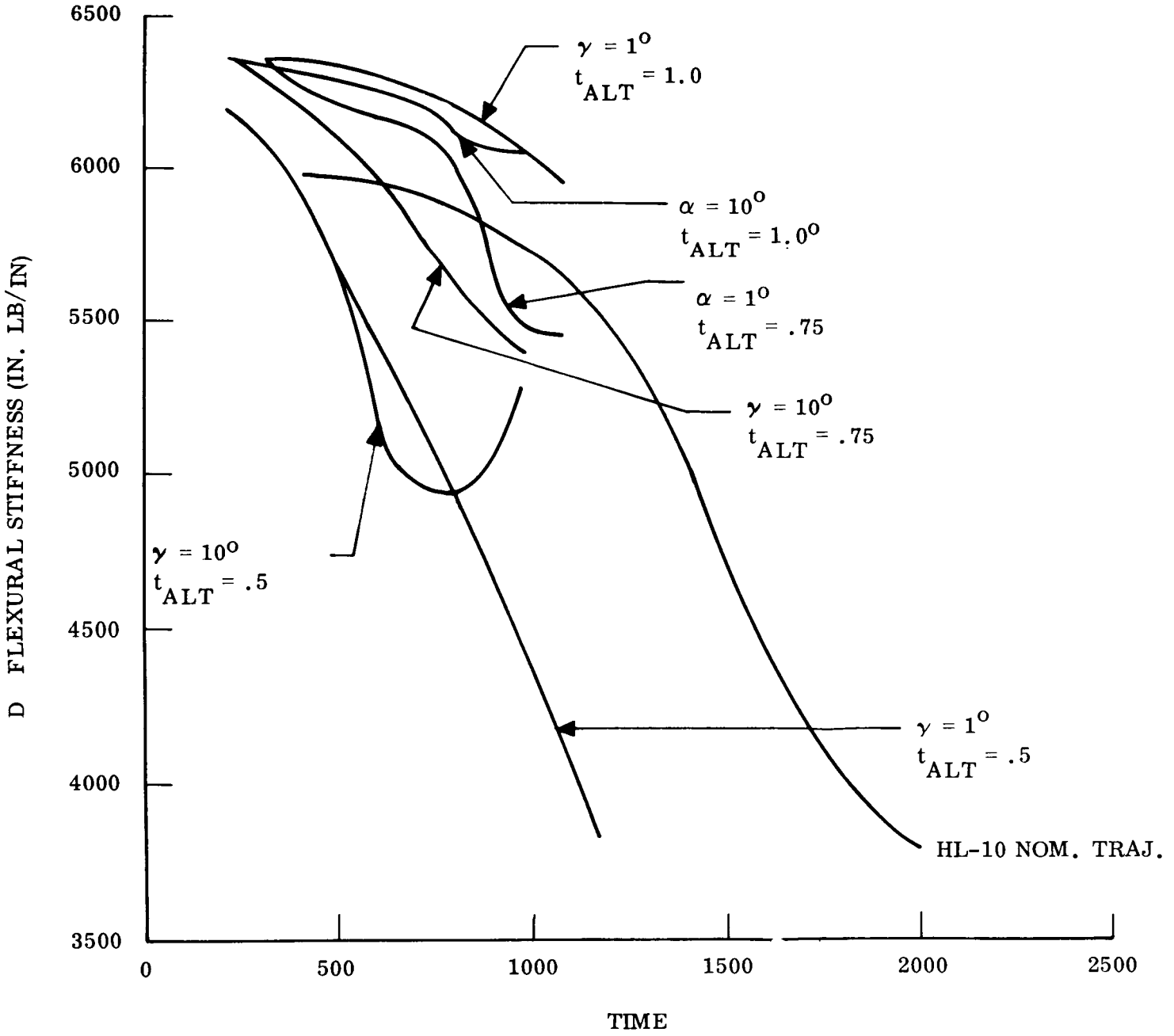

Figure 4-5. - Flexural Stiffness Versus Time, HL-10 and SLAMAST Trajectories

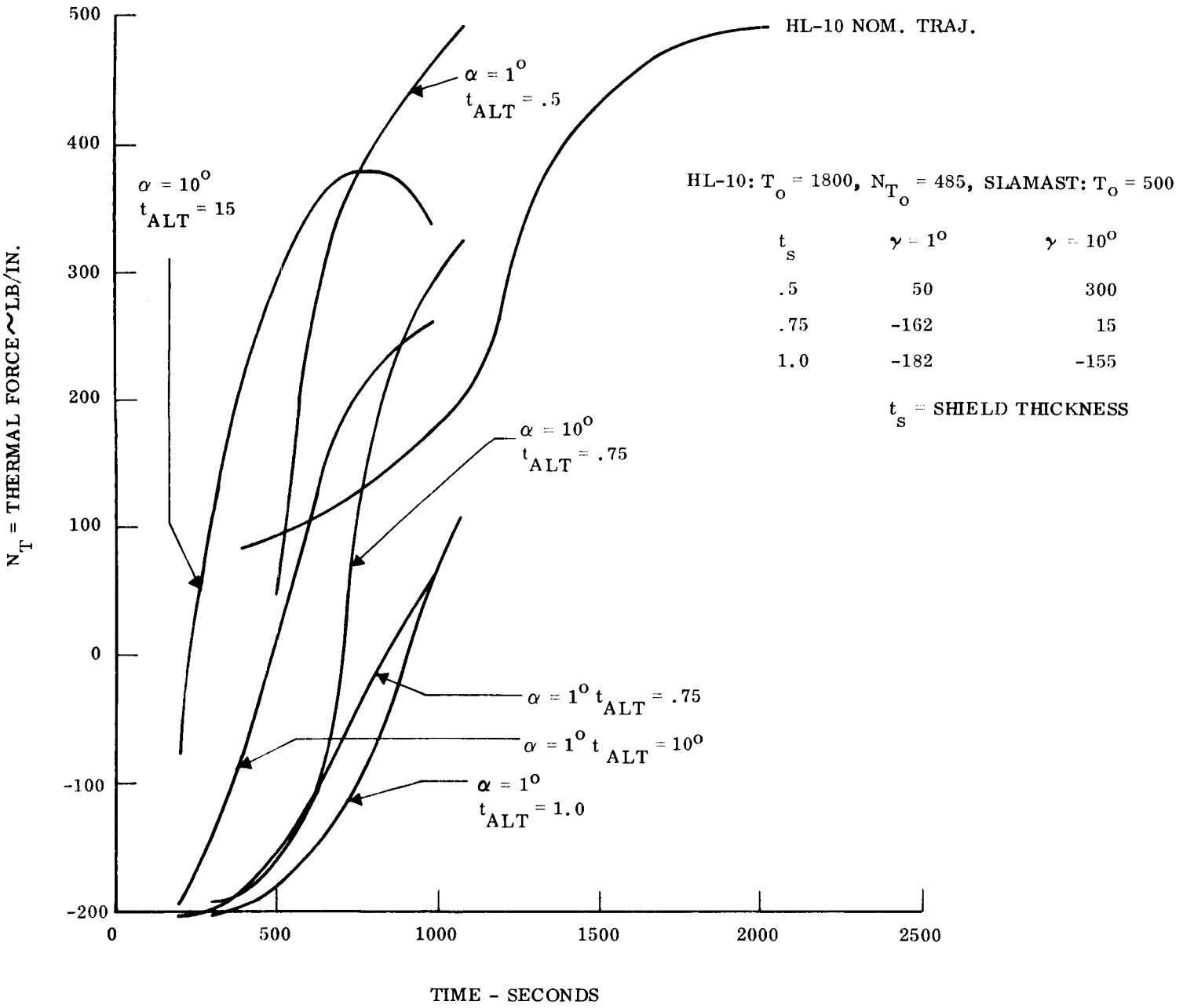

Figure 4-6. - Thermal Flow

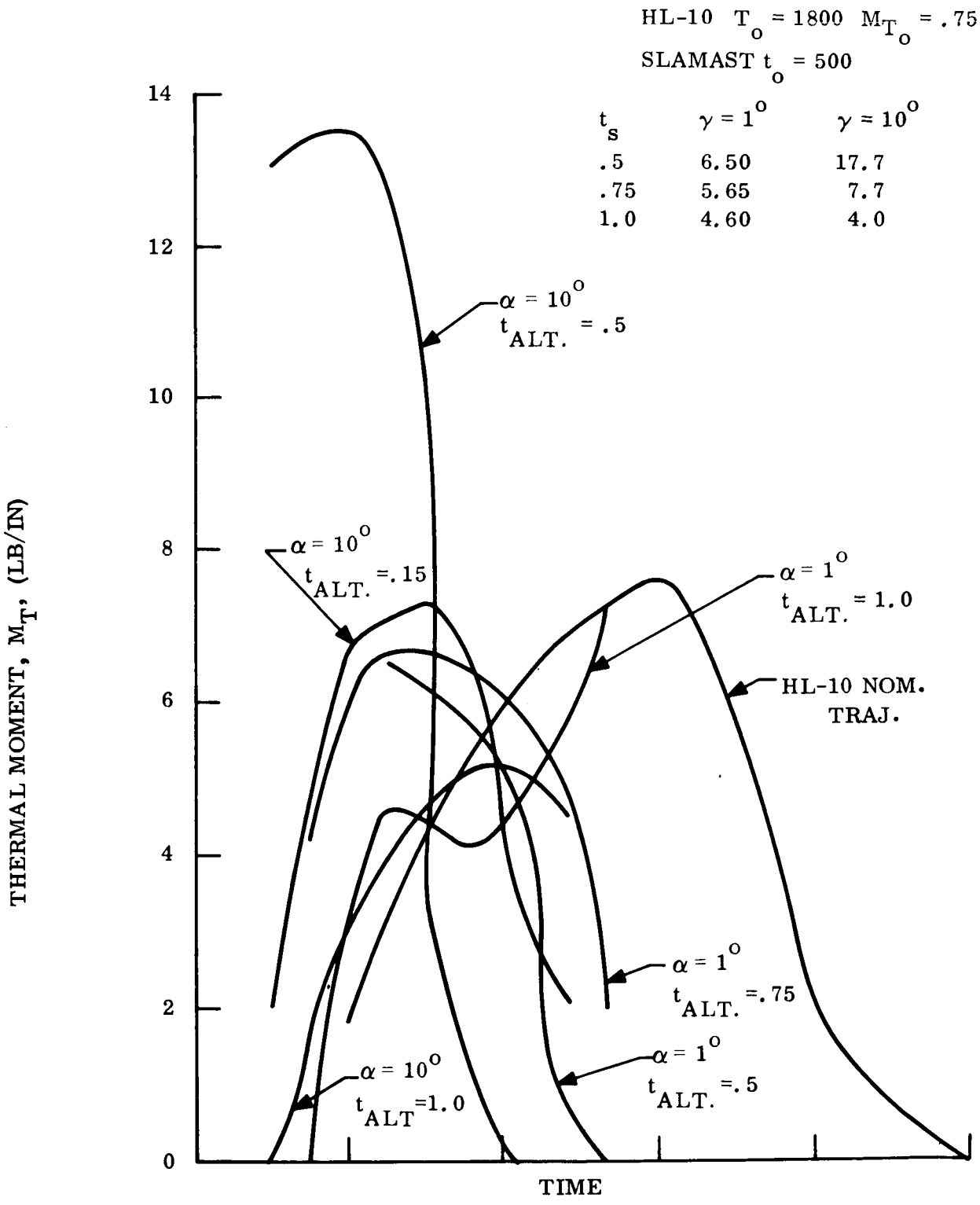

Figure 4-7. - Thermal Moment Versus Time, HL-10 and SLAMAST Trajectories

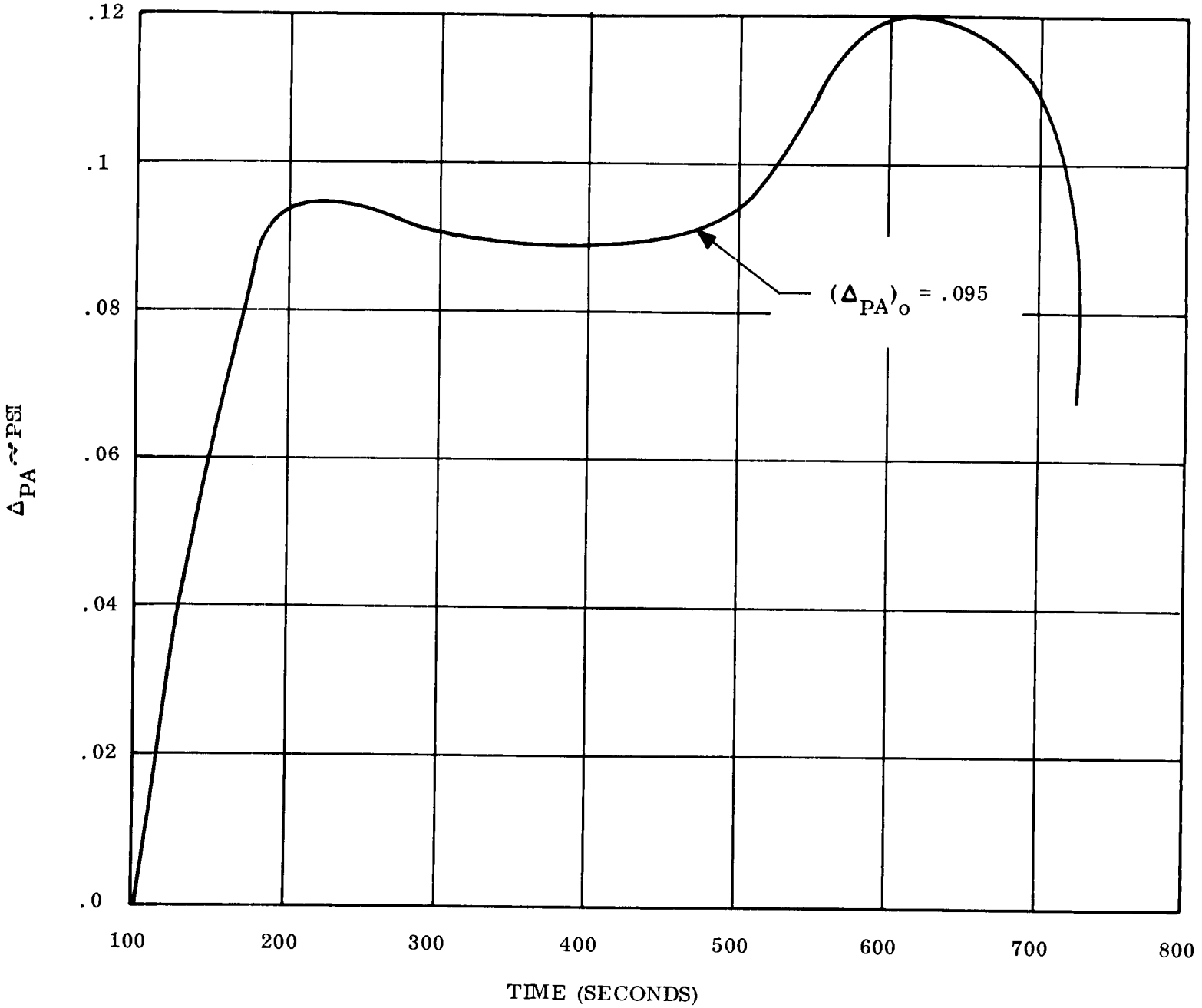

Figure 4-8. - External Pressure, SLAMAST $\gamma = 1^o$

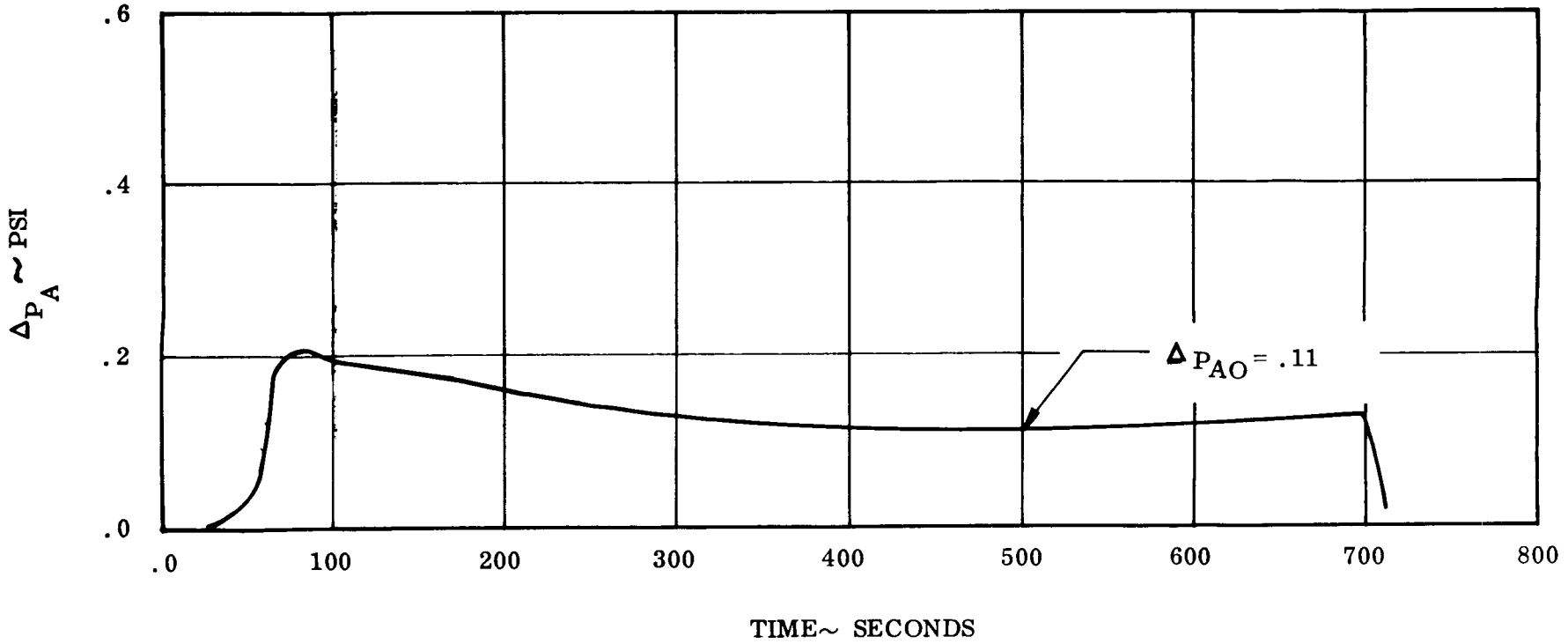

Figure 4-9. - External Pressure, SLAMAST, $\gamma = 10^{o}$

it can be seen that a true match of parameters is achieved only in two cases, i.e., N_T/N_O and B/B_O. For the other parameters a trajectory optimization would be required to achieve the proper combination of critical parameters. The trajectories used in these comparisons are the basic vehicle design trajectories and were used only for illustrative purposes. The inherent maneuvering capability of the vehicle would allow trajectory shaping to provide the proper environment. Thus, the case outlined here should be considered a first iteration in the process of experiment trajectory definition.

With the above constraints, the SLAMAST mode of failure and margin of safety is compared with the HL-10. This step is shown in Block 5. Two things can happen.

(1) Case A. - The comparison is satisfactory and the design is adequate (Block 6)

(2) Case B. - The comparison is not satisfactory and a design cannot be accomplished meeting this requirement due to minimum gage of facing thickness, supports not far enough apart, pressure too small, etc. (Block 6)

If a design can be accomplished, the next step is to review the critical times for other failure modes earlier in the flight to insure that the design satisfying the bending design criteria has not created a failure in the panel in other modes (Block 7). If no other modes of failure are critical earlier in the flight, the next step is in Block 9, where the panel design is analyzed to determine the margins of safety for the other noncritical modes of failure in the SLAMAST test panel. For example, suppose the following values were obtained:

SLAMAST

Mode of failure	Margin of safety
Strength - Bending	.02
Buckling	.50
Ablator Cracking	1.0
Deflection	8.2

The procedure described in Block 9 is to try to get the buckling margin of safety closer to the HL-10 value at 1800 seconds, namely 0.12. This is particularly important if the numbers are close because there will probably be mode of failure interaction as the margins decrease. Two ways of varying the buckling margin of safety are: changing the trajectory or changing the design. This should be done if it can be accomplished without affecting the 0.02 margin of safety in the bending failure mode. It would be desirable to have all the margins of safety on the SLAMAST panel identical to the ones on the HL-10, but as the values of margin of safety for the non-critical modes of failure increase, this matching becomes less important. If the SLAMAST mode of failure and margin of safety compare favorably with the HL-10 and

B = EXTENSIONAL STIFFNESS

B_o = EXTENSIONAL STIFFNESS AT REFERENCE TIME (t_o)

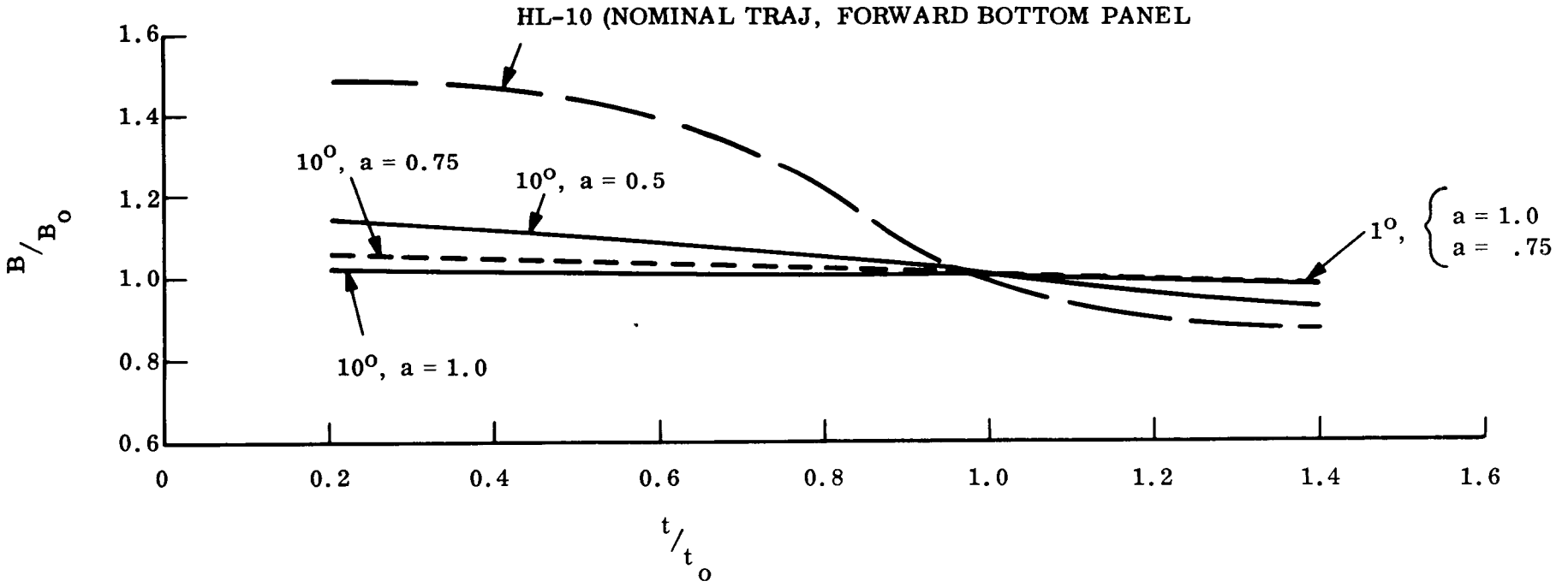

B_o VALUES

HL-10, t_o = 1800 SECS., B_o = 114X10^3 LBS./IN

SLAMAST, t_o = 500 SECS.

ABLATOR THICKNESS (a)	$\gamma = 1^o$	$\gamma = 10^o$
0.5 IN.	160 x 10^{-3} lbs/in	153 x 10^3 lbs/in
0. 75 IN.	175 x 10^3 lbs/in	172 x 10^3 lbs/in
1. 00 IN.	179 x 10^3 lbs/in	177 x 10^3 lbs/in

Figure 4-10. - Comparison of HL - 10 and SLAMAST Trajectories, Non-dimensional Similarity Parameters $\frac{B}{B_o}$

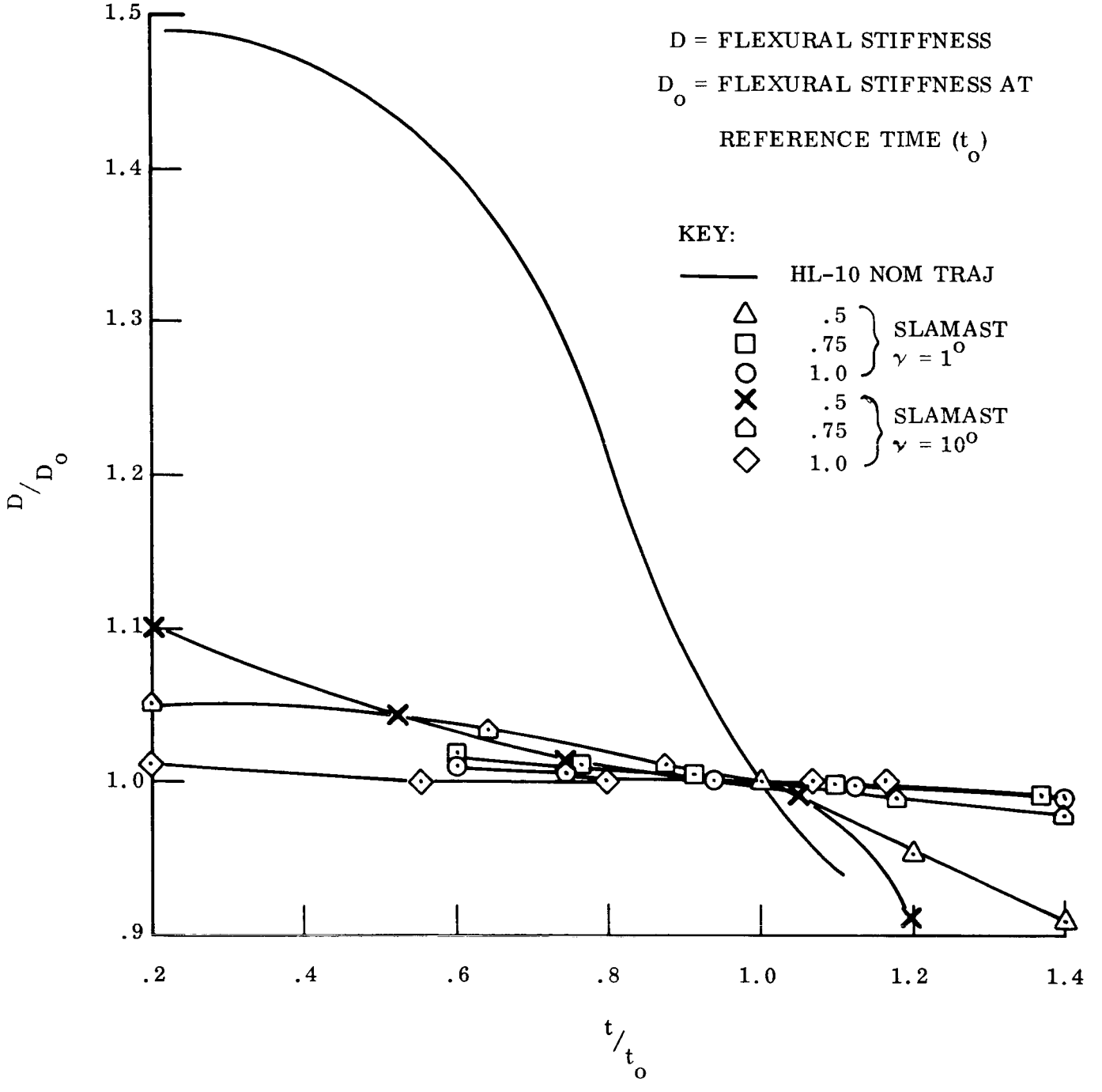

Figure 4-11. - Comparison of HL - 10 and SLAMAST Trajectories, Non-dimensional Similarity Parameters $\frac{D}{D_o}$

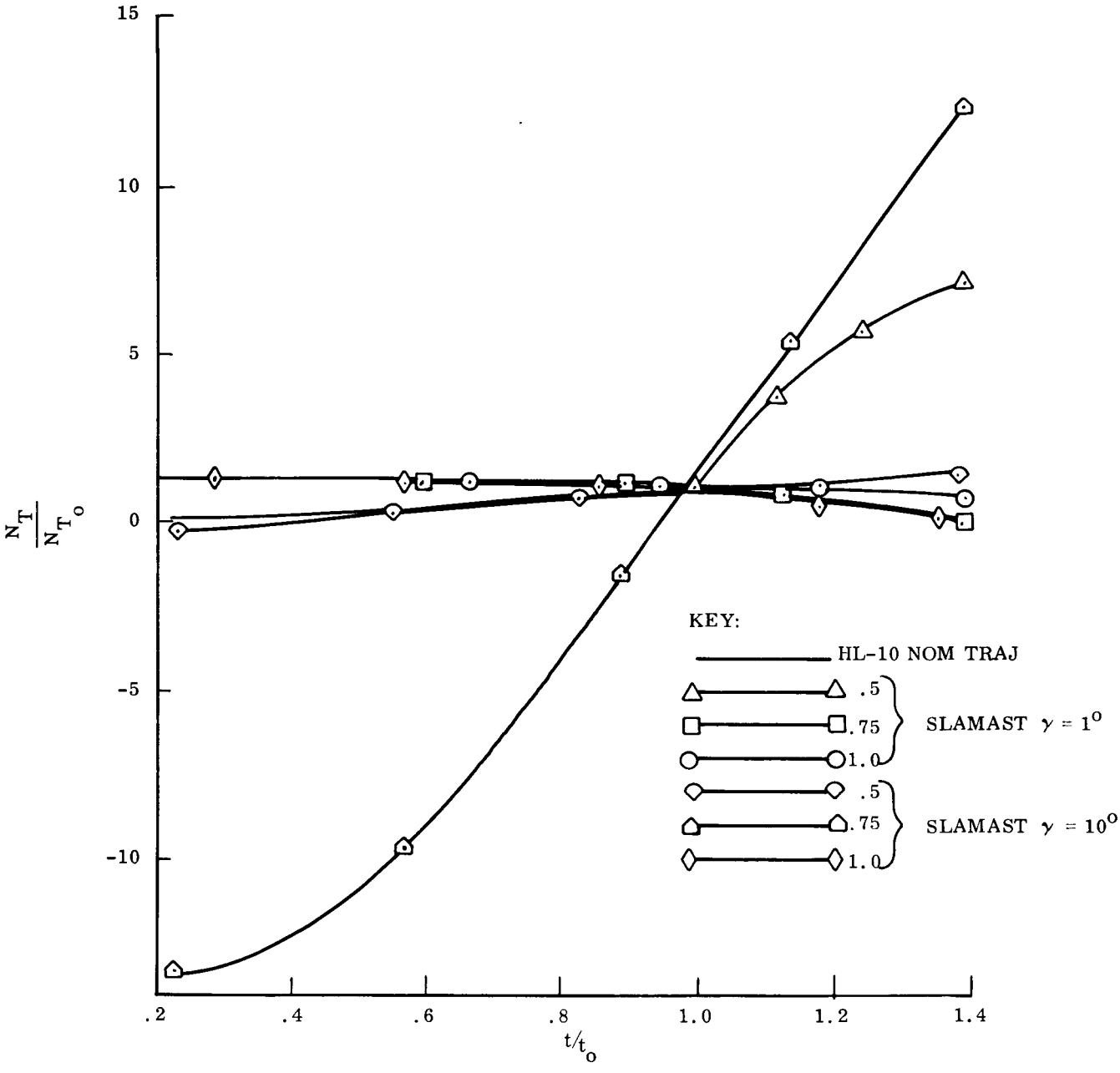

Figure 4-12. - Comparison of HL - 10 and SLAMAST Trajectories, Non-Dimensional Similarity Parameters $\frac{N_T}{N_{T_o}}$

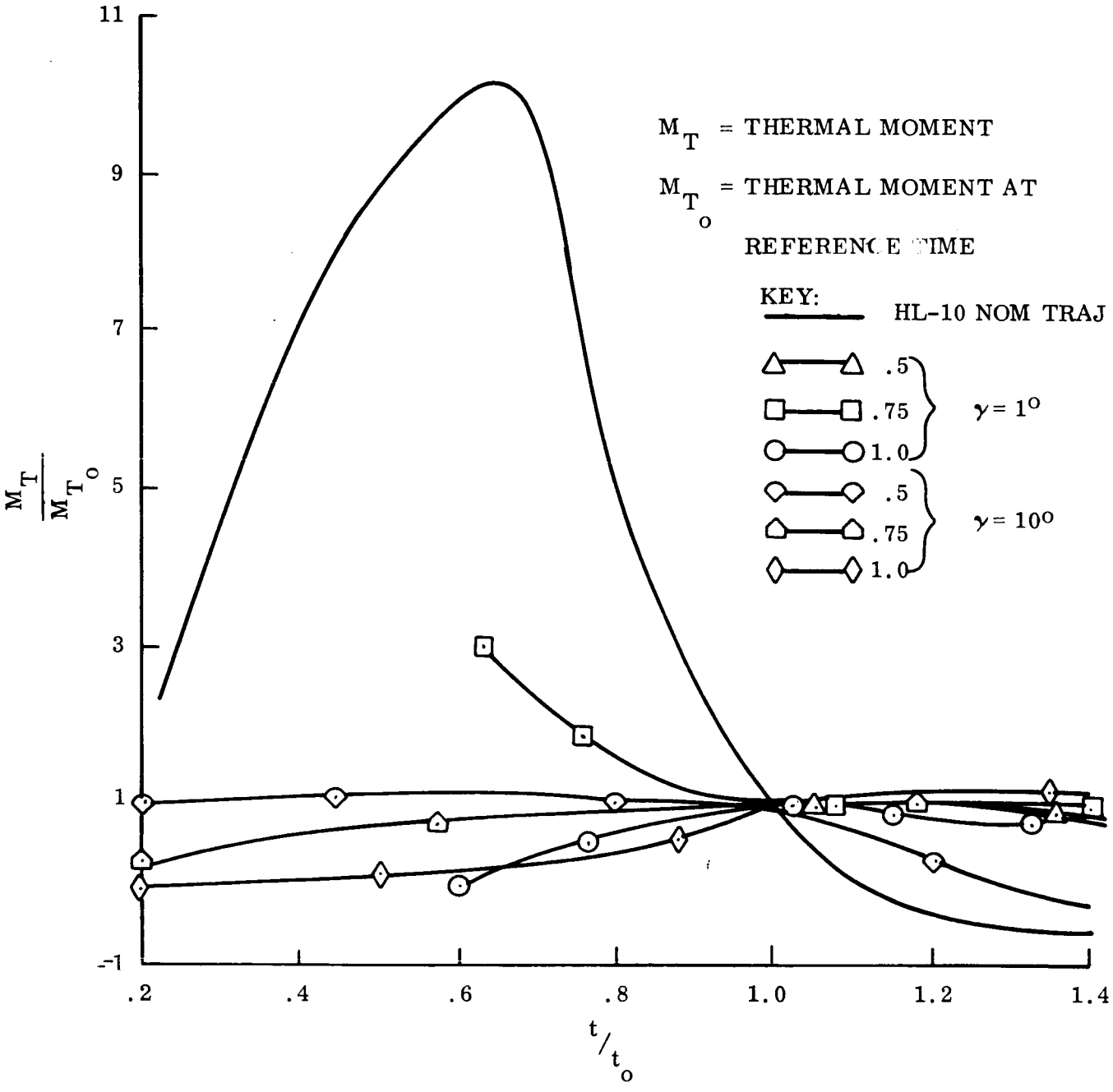

Figure 4-13. - Comparison of HL - 10 and SLAMAST Trajectories, Non-dimensional Similarity Parameters $\frac{M_T}{M_{T_o}}$

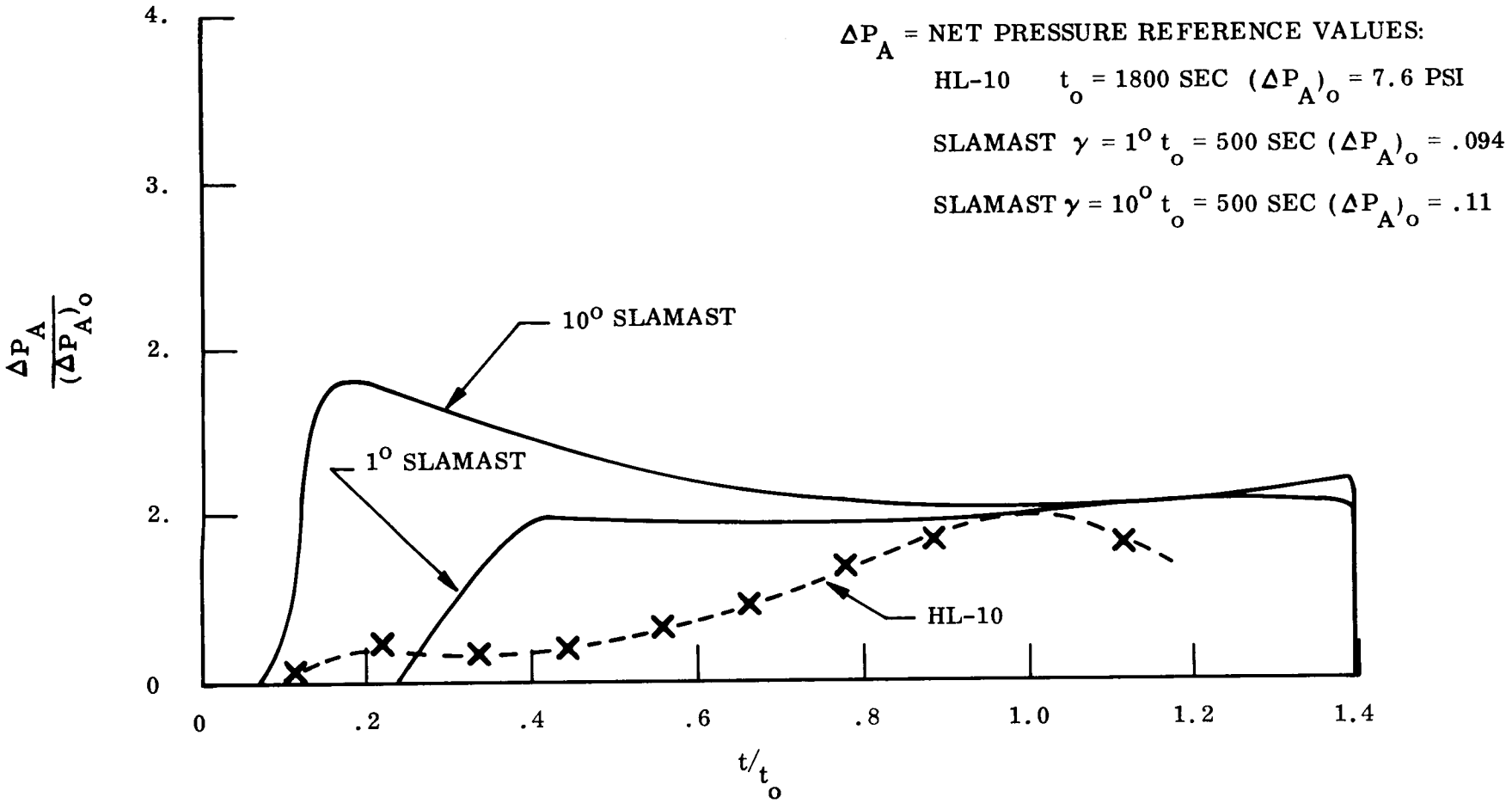

Figure 4-14. - Comparison of HL - 10 and SLAMAST Trajectories, Non-dimensional Similarity Parameters, $\Delta P_A/(\Delta P_A)_o$

no other modes are critical earlier and the mode of failure having the nearest margin of safety to the minimum has been adjusted to come as close as possible to the HL-10 values, the SLAMAST panel design and trajectory can now be specified to achieve the HL-10 simulation desired (Block 10). If the margin of safety of the next closest mode of failure is very close to the critical mode, the importance of interaction between these failure modes becomes crucial and margins of safety must be carefully determined with accurate tolerances to assure proper thermostructural response in the truly critical mode.

Returning to Case B now, where a design cannot be accomplished (Block 6), a different trajectory can be flown and/or an earlier time or later time can be selected (Block 11). The test panel is then redesigned using the information gathered from Block 11 (Block 12) and the SLAMAST mode of failure and margin of safety is again compared with the HL-10 (Block 5); and the procedure continues to Blocks 6, 7 and 8.

If other failure modes are critical earlier (Block 8), the trajectory can be changed earlier in the flight to eliminate the other failure modes and/or the design can be changed to strengthen the panel in the other failure modes (Block 13). The procedure then returns to Block 5 where the SLAMAST panel is compared to the HL-10, and continues along the path of Blocks 6, 7, 8 etc.

The flow chart indicated in Figure 4-2 with its trial and error processes and its iterative loops will be amenable to computer mechanization whereby a design can be accomplished more quickly and effectively.

The SLAMAST panel design would then be complete and the particular trajectory designated to accomplish the intended experiment for investigating one or two particular critical modes of failure. The flight test would be conducted with complete instrumentation particularly in the area of the test panel. Test data would be recorded during the complete flight. The data will be thoroughly evaluated to identify how well the predicted behavior coincided with the actual. Were the aerodynamic, thermodynamic, and acoustic prediction verified? Did the materials (both structural and non-structural) behave in accordance with the predicted characteristics, particularly at the higher temperatures? Were the analysis techniques used in determining loads, stresses, deflections and dynamics adequate in predicting the actual panel response measured?

By careful evaluation of the thermal gradients, the pressures recorded, the depth of ablation, panel deflections and honeycomb face strains, the area in which the thermostructural panel response is greatly different than the predicted will be isolated.

If the flight is completely successful and the test panel is recovered intact, and all the test data shows the predicted values to be within reasonable tolerances, the SLAMAST vehicle will have been a truly useful tool. Complete verification of all aerodynamic, thermodynamic, and material properties inputs would be extremely significant. Greater confidence would be placed on the analytical model and the techniques used in deriving the margins of safety for the various modes of failure in the HL-10 design or the particular prototype under study.

If some unexpected phenomena occurs during flight, the test data would be used to determine if such an event could indeed occur under similar conditions on the prototype vehicle.

REFERENCES

4-1. Newell, J., "A Study of Thermo Structural Design Concepts for Lifting Re-entry Vehicle", NASA CR-240, June 1965.

4-2. LaPorte, A. H., "Research on Refurbishable Thermostructural Panels for Manned Lifting Re-entry Vehicles", NASA CR-638, November, 1966.

4-3. Rieckmann, R. E., "Research Study to Provide Concepts of Panel Attachment Mechanisms Suitable for Refurbishable Panel Application", NASA CR-640, November, 1966.

4-4. Vinson, J. R. and Shore, S., "Methods of Structural Optimization for Flat Sandwich Panels"; U.S. Naval Air Engineering Center, Report No. NAEC-ASL-1083, 15 April, 1965.

5. EXPERIMENT SIMULATION

Two sentences from Section 3 of this report may be quoted which relate to the purpose and requirements of testing:

> "Testing with proper instrumentation will reveal these definciencies if they indeed exist",

and

> "Testing becomes a job of demonstrating the accuracy with which environment can be predicted, material behavior in the presence of that environment is known, and structural response in the presence of both of these can be predicted."

The underlined phrases are the key elements to which the discussion in this section is directed.

It is clear that meaningful conclusions can be drawn only from a well conceived and well executed experiment. We propose that experiment simulation be used to ensure the proper design and execution of each of the various experiments that may be performed with the SLAMAST vehicle. Simulation is the tool by which the experiment can be studied; it begins by recognizing the experiment to be a "system" and by defining the various system components and their interactions. The obvious components of an experiment system are the instrumentation and data acquisition or telemetry. (Telemetry is here meant to include everything between the generation of some signal by the instrumentation, and the reception of that signal on the ground.) Whatever a particular experiment may require in terms of these two components, the significance of the experiment lies not in the data itself, but in what this data tells about the performance of whatever was tested; more precisely the data is meaningful only in relation to the performance of the test subject in a particular environment. To the obvious components, instrumentation and data acquisition must therefore be added data reduction, which transforms the raw data (resulting from data acquisition) to engineering data, and analysis, which interprets the engineering data in drawing conclusions about the performance of the test object in its environment. Lastly, the environment itself, possible together with instrumentation that will make the environment known, must be considered as a component of the total experiment system.

Any attempt to design an "optimum" experiment, that is an experiment which will yield the best or most meaningful data in the presence of certain constraints (vehicle, cost, environment, practicality, etc.), must necessarily consider all the components of the experiment system. This can be done, and is often done in an informal manner, by much trial and error and by trying to "make the best of what we have". A more formal way will give better results. This formal way exists in experiment simulation. Fig. 5-1 shows how such a simulation can be performed. The essence of the simulation is the performance of four steps:

(1) determine nominal experiment data

(2) add instrumentation and telemetry errors

(3) perform data reduction and analysis

(4) compare the results of data analysis with the nominal data

By varying the inputs to each of these elements, conclusions can be drawn about the design and the requirements of each of the experiment system components. For instance, by putting in various arrangements of instrumentation (location and numbers of sensors) a particular arrangement may be found which gives the most meaningful results when subjected to a particular method of data analysis. Or, in the presence of certain inherent or unavoidable errors in sensor response, it may be found that a high sampling rate is required. In such a case, any improvement would be sought in providing better or different sensors. The actual elements of simulation and the particular cases to be studied depending, of course, on whatever experiment is to be performed. But, in each case, the fundamental nature of this approach is that all judgments on the performance of an experiment system are made on the basis of the interactions between the system components as defined above.

In summary then, the purpose of experiment simulation is as follows.

(1) Design experiment. - Ideally no component of the experiment system should be over or under designed with respect to any other.

(2) Provide a preview of the data. - What the data looks like will determine how to handle it with respect to sampling, recording.

(3) Exercise the data analysis. - Various methods of data analysis may be available; which method to choose depends on the quality of data available.

(4) Prepare for post-flight analysis. - A thorough understanding of the entire experiment may appreciably reduce the time necessary for post-flight analysis.

(5) What to do in case of contingencies. - An important problem in post-flight analysis is how to get useful data in case some sensor has failed.

Finally, the simulation will tell how much uncertainty is to be expected to remain after having provided the best possible instrumentation, data acquisition and analysis. If, in the real experiment, results appear to be different than expected, it can be decided that something new has been learned if on the basis of simulation it is known that the anomalous result does not simply fall within the uncertainty band.

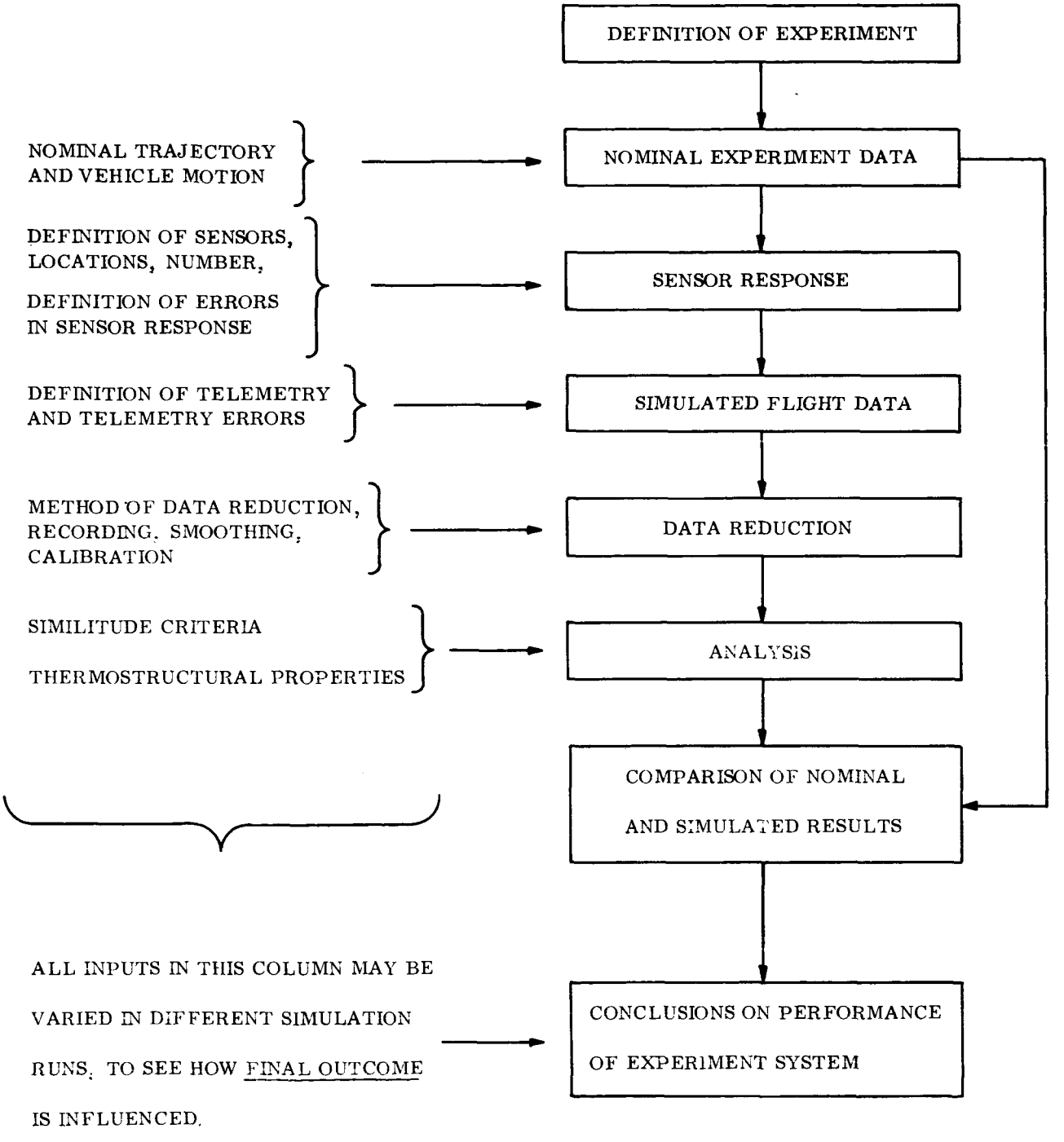

Figure 5-1. - Block Diagram of Experiment Simulation

6. DETAILED SUMMARY OF SIMILARITY PARAMETERS

6.1 STRUCTURAL SIMILITUDE

Several investigations (ref. 6-1 to 6-11) have been performed to define the similarity pertinent to the general aerothermoelastic modeling problem. These studies have defined the similitude parameters of importance for complete aerothermoelastic simulation as those presented in Table 6-1. Results are shown for three separate investigations. It appears the work of Dugundji and Calligeros (ref. 6-2) is the most comprehensive and, accordingly, it is explored further in Tables 6-2 and 6-3. Table 6-2 presents the similarity parameters in terms of the individual disciplines to which they apply. These disciplines are aerodynamics (pressures and aerodynamic heating), heat conduction, and structures.

Two sets of parameters are shown for structural similarity in Table 6-2. The parameter u_o/L comes in only for large deflections and can be dropped if only small deflections are pertinent. If retained, it serves to define the reference deflection u_o ; otherwise, if dropped, the reference deflection u_o can be obtained more freely from the first parameter $(\sigma_o L/E_o u_o)$. The next two parameters serve to define the reference stress, σ_o, either from the aerodynamic loading, p_A, or from any non-aerodynamic loading, p_F. The $(\rho_B u_o L/\sigma_o t_o^2)$ condition relates to dynamic vibrations and serves to define the reference time, t_o. The $\rho_B gL/\sigma_o$ parameter relates to gravitational loadings and may also serve to define the reference stress, σ_o, if these are significant. The Poisson's ratio condition (ν) can usually be met for many elastic materials, while the circumflexed quantities $(\wedge)$ require that temperature variations of these quantities be of the same form for both model and prototype. The remaining (T) condition would be automatically satisfied if the similarity conditions on aerodynamic and heat conduction similarity are maintained.

Also shown in Table 6-2 are the similarity parameters derived from plate theory. The plate or panel type structure is very often encountered in flight vehicle structures. Some less restrictive similarity parameters than those for an aribtrary elastic body may be arrived at when considering heated and laterally loaded plates. Thin plate theory similarity parameters seem particularly appropriate for some of the experiments envisioned for the SLAMAST vehicle. For small deflections of plates, the $B_o u_o^2 /N_o L^2$ parameter, which arises from a nonlinear coupling term in the governing differential equation, may be neglected.

Table 6-3 presents the pertinent similarity parameters for some specialized situations (ref. 2). The thermostructural behavior of a solid thin plate leads to the similarity parameters shown under item 3 in Table 6-3. For a solid plate of thickness $\delta = \tau L \bar{\delta}$, the quantities B_o, D_o, N_{T_o}, M_{T_o}, and N_o of general plate theory can be related to δ, thus simplifying the general plate parameters of Table 6-2. These similarity parameters (Table 6-3) are less restrictive than the general ones of Table 6-2, since they permit variation in the thickness ratio (τ) of the plates. Again, if small deflections are to be considered, the separate $(u_o/L\tau)$ parameter arising from the nonlinear coupling term may be dropped. However, then, if thermal forces N_{T_o}

TABLE 6-1. - SUMMARY OF PARAMETERS FOR AEROTHERMOELASTIC SIMILITUDE

Reference	Parameters
Dugundji and Calligeros	M_∞, Re_∞, $\frac{k_\infty}{K_o}$, $\frac{\rho_\infty V^2}{E_o}$, $\alpha_o T_o$, $\frac{\rho_B}{\rho_\infty}$ $\frac{T_o}{T_\infty}$, $\frac{K_o t_o}{L^2}$, $\frac{V t_o}{L}$, $\frac{U_o}{L}$, $\frac{\sigma_o}{E_o}$, $\frac{P_E}{E_o}$ $\frac{\epsilon_o \sigma T_o^3 L}{K_o}$, $\frac{\rho_B g L}{P_\infty V^2}$, Pr, γ, v, $\hat{k}$, $\hat{C}_p$ $\hat{\mu}$, $\hat{K}$, $\hat{C}$, $\hat{E}$, $\hat{\alpha}$, ϵ_w, T_{B_i}/T_o
O'Sullivan	M_∞, R_e, P_r, $p/\rho_\infty V_\infty^2$ γ, T_w/T_∞ α, $\frac{\dot{\alpha} L}{V_\infty}$, $\frac{\ddot{\alpha} L^2}{V_\infty^2}$
Molyneux	$\frac{L}{vt}$, $\frac{p}{\rho V^2}$, R_e, $\frac{gL}{V^2}$, $\frac{p}{\rho C_p T}$, $\frac{k}{V \rho c_p L}$, γ, $\frac{k}{K}$, $\frac{\epsilon T^3 L}{K}$, $\frac{Kt}{c \rho_B L}$ v, $\frac{\sigma u}{EL}$, $\frac{\alpha T L}{b}$, $\frac{\rho_B g L}{\sigma}$, $\frac{\rho_B u L}{\sigma t^2}$, $\frac{p}{\sigma}$, $\frac{u}{L}$

TABLE 6-2. - IDENTIFICATION OF GENERAL SIMILARITY PARAMETERS

Discipline \ Reference	Dugundji Calligeros	O'Sullivan
Aerodynamic Similarity	M_∞, Re_∞, Pr, γ $\frac{Vt_o}{L}$, $\frac{u_o}{L}$, $\frac{T_o}{T_\infty}$, $\frac{k_\infty}{K_o}$ C_p, k, μ, $\bar{T}_B$, $\bar{u}_j$	M_∞, Re_∞, Pr, γ N_u, $\frac{T_W}{T_\infty}$ α, $\frac{\dot{\alpha} L}{V_\infty}$, $\frac{\ddot{\alpha} L^2}{V_\infty^2}$
Structural Similarity	(Elasticity Theory) $\frac{\sigma_o L}{E_o u_o}$, $\frac{\alpha_o T_o L}{u_o}$, $\frac{u_o}{L}$, $\frac{P_A}{\sigma_o}$, $\frac{P_F}{\sigma_o}$ $\frac{\rho_B U_o L}{\sigma_o t_o^2}$, $\frac{\rho_B g L}{\sigma_o}$, v, $\hat{E}$, $\hat{\alpha}$, $\bar{T}$ (PLATE THEORY) $\frac{\Delta p_{A_o} L^4}{D_o U_o}$, $m_o L$ $\frac{(\Delta p_A)_o L^4}{D_o U_o}$, $\frac{m_o L^4}{D_o t_o^2}$, $\frac{m_o g L^4}{D_o u_o}$, $\frac{p_F L^4}{D_o u_o}$ $\frac{N_o L^2}{D_o}$, $\frac{L^2 M_{T_o}}{D_o u_o}$, $\frac{B_o u_o^2}{N_o L^2}$, $\frac{N_{T_o}}{N_o}$, v $\hat{B}$, $\hat{D}$, $\hat{N}_T$, $\hat{M}_T$, $\bar{m}$, $\overline{\Delta p_A}$	$\frac{u}{L}$, $\frac{\sigma}{E}$, v, αT, $L\alpha\frac{dT}{dL}$, $L^2\alpha\frac{d^2T}{dL^2}$ $\frac{F}{L^2 E}$, $\frac{pF}{E}$, $\frac{M}{L^3 E}$

and thermal moments M_{T_o} were present simultaneously in a given heating situation, the $(u_o / L\tau)$ requirement would still be necessary (through mutual satisfaction of the sixth and eighth parameters of item 3 in Table 6-3).

One specialized situation that deserves particular attention is panel flutter. For thin panels at $M > 2.5$, aerodynamic piston theory is often assumed to give a reasonable estimate of the pressure distribution. For these thin panels, the assumption of small heat conduction in the x_1 and x_2 directions is apt to be reasonable. Under these conditions, the parameters reduce to those shown in item 4 of Table 6-3. The first parameter $(\rho_\infty V^2/E_o M_\infty \tau^3)$ is the basic panel flutter parameter, while the second parameter relates to thermal strains in the panel. The third (mass density parameter) can usually be ignored if it is large enough. An example of scaling for panel flutter is given in reference 6-2.

The high structural temperatures and air loads associated with flight at high Mach numbers may no longer justify the assumption of an elastic structure, so that additional structural and material considerations are necessary. Structural deflections may extend into the plastic range in which case material yield and ultimate stresses and plastic stress-strain behavior must be considered. Furthermore, the assumption of small deflections may have to be removed and it may be necessary to scale the structural deflections in the same scale as the characteristic dimensions of the body. At high temperatures the creep and fatigue characteristics of a structure may have to be considered which introduce time, temperature level, and stress level as additional parameters. For convenience, the stress and deflection problem is divided into two major categories, namely, short - time loading and long - time loading.

6.1.1 SHORT-TIME LOADING

6.1.1.1 General. - This cateogry is concerned with loads of sufficiently short duration that the stress deformation behavior of the material is not influenced appreciably by the time under load, i.e., creep and fatigue effects are absent. The material behavior can then be described solely by means of stress-strain curves that for very short duration loads (high strain rates) tend to become additionally dependent on strain rate $\dot{\epsilon}$. The stress deflection behavior considered here will be at stress levels between the yield point and the ultimate stress. The parameters for the elastic range have been derived in reference 6-5.

Nonrecoverable deformations may result in this regime which may alter the steady-stage deflections of the outer shell and the internal structural geometry. These deformations may subsequently alter the air load distribution acting on the structure. Plastic buckling may also occur in members subjected to compressive forces. Essentially then, this category is an extension of an elastic structure study into the plastic range and the additional parameters which must be included relate to the short-time plastic stress-strain behavior of a material. The similarity parameters required for the same stress distribution are:

TABLE 6-3. SIMILARITY PARAMETERS FOR SPECIALIZED SITUATIONS

1. Aerodynamic Pressure Distribution
(non - viscous flow)

M_∞, γ, $\frac{Vt_o}{L}$, $\frac{u_o}{L}$, $\hat{C}_p$, $\bar{u}_j$ (note absence of R_e)

2. Aerodynamic Heat Transfer (non-ablating body)

$\frac{T_{AW}}{T_o}$, $\bar{T}_W$, $\hat{k}$, $\hat{u}$

Laminar flow $(k_\infty/K_o)\ R_{e_\infty}^{.5}\ P_r^{.333}$

Turbulent flow $(k_\infty/K_o)\ R_{e_\infty}^{.8}\ P_r^{.333}$

3. Structural Behavior of a Solid Plate

$\frac{(\Delta p_A)_o L}{E_o \tau^3 u_o}$, $\frac{\rho_B L^2}{E_o \tau^2 t_o^2}$, $\frac{\rho_B g L^2}{E_o \tau^2 u_o}$, $\frac{P_F L}{E_o \tau^3 u_o}$, $\frac{\sigma_o}{E_o \tau^2}$, $\frac{\alpha_o T_o L}{u_o \tau}$, $\frac{u_o}{L\tau}$, $\frac{\alpha_o T_o}{\tau^2}$, ν, $\bar{T}$, $\bar{\delta}$, $\bar{\Delta}_{p_A}$

4. Panel Flutter

$\frac{\rho_\infty V^2}{E_o M_\infty \tau^3}$, $\frac{\alpha_o (T_o - T_{Bi})}{\tau^2}$, $\frac{\rho_B M_\infty \tau}{P_\infty}$, $\frac{T_o - T_{Au}}{T_{AW} - T_{Bi}}$, $\frac{k_\infty (\rho_\infty)^{0.8} P_r^{1/3} t_o}{\rho_B C_o L^2 \tau}$, $\frac{Vt_o}{L}$, $\frac{u_o}{L\tau}$, $\frac{\sigma_o}{E_o \tau^2}$

$\frac{pF}{E_o \tau^4}$, $\frac{\epsilon_o \sigma L \left[(T_o - T_{Bi})\bar{\theta} + T_{Bi}\right]^4}{k_\infty (R_e)^{0.8} \rho_r^{1/3} (T_o - T_{Bi})}$, $\frac{\rho_B g L M_\infty}{\rho_\infty V^2}$, ν, $\hat{k}$, $\hat{\mu}$, $\hat{K}$, $\hat{C}$, $\hat{E}$, $\hat{\alpha}$, ϵ_W

$$\frac{\sigma_o}{E_o}\ ,\quad \text{shape of stress-strain curve,}\quad \alpha_o T_o\ ,$$

$$\overline{T}_B\ ,\ \frac{u\,\ell}{L}\ ,\ \frac{P_B L^2}{\sigma_o t_o^2}\ ,\ \frac{P_B g L}{\sigma_o}\ ,\ \hat{E}\ ;\ \hat{\alpha}\ ,\ \nu \qquad (6\text{-}1)$$

The first three parameters above relate to static stress-strain behavior, the fourth to the body temperature distribution, the fifth to scaled structural deflections, the sixth to structural dynamic effects, and the seventh to gravitational forces. The last three are conditions on material properties which are automatically fulfilled if the same materials and temperatures are utilized. For convenience, the reference stress σ_o may be taken as the yield stress of the material. Note that for an elastic body the condition on the shape of the stress-strain curve above is automatically met.

The simulation of the general shape of the stress-strain curve is a very difficult task for anything except the same material at the same temperature. An attempt at this can be made, through the Ramberg-Osgood approximation. It has been shown that for many metals at various temperatures and various soaking times the following Ramberg-Osgood expression is a reasonable approximation

$$\epsilon = \frac{\sigma}{E}\left[1 + \frac{3}{7}\left(\frac{\sigma}{\sigma_{.7}}\right)^{n-1}\right] \qquad (6\text{-}2)$$

where $\sigma_{.7}$ is the stress corresponding to a secant modulus of .7E and n is the shape factor of the curve. Both E and $\sigma_{.7}$ are now functions of temperature T. Nondimensionalizing, Eq. (6-2) becomes

$$\epsilon = \frac{\sigma}{E_o}\,\frac{\overline{\sigma}}{\hat{E}}\left[1 + \frac{3}{7}\left(\frac{\sigma_o}{(\sigma_{.7})_o}\,\frac{\overline{\sigma}}{\hat{\sigma}_{.7}}\right)^{n-1}\right] \qquad (6\text{-}3)$$

where

$$\overline{\sigma} = \frac{\sigma}{\sigma_o}\ ,\quad \hat{\sigma}_{.7} = \frac{\sigma_{.7}}{(\sigma_{.7})_o}$$

In the above, $(\sigma_{.7})_o$ is the $\sigma_{.7}$ at some reference temperature.

Thus the entire shape of the stress-strain curve is reasonably well reproduced if the following parameters are duplicated

$$\frac{\sigma_o}{E_o}\ ,\ \hat{E},\ \frac{\sigma_o}{(\sigma_{.7})_o}\ ,\ \hat{\sigma}_{.7}\ ,\ n,\ \frac{\sigma_{ult}}{\sigma_{.7}} \qquad (6\text{-}4)$$

The first and second conditions above were previously derived for a body in the elastic region; the remaining ones are now additional conditions for the plastic portion of the stress-strain curve. The parameter $(\sigma_o/\sigma_{.7})_o$ serves to define the reference stress level σ_o, while the $\sigma_{.7}$ condition requires the $\sigma_{.7}$ to have the same variation with temperature on model and prototype. The parameter $\sigma_{ult}/\sigma_{.7}$ is introduced to account for the extent of the plastic region and may be dispensed with if both model and prototype operate below their ultimate strengths. With regard to the shape parameter n, for 4340 steel, stainless steel W and Inconel X, for example, $n > 10$ up to 1200^oF and $n \approx 10$ approximates many of the airframe metal alloys at room and elevated temperatures. The shape parameter, n, being approximately the same for many airframe materials, may therefore be dispensed with. Under all the above conditions, the first two parameters of Eq. (6-1) may then be replaced by the following:

$$\frac{\sigma_o}{E_o}\ ,\quad \frac{\sigma_o}{(\sigma_{.7})_o}\ ,\quad \hat{\sigma}_{.7} \tag{6-5}$$

where it has been assumed that all stresses are acting below the ultimate stress of the material. An additional condition is necessary relating to the normal stress boundary condition on the structure. At the surface of the body, the normal stress σ_n equals the sum of the aerodynamically applied pressure P_A and any additional non-aerodynamic loading, P_F. This then introduces the additional non-dimensional parameter,

$$\bar{\sigma}_n = \frac{\sigma_n}{\sigma_o} = \frac{P_A + P_F}{\sigma_o} \tag{6-6}$$

which is to be added to those originally given in Eq. (6-1). Summarizing then for a material whose plastic stress-strain curve is matched by the Ramberg-Osgood approximation as stated previously, the general parameters for stress and deflection similarity are,

$$\begin{gathered}\frac{\sigma_o}{E_o}\ ,\quad \frac{\sigma_o}{(\sigma_{.7})_o}\ ,\quad \hat{\sigma}_{.7}\ ,\quad \alpha_o T_o,\quad \bar{T}_B,\quad \frac{u_o}{L} \\ \frac{P_B L^2}{\sigma_o t_o^2}\ ,\quad \frac{P_B g L}{\sigma_o}\ ,\quad \frac{P_A + P_F}{\sigma_o}\ ,\quad \hat{E},\ \hat{\alpha},\ \nu\end{gathered} \tag{6-7}$$

The form of the boundary condition Eq. (6-6) as given above, permits the addition of non-aerodynamic loads P_F on a model to adjust for a purely aerodynamic loading on the prototype, provided this aerodynamic loading is known. If the aerodynamic loading is not known in advance, as in aeroelastic type models, it is then required to simulate both P_A/σ_o and P_F/σ_o separately.

For example, for such aerodynamic type testing over the surface of bodies in hypersonic flow, $P_F = 0$ and P_A/σ_o becomes

$$\frac{P_A}{\sigma_o} = \frac{\rho_\infty V^2}{\sigma_o} \overline{P} \qquad (6\text{-}8)$$

Maintaining the required aerodynamic similarity $\overline{P}$ for this general body, the above reduces to the condition of

$$\frac{\rho_\infty V^2}{\sigma_o} \qquad (6\text{-}9)$$

which replaces the $(P_A + P_p)/\sigma_o$ condition of Eq. (6-7) for these purely aerodynamic type loadings.

6.1.1.2 Stresses and deflections of plates. - A specific type of structure that is often encountered in aeroelastic work is the plate. Panel sections of the shield-structure composite used as the outer shell of a re-entry vehicle may be regarded as plates. A convenient means of representing the deflections of a composite panel of this type is to transform the actual shield-structure into an equivalent plate of varying bending and extensional stiffness. It might be of interest therefore to examine the specific similarity parameters associated with heated and laterally loaded plates. The governing differential equations of a heated isotropic plate are,

$$\frac{\partial^2}{\partial X_1^2}\left[D\left(\frac{\partial^2 u_3}{\partial X_1^2} + \nu \frac{\partial^2 u_3}{\partial X_2^2}\right)\right] + \frac{\partial^2}{\partial X_2^2}\left[D\left(\frac{\partial^2 u_3}{\partial X_2^2} + \nu \frac{\partial^2 u_3}{\partial X_1 X_2}\right)\right]$$

$$+ 2(1-\nu)\frac{\partial^2}{\partial X_1 \partial X_2}\left[D \frac{\partial^2 u_3}{\partial X_1 \partial X_2}\right] = \Delta p + \frac{\partial^2 F}{\partial X_2^2}\frac{\partial^2 u_3}{\partial X_1^2}$$

$$+ \frac{\partial^2 F}{\partial X_1^2}\frac{\partial^2 u_3}{\partial X_2^2} - 2\frac{\partial^2 F}{\partial X_1 \partial X_2}\frac{\partial^2 u_3}{\partial X_1 \partial X_2} - \frac{1}{1-\nu}\left(\frac{\partial^2 M_T}{\partial X_1^2} + \frac{\partial^2 M_T}{\partial X_2^2}\right)$$

(6-10)

$$\frac{\partial^2}{\partial X_1^2}\left[\frac{1}{B}\left(\frac{\partial^2 F}{\partial X_1^2} - \nu \frac{\partial^2 F}{\partial X_2^2}\right)\right] + \frac{\partial^2}{\partial X_2^2}\left[\frac{1}{B}\left(\frac{\partial^2 F}{\partial X_1^2} - \nu \frac{\partial^2 F}{\partial X_2^2}\right)\right]$$

$$+ 2(1+\nu)\frac{\partial^2}{\partial X_1 \partial X_2}\left[\frac{1}{B}\frac{\partial^2 F}{\partial X_1 \partial X_2}\right] = (1-\nu^2)\left[\left(\frac{\partial^2 u_3}{\partial X_1 \partial X_2}\right)^2\right.$$

$$\left. - \frac{\partial^2 u_3}{\partial X_1^2} \cdot \frac{\partial^2 u_3}{\partial X_2^2}\right] - \frac{\partial^2}{\partial X_1^2}\left[\frac{N_T}{B}\right] - \frac{\partial^2}{\partial X_2^2}\left[\frac{N_T}{B}\right] \qquad (6\text{-}11)$$

where $\Delta p(X_1, X_2, t)$ is the distributed lateral loading per unit area of the plate.

These two equations are the Von Kármán equations for large deflections of a plate with variable stiffness properties under applied loads and thermal stresses. The quantity $u_3\ (X_1, X_2, t)$ is the lateral deflection of the neutral surface from its initial position, F is the stress function, B and D are the extensional and bending stiffness per unit length respectively, and N_T and M_T are the thermal force and moment per unit length respectively. These latter are defined more generally as,

$$B = \int_{-\delta/2}^{\delta/2} \frac{E}{1-\nu^2}\, dX_3$$

$$D = \int_{-\delta/2}^{\delta/2} \frac{E X_3^2}{1-\nu^2}\, dX_3 \qquad (6\text{-}12)$$

$$N_T = \int_{-\delta/2}^{\delta/2} E\alpha \left[T - T_{Bi}\right] dX_3$$

$$M_T = \int_{-\delta/2}^{\delta/2} E\alpha \left[T - T_{Bi}\right] X_3\, dX_3$$

where δ is the plate thickness and ΔT is the temperature rise from some initial value.

Introducing the following non-dimensional parameters,

$$X_i = X_i/L \quad , \quad \bar{F} = F/N_o L^2 \quad , \quad \hat{N}_T = N_T/N_{To}$$

$$\bar{u}_3 = u_3/u_o \quad , \quad \hat{B} = B/B_o \quad , \quad \hat{M}_T = M_T/M_{To} \qquad (6\text{-}13)$$

$$\hat{N}_{ij} = N_{ij}/N_o \quad , \quad \hat{D} = D/D_o \quad , \quad \bar{\sigma}_{ij} = \sigma_{ij}/\sigma_o$$

the Von Kármán equations become,

$$\frac{\partial^2}{\partial \bar{X}_1^2}\left[\hat{D}\left(\frac{\partial^2 u_3}{\partial \bar{X}_1^2} + \nu \frac{\partial^2 \bar{u}_3}{\partial X_2^2}\right)\right] + - - - = \frac{L^4 \Delta p}{D_o u_o}$$

$$+\left(\frac{B_o L^2}{D_o}\right)\left[\frac{\partial^2 \bar{F}}{\partial X_2^2}\ \frac{\partial^2 u_3}{\partial X_1^2} + - -\right] - \left(\frac{L^2 M_{To}}{u_o D_o}\right)\left[\frac{\partial^2 \hat{M}_T}{\partial \bar{X}_1^2} + \frac{\partial^2 \hat{M}_T}{\partial \bar{X}_2^2}\right] \qquad (6\text{-}14)$$

$$\frac{\partial^2}{\partial \bar{X}_1^2}\left[\frac{1}{B}\left(\frac{\partial^2 \bar{F}}{\partial \bar{X}_1^2} - \nu \frac{\partial^2 \bar{F}}{\partial \bar{X}_2^2}\right)\right] + - - - = \left(\frac{u_o^2}{L^2}\right)\left[\frac{\partial^2 \bar{u}_3}{\partial \bar{X}_1 \partial \bar{X}_2}\right.$$

$$\left. + \frac{\partial^2 \bar{u}_3}{\partial \bar{X}_1^2}\ \frac{\partial^2 \bar{u}_3}{\partial \bar{X}_2^2}\right] - \left(\frac{N_{To}}{C_o}\right)\left[\frac{\partial^2}{\partial \bar{X}_1^2}\left(\frac{\hat{N}_T}{B}\right) + \frac{\partial^2}{\partial \bar{X}_2^2}\left(\frac{\hat{N}_T}{B}\right)\right] \qquad (6\text{-}15)$$

The first non-dimensional parameter appearing above, $L^4 \Delta p/D_o u_o$ may be split up further by noting that the lateral loading Δp may be due to aerodynamic, inertial, gravity, or externally applied forces

$$\Delta p = P_A - \frac{m \partial^2 u_3}{\partial t^2} - m g + P_F \qquad (6\text{-}16)$$

Hence the resulting non-dimensional parameters for a plate under lateral loads and varying temperature are

$$\left.\begin{array}{l} \dfrac{(\Delta P_A)_o L^4}{D_o u_o}, \quad \dfrac{m_o L^4}{D_o t_o^2}, \quad \dfrac{m_o g L^4}{D_o u_o}, \quad \dfrac{P_F L^4}{D_o u_o} \\ \dfrac{N_o L^2}{D_o}, \quad \dfrac{L^2 M_{T_o}}{D_o u_o}, \quad \dfrac{B_o u_o^2}{N_o L^2}, \quad \dfrac{N_{T_o}}{N_o}, \quad \nu \\ \hat{B}, \hat{D}, \quad \hat{N}_T, \hat{M}_T, \bar{m}, \bar{\Delta}_{P_A} \end{array}\right\} \qquad (6\text{-}17)$$

For the study of small deflections, u_3 of heated plates, the non-linear terms $(\partial^2 u_3/\partial X_1 \partial X_2)^2 - (\partial^2 u_3/\partial X_1^2)(\partial^2 u_3/\partial X_2^2)$ appearing in Eq. (6-11) may be neglected. In this case the u_o/L requirement in Eq. (6-15) would not appear. Further, it is seen that this would then uncouple the two equations and permit one to solve the second equation for the stress function in the form,

$$\bar{F} = \frac{N_{T_o}}{B_o} \bar{g} (\bar{X}_1, \bar{X}_2) \qquad (6\text{-}18)$$

where $\bar{g}(\bar{X}_1, \bar{X}_2)$ is some non-dimensional function depending on the temperature distribution and boundary conditions of the plate. Placing this back into the first equation for u_3 would result in the following non-dimensional parameters for the small deflections of a heated, laterally loaded plate

$$\frac{(\Delta P_A)_o L}{E_o \tau^3 u_o}, \quad \frac{\rho_B L^2}{E_o \tau^2 t_o^2}, \quad \frac{\rho_B g L^2}{E_o \tau^2 u_o} \qquad (6\text{-}19)$$

$$\frac{P_F L}{E_o \tau^3 u_o}, \quad \frac{\sigma_o}{E_o \tau^2}, \quad \frac{\alpha_o T_o L}{u_o \tau}, \quad \frac{u_o}{L\tau}$$

$$\frac{\alpha_o T_o}{\tau^2}, \quad \nu, \bar{T}, \quad \bar{\delta}, \quad \overline{\Delta P_A}$$

6.1.2 LONG-TIME LOADING

In this category the duration of loading is sufficiently long that time under load will appear as an additional parameter relating to such items as creep and fatigue.

The consideration of time under load as a parameter is in addition to requiring the reproduction of the parameters of Eq. (6-1) and Eq. (6-6) for similitude. Reproduction of the actual time experienced by a prototype for a given loading will in most cases be impossible for a ground test model because of the short operating times of wind tunnels. Furthermore, if the actual time spent at temperature is important for a transient temperature test, this too is impractical to reproduce since simulation of the transient heating problem requires the time scale to be reduced according to

$$\frac{(t_o)_M}{(t_o)_P} = \left(\frac{L_M}{L_P}\right)^2 \qquad (6\text{-}20)$$

However, this last restriction does not apply for a steady-state heating experiment.

Reproduction of strain-rate is important since it affects the creep and fatigue behavior of a structure. Therefore, it is important to consider both the load level and the rate of loading of a heated structure along with the thermal loading.

Duplication of the aforementioned long-time loading effects on a one-to-one time basis is impossible in practically all cases if wind tunnel testing is utilized. Certain alternatives are available however. It is possible, at least for structures in which a two dimensional state of stress exists, to utilize results of phenomena such as creep, tension and compression loadings at short periods of time and given stress and temperature levels to extrapolate to longer periods of time and different stress and temperature levels with the Larson - Miller parameter

$$T\,(C + \log t) \qquad (6\text{-}21)$$

where C is a constant characteristic of the material and t is the time to rupture or to achieve a given strain (ref. 6-12). This parameter has correlated data over a wide range of times and temperatures for many steels, high temperature alloys, and aluminum alloys.

Another alternative is to utilize short-time experimental data in a cumulative sense. As suggested by Gerard (ref. 6-13) for creep, the total cumulative creep may be taken as the sum of the creep increments due to the time spent at each stress and temperature level. The creep deformation of a prototype, to a first approximation, may thus be accounted for by conducting several model tests at a given load and temperature level where the total testing time is equal to the prototype time.

The problem of fatigue at present is not well understood, especially at elevated temperatures. However, some current experimental techniques can be suggested here. The cumulative-damage theory of Miner (ref. 6-14) may be used to correlate fatigue data for several tests on each run for a different number of cycles n_i at a specified stress and temperature level with which a fatigue life N is associated. According to this theory, the fatigue life of a prototype will be reproduced experimentally if

$$\left(\frac{n_1}{N_1} + \frac{n_2}{N_2} + \ldots\right)_M = \left(\frac{n_1}{N_1} + \frac{n_2}{N_2} + \ldots\right)_P \qquad (6\text{-}22)$$

where each term on the left side above represents a model test and each term on the right represents the percentage of time spent by the prototype at any given stress level. The fatigue life N at each stress level would have to be obtained from an σ - N diagram at the corresponding temperature level. The cumulative damage concept is based on the assumption that the cycling tests may be conducted in any desirable sequence with no effect on the fatigue life.

An alternative method consists of determining an equivalent stress σ_r of constant amplitude which would have the same overall effect as a variable loading at different stress levels σ_1, σ_2 , - - --, and at different cycles n_1, n_2, - -, (ref. 6-14). This equivalent stress σ_r may be expressed as

$$\sigma_r = \frac{\sigma_1^X n_1 + \sigma_2^X n_2 + \ldots}{n_1 + n_2 + \ldots} \qquad (6\text{-}23)$$

where the exponent x is the inverse slope of the σ - N diagram on a log-log plot. The equivalent stress σ_r of the prototype may be estimated and a series of tests conducted on the model at various stress levels and cycles satisfying Eq. (6-23) and the condition $(\sigma_r)_M = (\sigma_r)_P$.

Additional considerations are important when dealing with fatigue. Scale effect may be very significant but the extent of this has not been fully understood. One theory holds that a specimen in which a large volume is subjected to high stress has more chance of containing a weak spot that determines failure than does a smaller piece (ref. 6-15). Reproduction of geometric details and use of the same material is also necessary.

For the problem discussed in this category it appears desirable that the applied load and temperature spectrums of a model should be the same as the prototype wherever possible. In many cases this will not be possible and some of the suggestions mentioned above may be applied, accounting for these phenomena at least in an approximate manner.

6.2 SIMILITUDE OF AEROTHERMOCHEMICAL LAWS OF ABLATING BODIES

6.2.1 INTRODUCTION

An analytically derived equation is considered correct for any system of units. Thus, each group of terms in the equation will have identical dimensionless representation. If the variables in a physical situation are known, where the relationship between the variables is not known, a situation can be formulated as a relation between groups of dimensionless variables where the groups number less than the variables. Such a process is termed "dimensional analysis". Hopefully, this procedure allows for less experimentation to establish a relationship between the variables while simplifying the experimentation. The two methods in which the dimensionless groups can be postulated include, the Buckingham π theorem, and examination of the governing differential equations and appropriate boundary conditions.

In connection with the theory of dimensional analysis is the concept of similitude which is an important criteria in model-prototype studies. Similitude may be considered a link between the two phenomena. Thus, similitude can be defined as the theory that includes a consideration of the conditions for which the behavior of two separate phenomena will be similar. The techniques of predicting the results of one phenomena from the observations of the other will be the course of study in this report.

When considering combined aerothermal similarity parameters (with regard to heat shield requirements) such as aerodynamics, heat conduction, and stress deformations at high temperatures and Mach numbers, reproducibility on scaled models becomes impossible. This is a result of such phenomena as property variations with temperature, transient effects, real-gas effects, radiation effects, ablation (chemical) effects, and boundary layer interaction effects. One method of treating these complicated phenomena is with the use of "incomplete aerothermoelasticity" (ref. 6-16). Incomplete aerothermoelasticity, or testing in successive steps, implies a knowledge of the pressure and/or heating a priori artificially applied to the scaled model. Specific purpose tests of this nature could yield more realistic knowledge of model-prototype behavior.

When the similarity laws are used in the hypersonic flow regime, use can be made of the Mach Number Independence Principle (ref. 6-17). This implies that the pressure distribution is independent of the Mach number. Another advantage associated with this speed range is the altitude, in particular with boost-glide vehicles, where the Reynolds number are lower and laminar flow exists over the entire structure. On the other hand, thermal radiation must be considered at hypersonic speeds.

Inasmuch as the materials to be used for the prototype must exhibit certain thermophysical properties for heat protection, it is expected that the model materials might have to be exactly duplicated. Thus, what will be required is some clear delineation of specific aerothermo problems associated with realistic materials at flight conditions. With this in mind, the pertinent parameters will be maintained and approximations can be made according to the specific problems using incomplete similitude.

The salient quantities involved in aerothermo modeling are the pressure distributions and the heat transfer imposed on the vehicle as a result of the external flow field. Consequently, when formulating a general model, one can direct the investigation into three distinct regions. These are the aerodynamic flow field, the material response region (char layer), and the transient heat conduction into the solid interior region.

6.2.2 SIMILITUDE FOR CHARRING ABLATORS

The important similarity parameters, for a char type ablator, which result from the governing differential equations and boundary conditions have been developed by Laganelli (ref. 6-18) and may be listed as

$$\frac{\dot{m}_g L C_{P_o}}{k_o}, \quad \frac{\dot{m}_c}{\dot{m}_g}, \quad T_x \tag{6-24}$$

The first term represents the ablation rate, the second represents the ratio of the solid-char mass fraction, and the third represents the temperature distribution within the virgin material. Equation (6-24) is subject to the following dimensionless groups:

$$\frac{\dot{q}_A L}{R_o T_o}, \quad \frac{\epsilon_o T_o^3 L}{k_o}, \quad \frac{L^2}{t_o K_o}, \quad \frac{T_w}{T_o}, \quad \frac{H_{cg}}{C_{P_o}} \quad \frac{V_o L}{K_o}$$

$$\frac{\left(h_c - h_w\right)_w}{C_{P_o} T_o} \quad \frac{\left(h_g - h_w\right)_w}{C_{P_o}' T_o} \quad \frac{L^2}{K_o T_o}\left[+ \dot{w}_c'' \left(h_g - e_c\right)\right], \quad \frac{L}{k_o T_o} \quad (q_b) \tag{6-25}$$

$$\frac{H_{deg}}{T_o C_{P_o}}, \quad \frac{T_{deg}}{T_o}, \quad \bar{k}_s, \quad \bar{C}_{P_s}, \quad \bar{\rho}_s, \quad \bar{k}_c, \quad \bar{C}_{P_c}, \quad \bar{\rho}_c, \quad \bar{\bar{C}}_{P_g}, \quad \bar{\rho}_g, \quad \bar{\mu}_g$$

with

$$\frac{\tau_A L}{\mu_o V_o}, \quad \frac{V_o \mu_o L}{P_o p}, \quad \frac{P_A}{P_o} \tag{6-26}$$

The first three terms of Eq. (6-25) are the similarity parameters associated with a non-ablative vehicle. The fourth through tenth parameters of Eq. (6-25) and the first two parameters of Eq. (6-26) represent the charring ablative process. The remaining terms of Eq. (6-25) represent similarity requirements for temperature response with material properties in the solid, char, and gas phases. Finally, the last parameter of Eq. (6-26) represents similarity for a geometric condition.

As might be expected, complete similarity of the parameters represented by Eq. (6-25) and (6-26) would be fortuitous. However, restricted purpose analysis such as viscous interaction for given body geometrics (boost-glide vehicles), stagnation point phenomena, and ablation effects lend a knowledge to the more significant parameters in the process. Even with these relaxations, one to one scaling would be virtually impossible. The probability of simulating the significant parameters in static and wind tunnel tests, with regard to incomplete aerothermoelasticity, is infeasible since scaling the required aerodynamic heat flux and pressure distributions becomes extremely difficult with existing facilities. It must also be kept in mind that the governing differential equations are themselves approximations and do not necessarily represent the true characteristics of the ablating process from which the similarity parameters evolved. On this basis, therefore, a more realistic approach was developed for model-prototype studies. It should be noted, however, that the similarity parameters previously developed do indeed indicate the more significant parameters which should be considered in the scaling studies.

6.2.3 SIMILITUDE PHILOSOPHY

As indicated previously, the reason for similitude studies is to predict the results of one phenomena from the observations of another. On the other hand, if we are able to predict the performance of a prototype vehicle, based upon our knowledge of existing materials and environmental conditions, it would be meaningful to simulate this performance on a scaled model to ensure its reliability. However, in the design of such a prototype it is inevitable that certain characteristics of the design will fail before others. With this in mind, a basis for formulating a similitude philosophy ref. (6-19) can be established. In connection with this philosophy, it will be shown that flight tests can yield information that could not otherwise be determined in ground tests.

Consider then, those particular parameters which are associated with potential failure modes of a charring ablator shield. As might be expected, the design criteria is mostly dependent upon the aerodynamic environment and material property variations which in turn predictate the structural size, thickness, etc. Based on past experience, several of the failure modes may be classified as:

(1)	Aerodynamic pressure	Aerothermochemical Considerations
(2)	Recovery enthalpy	
(3)	Blowing rate	
(4)	Char recession	
(5)	Aerodynamic shear stresses	Mechanical Considerations
(6)	Spallation	

These phenomena are particularly concerned with various flight regimes which include:

(1) Powered Flight

(2) Re-entry

(a) Nominal, (b) Overshoot, (c) Undershoot, (d) Abort

Having established the limitations in design, each potential mode of failure can be characterized by a margin of safety which is defined as

$$M.S. = \frac{\phi_{allowable}}{\phi_{calculated} \times F.S.} - 1 \geq 0 \qquad (6\text{-}27)$$

where ϕ represents any of the modes of failure and F.S. the factor of safety. If the margins of safety are plotted as a function of time, as shown for example in Figure 6-1, it is observed that a minimum value is obtained which will be designated as the critical mode of failure at some time t_o. This prediction is, of course, predicated upon our knowledge of the environment and material response analytically derived a priori for the prototype. Figure 1 indicates that the mode of failure, represented by the minimum margin of safety, should occur in flight before the other potential modes of failure.

Notice that it is no longer necessary to simulate all the modes of failure on a one to one basis, as was the case for the parameters of Eq. (6-25) and (6-26), but merely to simulate the critical mode of failure in model studies. Thus, by constraining the model to a flight path which simulates the critical mode of failure, within the flight time of the model, any unexpected phenomena which may occur before the critical failure mode time will be revealed. If on the other hand the model indicates the failure mode (for which it was constrained) has occurred, one has indeed simulated this event for which the prototype was designed. All other parameters, in the prototype design, are automatically satisfied. This implies that the other modes of failure have been essentially over-designed and can indicate areas where, for example, weight restrictions may be relaxed.

If the model fails in time prior to the critical mode of failure time, onboard instrumentation can yield valuable information as to which failure mode will require further investigation. In connection with this concept suppose, for the purpose of illustration, that the critical margin of safety was unity and the next lowest margin of safety (for another mode of failure) was 1.1. One can expect as a result of inaccuracies in the computations, the environment, material response, or data correlations that an overlap of the tolerances between the two modes of failure is quite imminent. This would require simulation of the two modes of failure in question. Of course, it would be desirable to match all the margins of safety for the prototype-model studies; but this is not necessary for the criteria to work.

Having established the nature of the philosophy, it would perhaps be meaningful to state the concept in composition form. All aerothermostructural concepts should be established for the prototype vehicle with regard to intended mission, loads, materials, factor of safety, analytical, and designs procedures. Having developed the necessary components of the prototype vehicle, the model is designed to determine critical modes of failure, sizes, and other pertinent details. The model is then studied to determine that particular flight profile which simulates the condition represented by the critical design criteria for each of the modes of failure, and involves all the phenomena associated with the prototype. Thus, at this particular flight profile, the model should be so designed with the same material, factor of safety, analysis, and design procedures used in designing the prototype. It should be noted that the model design must be identical with the prototype when considering the modes of failure and margins of safety, even though the model may vary in geometric quantities.

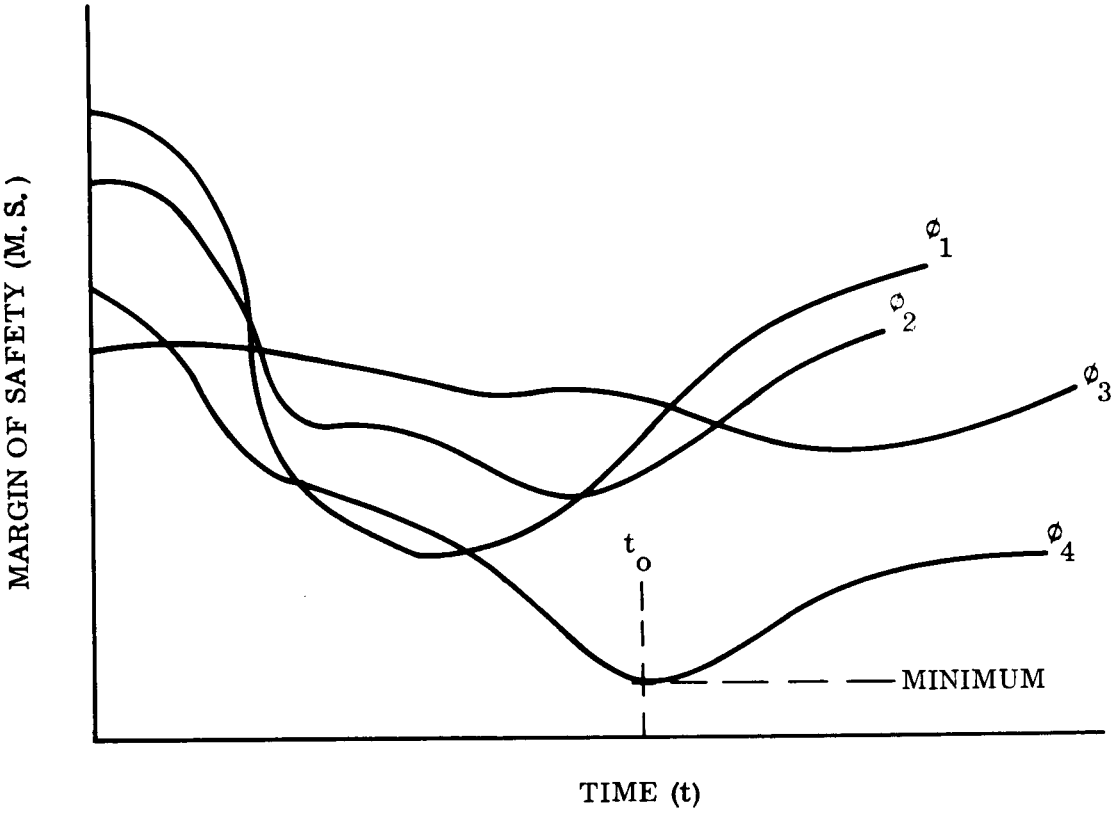

Figure 6-1. - Margin of Safety versus Time

It can be clearly seen that the need for a flight controlled vehicle is necessary in order to establish any practical similitude studies for ablating bodies. This procedure not only accomplishes this intention but is capable of uncovering by suitable instrumentation any unsatisfactory knowledge of the environment; any deficiencies in the analysis, design, or material behavior; and any unforeseen phenomena which would not be possible in ground simulated flights. In other words, by constraining the model flight profile to simulate as nearly as possible the critical aspects of the intended prototype flight profile, by using the same materials and structural concepts, and by forcing the model to have the same critical modes of failure, with the same factors of safety and margin safety, the salient parameters of aerothermostructural simulation are achieved without the complications of the less important considerations.

Although a large number of critical conditions occur over the prototype structure during the various flight regimes (abort, over and undershoot flight paths), through use of the philosophy stated above, a controlled flight model is capable of studying these critical conditions even though it has no abort or particular flight path considerations itself. Thus, the philosophy is considered both theoretically sound and provides a basis for a program that has a high degree of engineering overtones of being physically practical.

6.2.4 CHEMICAL SIMILARITY AND REQUIRED MODEL FLIGHT PROFILES

In order to demonstrate the applicability of the similitude philosophy suppose we consider, for example, that the most pertinent parameter associated with aerothermochemistry is the mass injection coefficient (B_g). It is necessary that the margin of safety is determined for all the modes of failure on the prototype; however, we will assume that B_g is the critical parameter for illustration. Having established the critical mode of failure, it is necessary to find a particular flight time on the model (SLAMAST) which will simulate this failure mode. Before proceeding, the reason for the choice of B_g as a potential critical parameter is associated with flight tests that have demonstrated coagulation characteristics of the char layer (as a result of chemical reactions) due to certain gas species. This in turn drastically changes the temperature gradients in the material, thereby, changing the required backface temperature. This particular phenomena, which occurred in flight tests, was not observed in wind tunnel studies.

According to the similitude philosophy it is necessary to establish a critical margin of safety. However, this is not possible when considering chemistry, in that, an allowable value of B_g is not known explicitly for the prototype (M2-F2). Since data was available for M2-F2, which exhibits similar characteristics to HL-10, it was used as the prototype. Fogaroli (ref. 6-20) has shown that certain species can cause probable surface sealing, thereby establishing an allowable value for mass injectant coefficient. Figure 6-2 represents char surface composition as a function of local pressure and B_g for an ESM in air. The case in question is for a char recession rate (B_c) equal to zero. This constraint will be forced on the model (SLAMAST). Notice that a transition occurs when the mass injection coefficient reaches a value of approximately 0.5 where the species SiO_2 can cause probable surface sealing. Based on this constraint, observation of Figure 6-3 indicates that failure is not probable in

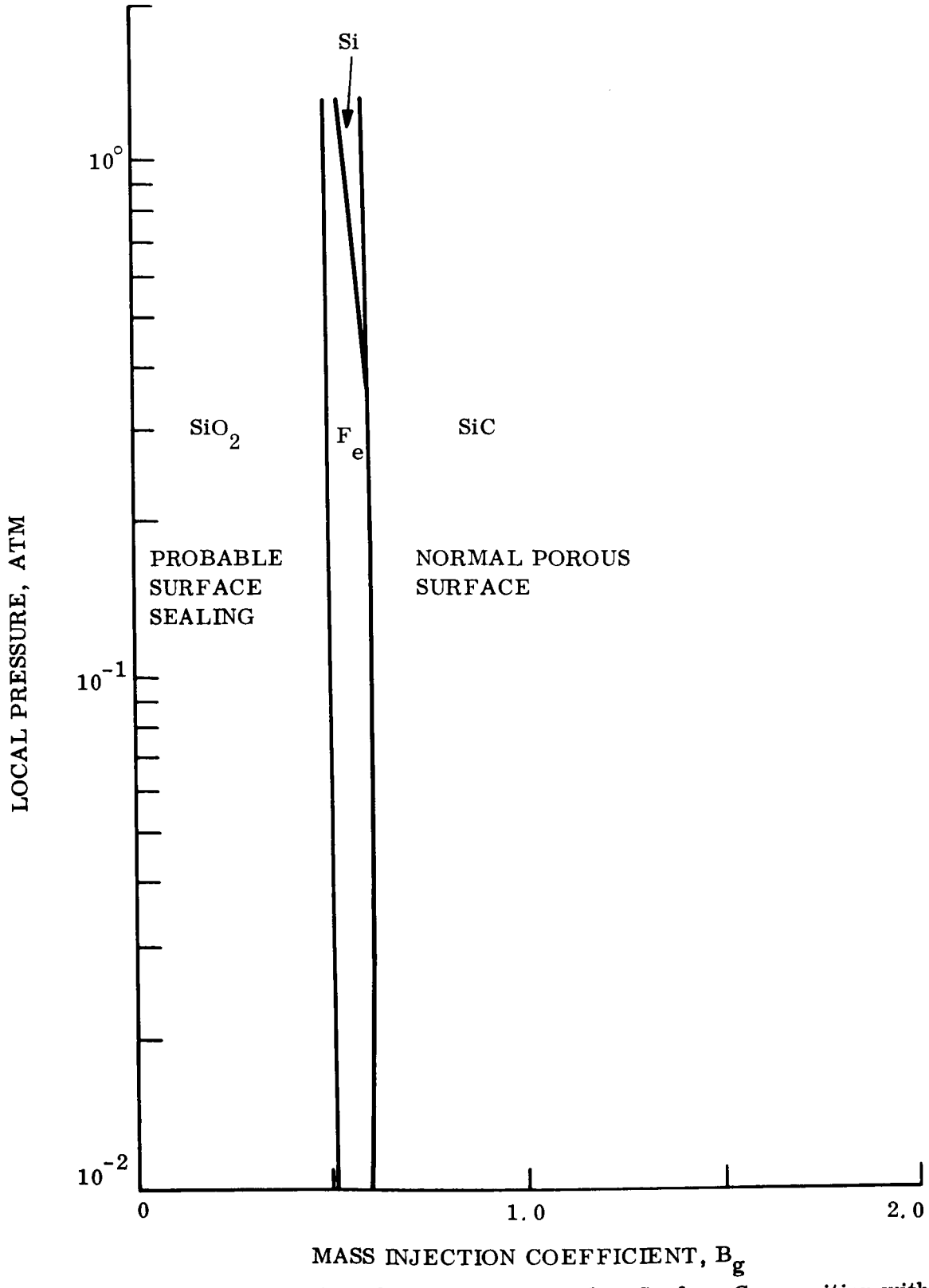

Figure 6-2. - Variation of Predicted ESM Char Surface Composition with B_g and Pe in air for $B_c = O$

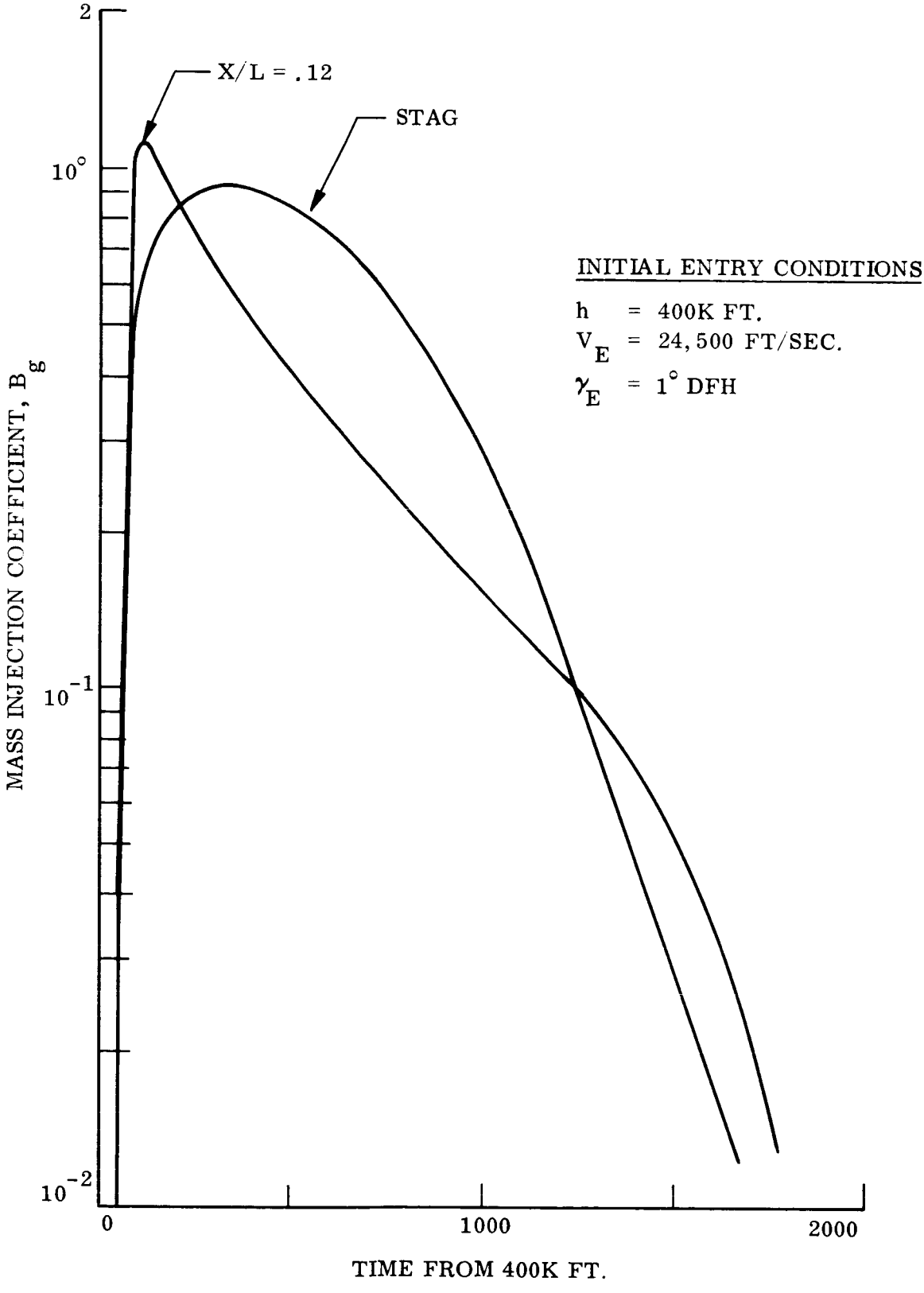

Figure 6-3. - M2-F2 Mass Injection Coefficient Histories, $B_c = O$

the first 80 seconds due to the very rapid traversal of the critical regime. However, failure may be possible during the remainder of the flight after 800 seconds (with respect to M2-F2 stagnation conditions). On the other hand, for a location X/L - .12 on the prototype, failure is not probable in the first 60 seconds but is possible during the remainder of the flight after 420 seconds. The reason that failure would not likely to occur in the beginning of the flight path is stated above.

Assuming that Bg represents the critical mode of failure (a criteria based upon chemical reactions causing a transition of this parameter from probable surface sealing to a normal porous surface), it is necessary to establish the proper flight profile on the model (SLAMAST) that simulates the critical mass injection coefficient. Eq. (6-27) states:

$$(M.S.)_{M2-F2} = \frac{(B_g)_{allow.}}{(B_g)_{actual}} - 1$$

or

$$(B_{g_{calcul.}})_{model} = \frac{(B_{g_{allow}})_{model}}{(1 + M.S.)} \qquad (6-28)$$

From Figure 6-3 consider some value of B_g (= .13) about t_o equal 1200 seconds. For an allowable value of B_g equal to 0.5, the margin of safety becomes 0.28 for the prototype (M2-F2).

In keeping with the similitude philosophy, the same margin of safety and the same factor of safety are maintained with the same material. The required value of the mass injection coefficient can now be determined for the model (SLAMAST). Notice that the Eq. (6-28) the allowable value of B_g is required for the model. This is usually determined pending the characteristics of the model (material, shape, etc.). However, since we are simulating a chemical phenomena Figure 6-2 can be used, in that it represents variations of an ESM char surface composition (for B_c = 0) for any vehicle. Hence, the same allowable value for the prototype will be characteristic of the model and the actual value of Bg for the model will be identical. It is necessary now to find that particular flight profile of the model (SLAMAST) to simulate the required critical mode of failure.

Figure 6-4 represents a typical flight path for the SLAMAST vehicle indicating the value of the mass injection coefficient as a function of time at two body points. Notice, for example, that the critical mode of failure can be simulated on the windward ray flight profile at a time of approximately 270 seconds. It should be kept in mind that the above profiles are arbitrary, and that a more meaningful profile can be procured to simulate our objective. If it is found that the shield material did indeed fail at this predicted time, we have demonstrated that Bg was the most critical parameter of concern. On the other hand, if it was found that the vehicle failed prior to the predicted time, a further investigation would be necessary. Nevertheless, the philosophy has demonstrated that it is possible to ensure a technique of evaluating prototype designs by inexpensive model studies.

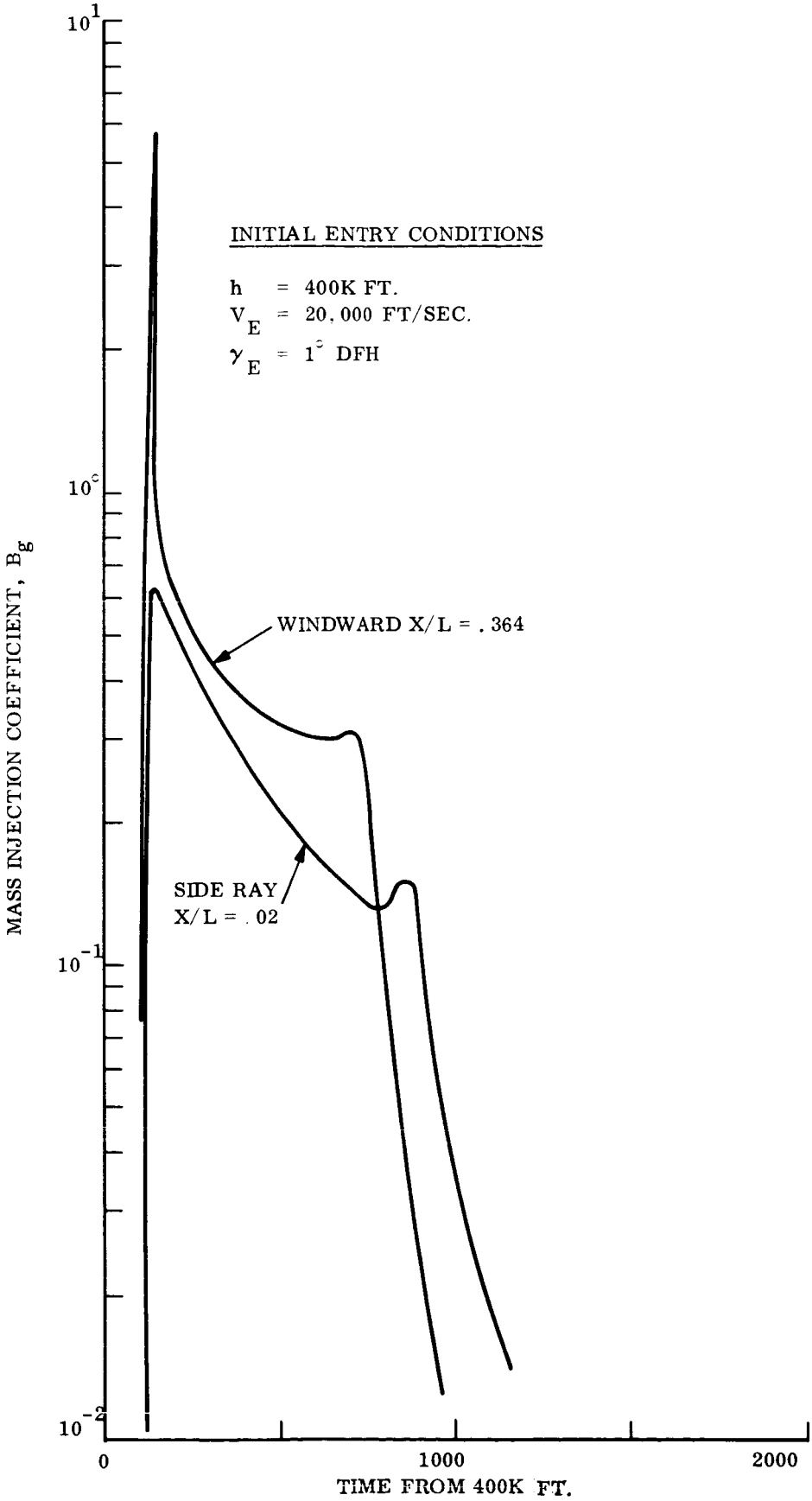

Figure 6-4. - SLAMAST Mass Injection Coefficient Histories, $B_c = 0$

NOMENCLATURE

B	Extensional Stiffness
$B_c = \frac{\dot{m}_c}{\rho_e u_e St}$	Char recession rate
$B_g = \frac{\dot{m}_g}{\rho_e u_e St}$	Mass injection coefficient
C	Specific Heat of Body
c_p	Specific Heat of Gas
D	Flexural Stiffness
E	Modulus of Elasticity
e	Specific Internal Energy
F	Stress Function
f_c	Fraction of Unreacted Material that Forms Char
g	Gravitational Constant
H	Heat
H_c	Heat of Combustion
H_{cg}	Heat of Cracking
H_{deg}	Heat of Degradation
h	Heat Transfer Coefficient (or Joint Resistance), also enthalpy
K	Body Heat Conductivity
k	Gas Heat Conductivity
L	Characteristic Length
M_∞	Mach Number
M_T	Thermal Moment
m	Mass/Unit Area
N_T	Thermal Load
n	Shape Factor or Scale Factor
P	Porosity (char layer)
Pr	Prandtl Number
p	Pressure
q	Dynamic Pressure
q_A	Aerodynamic Heat Flux

$\dot{q}_b$	Heat Flux Due to Blocking
R_e	Reynolds Number
T	Temperature
t	Time
U	Free Stream Velocity
u	Displacement
V	Velocity
w	Deflection (u_3)
$\dot{w}$	Net Rate of Production Due to Chemical Reactions
$\dot{w}''$	Net Rate of Production at the Gas Due to Gas - Solid Phase Reaction
x	Coordinate
Z	Thickness Coordinate
α	Coefficient of Expansion
δ	Plate Thickness
ϵ	Emissivity (or Strain)
γ	Specific Heat Ratio
μ	Gas Viscosity
K	Diffusivity
ρ	Density
τ	Thickness Ratio
σ	Stress
ν	Poisson's Ratio

Sub and Superscripts

$(\ )_A$	Aerodynamic
$(\ )_B$	Body
$(\ )_F$	Force (non - aerodynamic)
$(\ )_M$	Model
$(\ )_o$	Initial or References
$(\ )_P$	Prototype
$(\ )_\infty$	Free Stream Value
$(\bar{\ })$	Nondimensional Quantity

$(\ )$	Nondimensional Temperature Quantity
$(\dot{\ })$	Time Derivative
w	Wall Conditions
$(\ )_s$	Solid Virgin Material
$(\ )_c$	Char Layer
$(\ )_g$	Gaseous State

REFERENCES

6-1. Molyneaux, W. G., "A Consideration of the Similarity Requirements for Aerothermoelastic Tests on Reduced Scale Models", Symposium on Aerothermoelasticity, ASD TR 61-65, October, 1961.

6-2. Dugundji, J. & Calligeros, J., "Similarity Laws for Aerothermoelastic Testing", J/IAS, August, 1962.

6-3. O'Sullivan, W. J., Jr., "Theory of Aircraft Structural Models Subject to Aerodynamic Heating and External Loads", NACA TN 4115, September, 1957.

6-4. Schlessinger, M., "Practical Aspects of Aerothermoelastic Modeling", ASD - TDR - 62 - 705, December, 1962.

6-5. Calligeros, J. M. & Dugundji, J., "Similarity Laws Required for Experimental Aerothermoelastic Studies", MIT Aeroelastic and Structures Research Laboratory Technical Report 75-1, ASTIA AD 219760, May, 1959.

6-6. Calligeros, J. M. & Dugundji, J., "Similarity Laws Required for Experimental Aerothermoelastic Studies, Part 2 - Hypersonic Speeds". MIT Aeroelastic and Structures Research Laboratory Technical Report 75-2, ASTIA AD 253790.

6-7. Molyneaux, W. G., "Scale Models for Thermo - Aeroelastic Research". Royal Aircraft Establishment (Farnberough) Technical Note No. Structures 294, ASTIA AD 258163, March, 1961.

6-8. Ting, L., "Similarity Conditions for Testing High Speed Aircraft Models", Polytechnic Inst. of Brooklyn, Dept. of Aeronautical Engineering and Applied Mechanics, PIBAL Report No. 308, AFOSR No. TN 56-548, November, 1956.

6-9. Scipio, L. A. II, & Teng, L. C., "Analytical Study of Similarity Parameters for Aerodynamic Model Testing at High Temperatures, Part I - Similarity Criteria for Solid and Shell Type Aerothermoelastic Models", WADC TR - 57-496, ASTIA AD 142264, November, 1957, "Part II - Design Criteria for Wing Type Aerothermoelastic Models", WADC TR - 57 - 496, ASTIA AD No. 974, August, 1957.

6-10. Heldenfels, R. R., "Models and Analogs", High Temperature Effects in Structures, Ed. N. J. Hoff, Pergamon Press, 1958.

6-11. Sobey, A. J., "Advantages and Limitations of Models", J. Royal Aeronautical Sciences, Vol. 63, No. 587 November, 1959.

6-12. Gatewood, B.E., "Thermal Stresses", McGraw - Hill Book Co., Inc. 1957.

6-13. Gerard, G., "Some Structural Aspects of Thermal Flight", ASME Symposium on the Thermal Barrier, December, 1954.

6-14. Shanley, F.R., "Strength of Materials", McGraw - Hill Book Co., Inc. 1957.

6-15. Grover, H.J., Gorden, S.A., & Jackson, L.R., "Fatigue of Metals and Structures", NAVAER 00-25-534, 1954.

6-16. Calligeros, J.M. & Dugundji, J., "Similarity Laws Required for Experimental Aerothermoelastic Studies Part 2 - Hypersonic Speeds", Aero. and Struct. Research Lab. MIT Technical Report 75-2.

6-17. Hayes, W.D. & Probstein, R.F., "Hypersonic Flow Theory", Academic Press, N.Y., 1959.

6-18. Laganelli, A.L., "Similarity Laws for Ablating Bodies at Hypersonic Speeds", GE Tech. Infor. Series (to be published).

6-19. Shore, S. & Vinson, J.R., "Philosophy Concerning the Use of SLAMAST in Thermostructural Similitude Studies for Lifting Re-entry Vehicles", Structural Mechanics Associates Letter Report, January, 1967.

6-20. Fogaroli, R.P., "Mass Transfer and Surface Chemistry for ESM in Air at Hypersonic Speeds", GE-RSD-PIR-HTT 8151-585, June, 1966.

7. POTENTIAL SLAMAST APPLICATIONS

7.1 MATERIALS PERFORMANCE

Over the past several years, ablation performance anomalies have been noted in both low and high density materials. Several of the anomalies are described below:

(1) Surface sealing of silicone elastomers observed in Langley 2500 KW ARC - leads to uncontrolled swelling.

(2) Boundary layer combustion observed on phenolic nylon at Hi oxygen partial pressures, ref. 7-1.

(3) Boundary layer combustion observed on low density filled epoxy in honeycomb (Avcoat 5026-39-Hc- G) in low heat flux regime, Ref. 7-2.

(4) Significant surface recession occurs on low density filled epoxy in honeycomb (Avcoat 5026-39-HC-G) for low pressure, low heat flux, low aerodynamic shear conditions due to combustion of pyrolysis gases at char surface, ref. 7-3.

As more emphasis is placed on optimization of the low density class of ablators, a good understanding of the in depth chemical reactions as well as the aerothermochemical interactions of the injected decomposition products with the hypersonic boundary layer is required. The complex chemical reactions are dependent on several parameters, of which temperature and pressure are of key importance. Internal pressure build-up is directly a function of the molecular weight and rate of the gas generation, and the char layer porosity. The char porosity is very dependent on time, hence only a true simulation of a time history of the prototype environment will result in an accurate duplication of the in depth and surface chemical reactions.

The purpose of this section is to outline briefly the activities involved in proceeding from the preliminary heat shield materials screening to flight qualification of a candidate material and how the SLAMAST concept fits into this overall flight qualification program. This series of activities is illustrated in Figure 7-1.

The fundamental thermophysical properties, e.g., thermal conductivity specific heat, density, decomposition kinetics (TGA), heat of decomposition (DSC) are determined experimentally in the laboratory, ①.* These properties are then assembled for use in a charring ablator mathematical model like REKAP (Reaction Kinetics Ablation Program), ②for use in making pretest predictions to design the plasma jet ground test program, ③. The virgin material, char and decomposition gases chemical composition is combined theoretically with the hypersonic boundary layer in ④ using the approach of ref. 7-4. The output of the analytical chemistry

* ① The encircled numbers refer to a single step in the flight qualification program illustrated in Figure 7-1.

activity, ④, is the resultant heat and mass transfer effects due to the aerothermochemical interactions between dissociated air and the candidate ablator. These effects are incorporated as boundary conditions to the stage 0 REKAP, ②.

Plasma jet ground test results including surface and substrate temperature response, mass loss histories, and substrate density profiles are now compared to the pretest predictions, ⑤, with any required modification to the REKAP model made, ⑥ and ⑦ to obtain better agreement between the predicted and measured ⑤ test results.

This Stage 1 REKAP model is now employed to evaluate the performance of the candidate material in the prototype environment, ⑧, and to generate the preliminary ablator thickness requirements, ⑨.

Examination of the time histories of the significant aerothermodynamic performance parameters for the prototype environment, $\dot{q}/\Delta h$, h_r, P_e, Bg, Bc allows one to define a subscale test model flight program, ⑩, that will truly subject the candidate material to the range of those parameters that will be encountered in the prototype flight.

After conduction of the subscale model (like SLAMAST) flight test program and recovery of the vehicles

(1) The substrate temperature and char depth histories are compared to the flight test predictions, ⑪,

(2) The recovered shield is sectioned with quantitative chemical analysis and density profiles done on the char layer.

This information is now employed for upgrading the Stage 1 REKAP model to a fully flight qualified REKAP model, ⑫.

This flight qualified REKAP model is now employed to re-evaluate the preliminary prototype heat shield design, ⑨, and provide the necessary re-definition (if required) of the prototype heat shield requirements.

Hence, it is now possible to proceed to the prototype flight test program with a fully qualified shield material without having previously flown a full prototype vehicle.

7.2 BOUNDARY LAYER TRANSITION STUDIES

The lifting re-entry vehicle as opposed to ballistic type, is exposed to longer heating periods (although lower attendant heat rates) and maintains lower Reynolds numbers as a result of higher altitude flight. The magnitude of the local heat flux is strongly influenced by the state of the local boundary layer, i.e., laminar or turbulent. Hence, an optimum lifting entry vehicle design is influenced by the boundary layer transition criteria employed. For example, some low density ablators

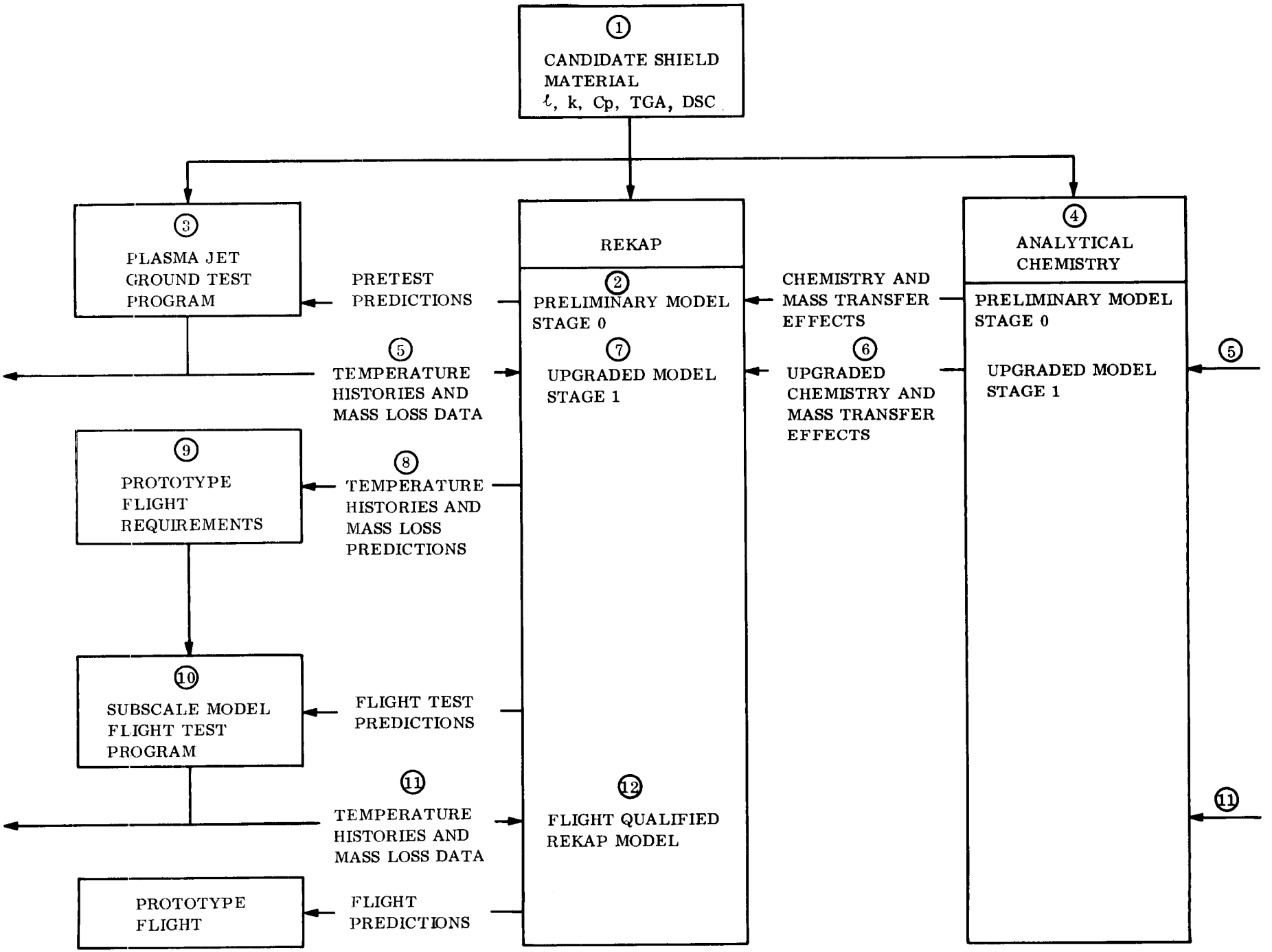

Figure 7-1. - Flight Qualification Program

(like silicone elastomers) exhibit a surface recession threshold above which surface melting occurs and the overall ablator efficiency decreases. Hence, the ablator that provides a minimum weight heat shield system for a predominately laminar flow regime may not provide the minimum weight system for a predominately turbulent flow regime due to the higher local heating rates, Figure 3.4-9.

From Figure 3.4-9 it can be determined that a turbulent boundary layer will result in increases in local time integrated heating by a factor of from 3 to 9 over major portions of the SLAMAST. From Figure 3.4-30, it is seen that this increase in time integrated convective heating results in an increase in heat shield requirement by 50 to 100 percent over major portions of the vehicle.

A study of available ground test transition data on SLAMAST type elliptical cones at an angle of attack was undertaken by ref. 7-5 to determine whether existing sphere cone transition prediction techniques, ref. 7-6 can be applied to an elliptical configuration. It was concluded that because of the dearth of transition data on elliptical bodies, a valid comparison with sphere-cone transition data could not be made. Therefore, no method is currently available by which a logical extension of sphere-cone correlation techniques will allow qualitative estimates of the expected conditions under which transition will occur on an elliptical vehicle at an angle of attack.

Therefore, an additional application of the SLAMAST vehicle would be to measure the on-set and propagation of boundary layer turbulence as it is influenced by the various combinations of flight parameters like angle of attack, surface temperature, mass injection rate, local Reynolds number, and local Mach number. This understanding of boundary layer transition can then be logically extended to application on the larger prototype vehicles, with the subsequent optimization of the low density ablator heat shield.

A flow chart is presented in Figure 7-2 illustrating the logical progression from ground test programs to a SLAMAST flight test in order to gain an understanding of the onset and propagation of the turbulent boundary layer. This program has evolved from the experience gained in several years of ballistic vehicle ground and flight testing where it has been consistently demonstrated that the observed flight boundary layer transition occurs at a local Reynolds number about one order of magnitude higher than that observed in wind tunnels.

Until the time when boundary layer transition on non-axisymmetric lifting re-entry vehicles at angle of attack is understood, it is necessary to have a guide to selection of the appropriate flight regime (i.e., laminar or turbulent) for the SLAMAST.

Based on the current axisymmetric cone boundary layer transition criteria, ref. 7-6, a Reynolds number based on local properties and wetted length of 500,000 is considered the most probable transition value for an axisymmetric cone for $Me < 1.5$. However, due to the complete lack of empirical data on boundary layer transition for a non-axisymmetric vehicle, ref. 7-7, it is felt that a most probable value of $R_{e_s} = 150,000$ at $Me < 1.5$ should be employed as a guide to SLAMAST trajectory selection.

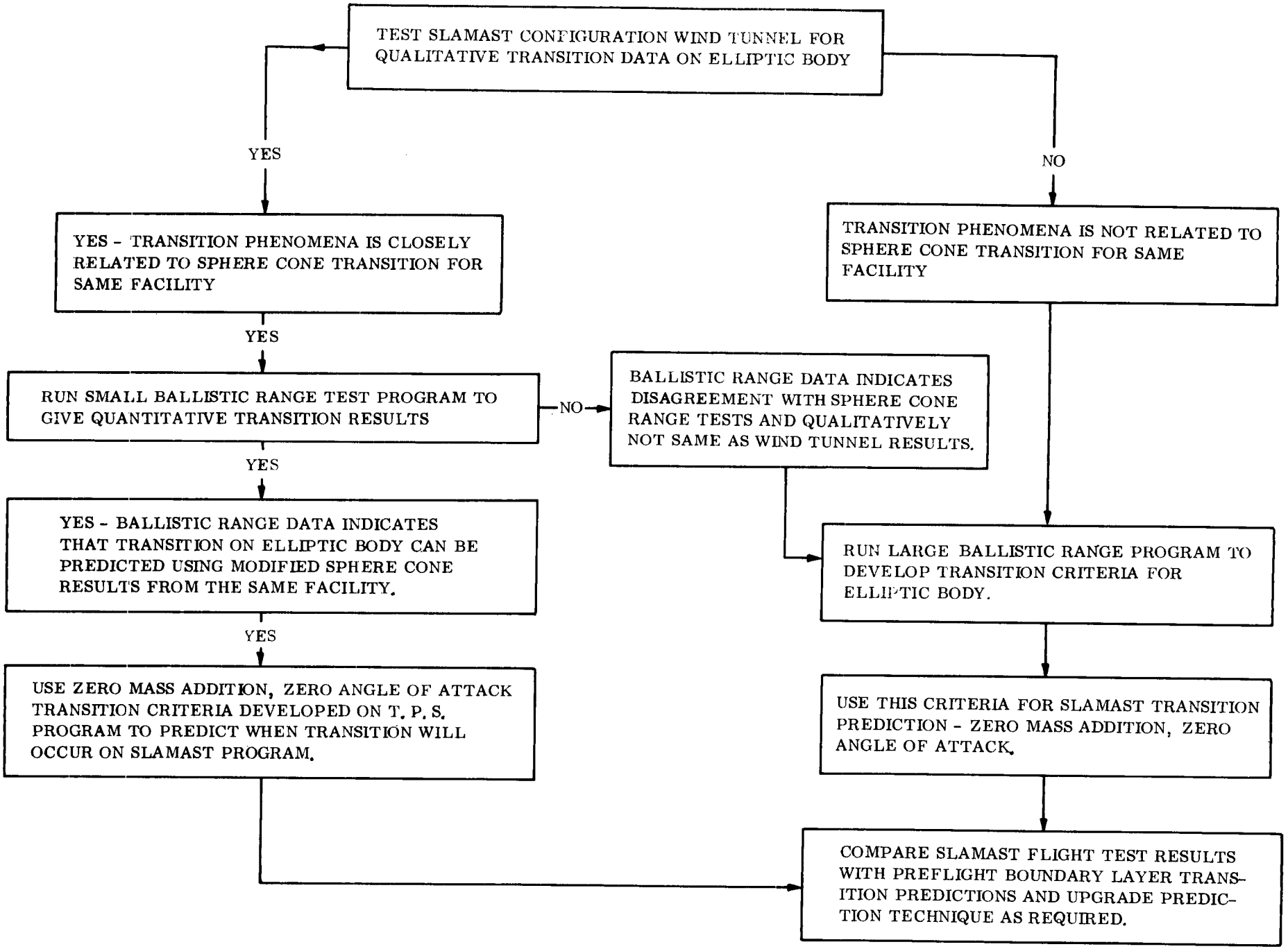

Figure 7-2. - Flow Chart

Aft on the skirt region where the local edge Mach number is about 5 at pull out, the boundary layer transition criteria of ref. 7-5 indicates a transition Reynolds number 1.5×10^6 for high mass addition materials. A review of the prototype nominal, over shoot and under shoot trajectories shows the constant altitude flight portions at 240K 300K and 170K feet respectively for entry velocities of 24,000 ft/sec, ref. 7-7. From inspection of Figure 7-2 it is apparent that the constant altitude portion of the prototype flight will be in the laminar flow regime for both the 1^o and 10^o entry path angle cases. However, a SLAMAST requirement for keeping the constant altitude flight in the laminar flow regime is determined from Figures 7-3 and 7-4 to be for $V_E = 20,000$ ft/sec

α P.O. $\geq 12^o$

$W/C_L S = 250$ lbs/ft^2

$\gamma_E \sim 0.5$ to 10^o DFH

In summary, it has been demonstrated that the onset of turbulent flow can increase the heat shield thickness requirement by 50 to 100 percent over major portions of a vehicle. Hence, an understanding of boundary layer transition is necessary for optimum design of the vehicle heat shield. Due to the complete lack of transition data on non-axisymmetric bodies it is proposed that the SLAMAST be used to obtain flight test experimental data on the onset and propagation of the turbulent boundary layer. This understanding of boundary layer transition can then be logically extended to application on the larger prototype vehicles with the subsequent optimization of the low density ablator heat shield.

7.3 SEPARATED FLOW AND PROTUBERANCE EXPERIMENTS

The aerothermodynamic characteristics of both the prototype (HL-10) and model (SLAMAST) can exhibit certain flow phenomena, which are not generally encountered in ballistic entry vehicles, such as protuberance interaction and corner flow phenomena. These phenomena would occur in regions where control flaps or extrusions are required for manuevering. If, for example, the test panel is located in a region near a control flap, as is the case in SLAMAST, flow separation is possible on the panel and reattachment of the flow on the control flap. Coupled with this phenomena, secondary shocks developed from the control flap coinciding with the vehicle bow shock and corner flow phenomena can greatly change the heat transfer characteristics on the test panel.

Any experimental data obtained in this region with different materials could prove to be invaluable when simulating critical design aspects in typical areas of the prototype (HL-10). It should also be kept in mind that any test panel located in a regime of a control flap must produce reliable data within the flight profile before the control flap is used, thus adding another constraint on the model.

With the general similitude laws developed in ref. 7-3 shown in Eqs. 6-24, 6-25, and 6-26, a study can be made with regard to changing the materials on the model in hopes of establishing a criteria between wind tunnel and flight data. It should be noted that the similitude philosophy previously described can be used as a constraint in developing approximate similitude in such a general study.

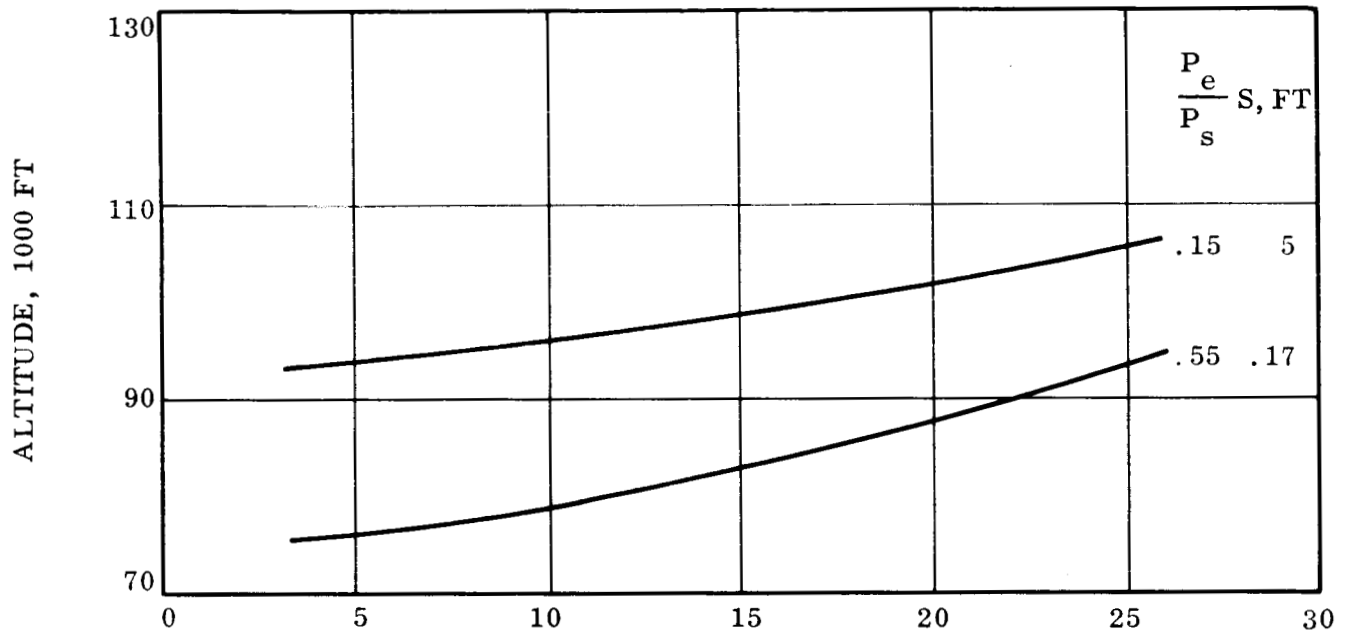

Figure 7-3. - Boundary Layer Transition Altitude for SLAMAST

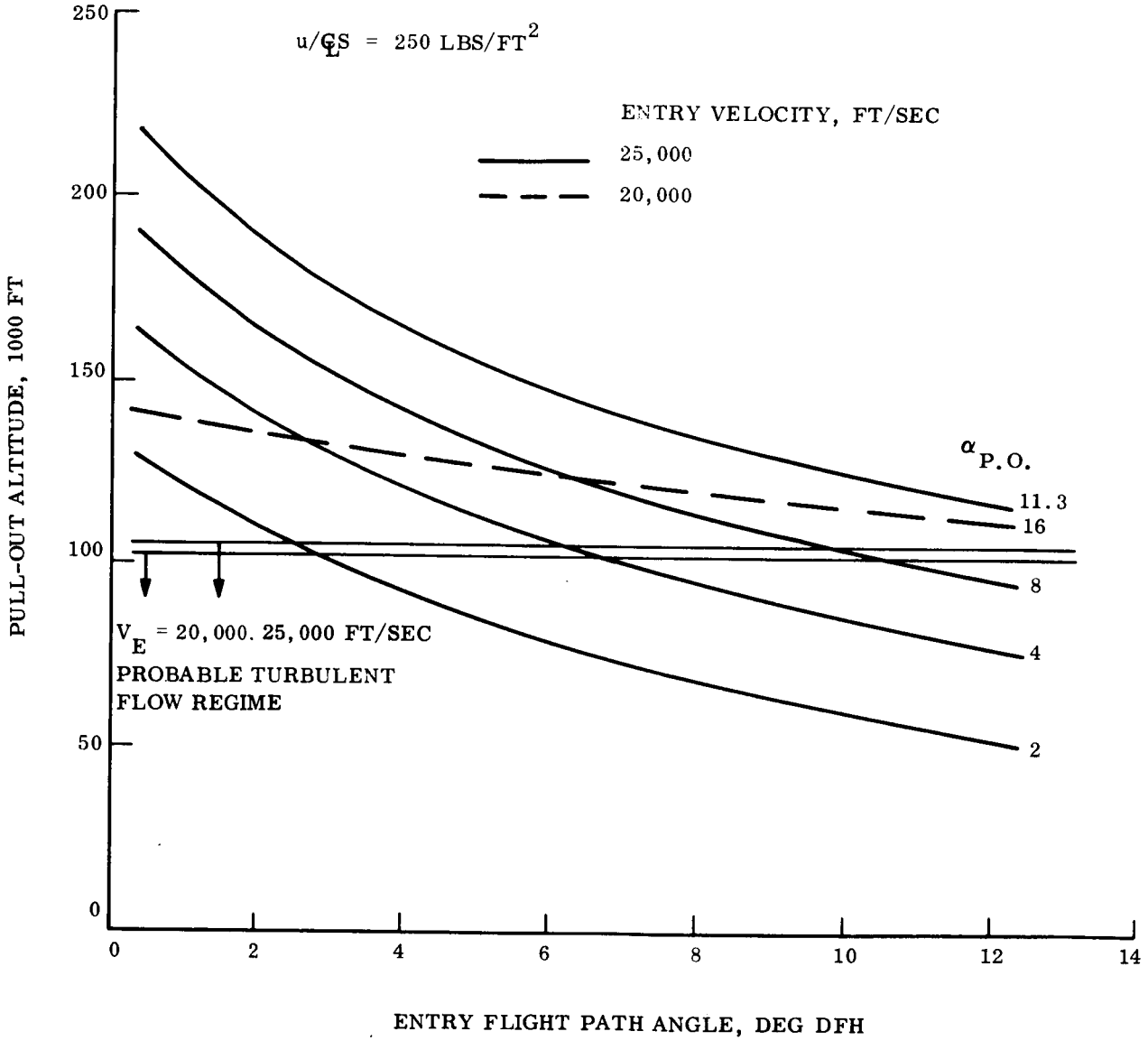

Figure 7-4. - SLAMAST Pullout Altitude for Various Combinations of Initial Re-entry Conditions

7.4 AERODYNAMIC FLIGHT EXPERIMENTS

SLAMAST class testbeds provide excellent facilities for investigation of aerodynamic characteristics in a true re-entry environment not otherwise obtainable in present ground test facilities. The SLAMAST flight investigations will provide aerodynamic data of considerable interest in the hypersonic-low-density flight environment over a large portion of the trajectory. Although these data may be of limited scope (depending on the primary experiment), they will include control effectiveness (derived from trim angle of attack as a function of control deflection), associated control loads, control duty cycles, stability characteristics, and lift and drag performance. These data are of importance to lifting vehicle technology and will be correlated with available ground test and analytical results. SLAMAST flights specifically oriented to provide aerodynamic information offer even greater opportunities for significantly advancing aerodynamic technology, as will be illustrated in this section.

The history of ballistic re-entry vehicle flights has revealed many significant and unexpected events including relatively large differences between flight data and those aerodynamic characteristics predicted on the basis of available analytical techniques and ground tests. For example, Figure 7-5 presents static stability, C_{M_α}, variations with altitude that were encountered during a recent flight of an ablating, conical, ballistic re-entry vehicle. The figure reveals the C_{M_α}, excursions and the variation of C_{M_α} from the predicted value by as much as a factor of four, for a flight portion during which the vehicle was flying at an essentially constant Mach number at or near zero angle-of-attack. Similar results have been obtained from other recent R/V flights.

The variations from predicted C_{M_α} values are attributed primarily to the vehicle's ablation characteristics, including both mass addition and shape change. Events such as those noted on the figure profoundly affect maneuvering/lifting vehicle design and require consideration during the design decisions relating to control sizing, center-of-gravity placement, and heat shield selection. Such events presently require flight evaluation to assess their levels, importance, and time-dependency. SLAMAST will make a valuable contribution towards achieving these goals.

Inherent in maneuvering lifting re-entry vehicle design is the very basic consideration of aerodynamic stability definition, the associated stability margin tolerances, and the related control performance requirements and characteristics. Knowledge of these characteristics is critical to the control system and to the autopilot design in terms of system complexity, weight, and reliability. However, an accurate definition of the aerodynamic stability and control characteristics and their related tolerances is necessarily restricted prior to flight test due to many considerations. These include:

(1) Ground test facilities provide only a limited flight environmental simulation. Involved are Mach and Reynolds' number, mass addition rates and distribution, etc., along with basic test accuracies and repeatability.

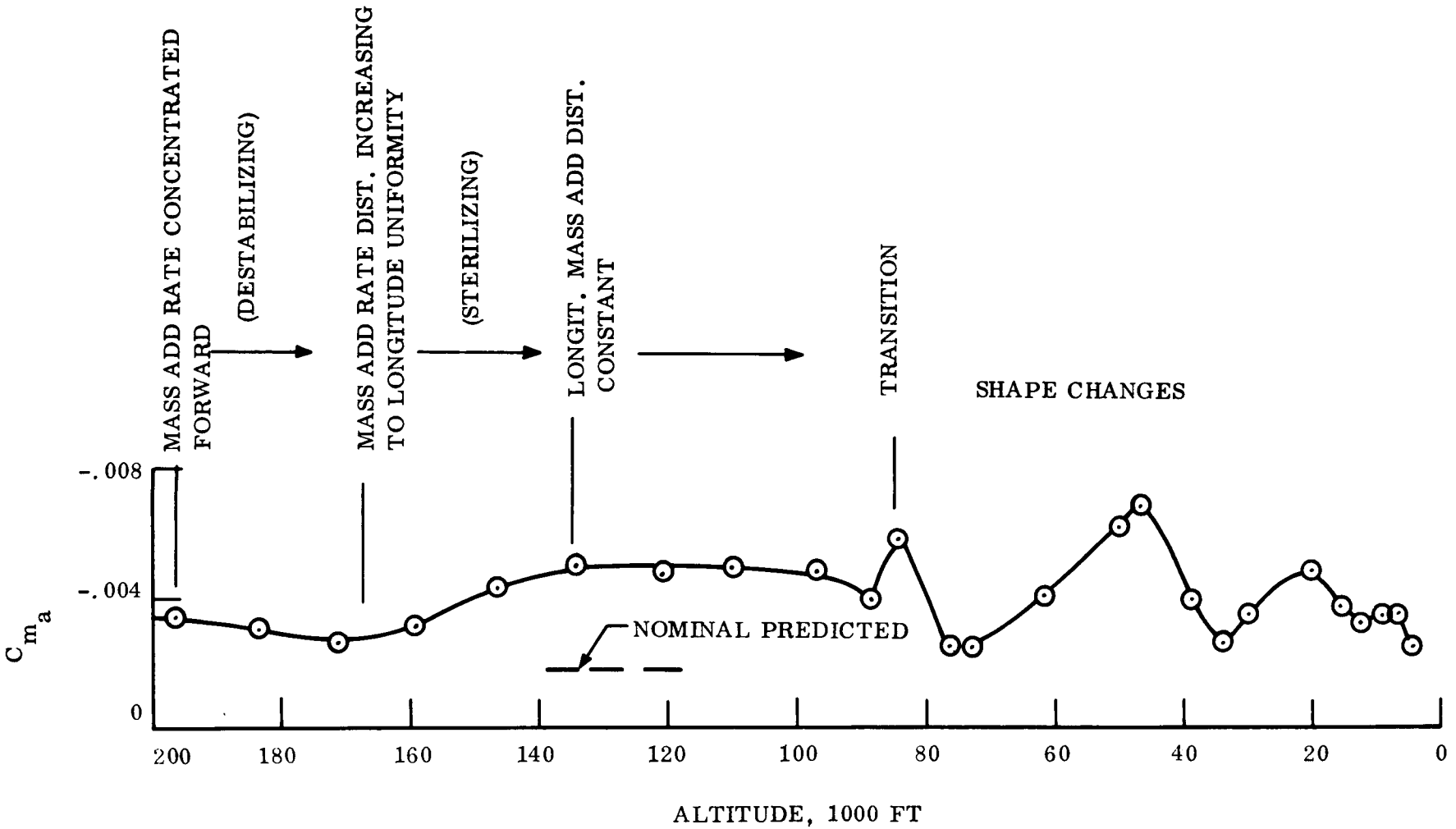

Figure 7-5. - Flight Data Aerodynamic Static Stability Variation With Altitude, Conical R/V With Ablating Heat Shield

(2) Available and calibrated analytical techniques cannot adequately predict environmental effects and have shown only limited validity in attempts to extrapolate wind tunnel data to flight conditions for ballistic vehicles

(3) Knowledge of ablation effects, both shape change and mass addition, on stability and control characteristics is sparse. Uncertainties in ablation charactistics, ablative mass loss rate and distribution exist to an undesirable degree. All these effects, in turn, are dependent upon accurate knowledge of heat shield material properties and response characteristics, which knowledge is incomplete if not minimal.

(4) Aeroelastic effects can exert major design perturbations, especially on high fineness ratio and high W/C_DS configurations.

(5) Manufacturing tolerances require continual monitoring and accommodation in detail design.

(6) Center of gravity uncertainties due to basic measurement accuracy, mass loss from ablation, aeroelastic deformation, fuel usage uncertainties, control movements, and etc. require vehicle design margins higher than desirable for minimum control system weight and size.

(7) Lack of flight data for maneuvering lifting re-entry vehicles is yet another handicap. With such data available, correlations enabling better predictions for future vehicle systems could be achieved.

On the basis of GE-RSD ballistic R/V flight experience and the items just enumerated, SLAMAST is considered a flight vehicle that will provide meaningful information and direct answers to many of the questions relative to these areas for consequent application to full scale lifting vehicle systems, manned and unmanned. Further, since a scaled testbed such as SLAMAST tends to exaggerate certain aerodynamic behavior indices, testbed flights provide a means for early identification of potential problem areas which might be masked on a full scale vehicle.

SLAMAST flight experiments directed toward providing the required aerodynamic flight knowledge are feasible. Selection of sufficient and accurate instrumentation, and comprehensive data acquisition will provide the definitions of the flight environment, vehicle altitude, control quantities, vehicle motions, etc., required for this evaluation. The flights themselves would be performed such that genuine transient attitude motions, such as pitch oscillations, can be generated. This would be effectively accomplished by momentary disablement or reduction of the pitch damping function, thus flying open loop. A programmed series of control displacement steps would then be extremely effective in generating meaningful transients point-by-point in the flight path. Such data would provide, in depth, such needed vehicle flight-determined information as C_{M_α}, C_{N_α}, rotary damping characteristics, measures

of control effectiveness, and available lift. Analog and/or digital simulations of this process would lead to more precise definition of the size and duration of the control displacement steps required, and of the accuracy required in the flight data to permit adequate determination of the desired parameters.

From the previous discussions in this section it can be seen that the SLAMAST vehicle offers a great flexibility to experimentally evaluate a number of the problems associated with lifting re-entry vehicle design. It is in this mode that the SLAMAST system offers its most efficient utilization as a facility for LRV flight systems qualification.

REFERENCES

7-1. Vojvodick, N. S. and R. B. Pope, "Effect of Gas Composition on the Ablation Behavior of a Charring Material", AIAA Journal March 1964

7-2. Diaconis, N. S., et. al. "Experimental and Analytical Study of the Behavior of Thermal Protection Systems in Convective Heating, Radiative Heating and Shear Stress Environments", Final Contractor Report on NASA Contract NAS 9-4771, February 1967

7-3. Nestler, D. E., "Evaluation of Micrometeoroid Penetration Effects on Heat Shield Performance Final Report, Vol. III", Final Contractor Report on NASA Contract 9-4119, September 1966

7-4. Fogaroli, R. P. "Ablating Boundary Layer Equilibrium (ABLE) Program", GE-PIR- HTT 81510516

7-5. Berkowitz, A. M., "Review and Applicability of Available Boundary Layer Transition Data on Elliptic Cones, GE-PIR-HTT-8151-668

7-6. Berkowitz, A. M., "Suppression of Re-entry Vehicle Transition to Low Altitudes" (u) GE-PIR-HTT-8151-646, Secret

8. SLAMAST LIMITATIONS

8.1 THERMOSTRUCTURAL

Consider first the potential difficulties associated with minimum gage design. It is quite reasonable to expect, at least in some cases, that in order to have a properly designed test panel of smaller overall size, smaller thicknesses would also be required. However, if the full scale vehicle has thicknesses which are minimum gage, the test panel could not utilize the required reductions in thickness. There are ways to possibly circumvent this problem and if it arises these potential solutions would be pursued. One of these possible solutions is to change the loads or temperatures to levels such that, even with an undesirable scaling in the size, the necessary margin of safety reproduction could be accomplished. As the details of an actual experiment design are delved into, it is possible that other solutions might be found depending on what factors consititute the weak link in the structure or shield system.

Another situation which could make experiment design not necessarily impossible, but at least difficult, is the simulation of an optimum structure. If a structure is the ultimate in optimum design the margins of safety against failure in all possible modes are equal. This can be accomplished in few, if any, structures. However, it is very common to achieve "partial optimization" where some of the margins are equal or very close. If an experiment is being designed to simulate this type of structure, it is obvious that the task could be more difficult, since it would be necessary to closely reproduce the margins which are close to one another. Again, the degree of difficulty is dependent on the details of the particular case.

One problem area that has not been mentioned and does not appear to be critical on present HL-10 designs, but which could be an important factor in some designs, is the area of fatigue and flutter. It may be possible that the same margin of safety approach can be applied here as has been applied throughout this report. However, this would have to be explored in more depth before such a conslusion could be drawn.

The thermostructural parameters evaluated in this report were not time dependent. Thus such failure modes as creep and fatigue were not candidates for simulation. In general it appears that the approach described in this report would preclude this type of simulation with SLAMAST. Before a definite conclusion can be stated in this regard would need additional investigations to be carried out.

9. OTHER TESTING ALTERNATIVES

9. OTHER TESTING ALTERNATIVES

At present, there are only two approaches available to verify or validate a design of a manned lifting re-entry vehicle, or, for that matter, any flight system. These are flight testing of a prototype vehicle or ground testing of critical items.

Although the actual flight testing of a prototype vehicle under its associated real flight environment does provide the most definitive data, the costs associated with these design verifications are usually high. The second approach, ground testing, while reduced in overall cost, provides only a limited amount of data on singular phenomena (i.e., the ground test results usually do not include interaction effects, which are quite important in total structural response).

There are basically four types of facilities in which structural re-entry environments simulations can be performed. These are:

(1) Large conventional wind tunnels,

(2) Arc heated tunnels,

(3) Rocket exhaust,

(4) Pressurized chambers with radiant heat sources.

Few wind tunnels are available which are large enough to accommodate test panels of the sizes proposed on SLAMAST (about 14 inches by 16 inches). None of these facilities can provide experiment times available on a flight vehicle such as SLAMAST. The largest continuous tunnels available today are those of the Arnold Engineering Development Center in Tennessee. That facility has two 50 inch diameter wind tunnels which range from Mach numbers of 6 to 12.5. However, in order to obtain the proper loading conditions, the model would have to be placed at a rather larger angle of attack. This approach would not permit the most severe flight conditions to be obtained, and more important, the large angles of attack required might cause tunnel blockage.

At the present time, there are no arc-heated facilities which are capable of operating for long times with a large flow field; and there are none planned for the near future. In order to obtain a large flow field, the flow must be expanded to very low pressures. This would minimize any possibility of obtaining the simultaneous thermodynamic and aerodynamic environments possible in the SLAMAST flight environment. At the present time there are no facilities which can achieve a flow field this large under any condition, or run for the times available in a SLAMAST flight.

Rocket exhausts such as those at the Malta facility are generally used for thermostructural tests. However, for the conditions being considered they are not acceptable because the maximum flow field is limited to 15 inches and the heat fluxes and pressures will be much too high for a lifting vehicle environment. Essentially, the result would be more a jet impingement with resulting, undesirable pressure and heat transfer gradients over the test panels.

The remaining choice would be to place the test panel in a chamber designed such that a differential pressure could be applied to the panel, with radiant heat sources providing the necessary thermal environment. The first step would require the design of a chamber which incorporates the panel as an outside wall to create a pressure drop across it. A radiant heat source would have to be placed in the chamber to radiate evenly to the panel. For the long duration tests necessary here, an extensive cooling setup would be required to keep the heat from building up. Such a facility is not known to exist.

The facilities described above would not be capable of varying the heat flux or pressure during testing, which would more closely simulate actual flight conditions. This effect could be minimized if the facilities had enough latitude in environmental control, i.e., such that those environments producing the minimum margins of safety in the critical modes of failure of the test panel, could be simultaneously achieved. It is essential that the thermostructural response of the test panel is not seriously impaired by producing artificial environments either too quickly or at unacceptable rates. The entire discussion in the philosophy section highlights the goal of matching as closely as possible the similarity parameters during the earlier flight times so as to approach the "critical conditions" in the same way as in the prototype vehicle. In this aspect, the ground test facilities with their specific capacities and limitations will not be able to come close to the innumerable flight trajectories and maneuvers which SLAMAST can fly to simulate most realistically the actual transient flight environment.

The real limitations of ground testing lies in its inability to combine simultaneously the effects of aerodynamics, variable heating rates, ablation phenomena, inertia loading, and dynamic loading which can only be achieved in flight. It is particularly important when the design margins of safety for several of the most critical failure modes are close. The interaction of these failure modes under a combined environment may seriously affect the thermostructural response of the test specimen.

It is during these combined environments that unforeseen events occur; events that were not predicted on the basis of ground tests which at best could only combine parts of the flight environment. For example, only after flight testing in which aerothermal effects were included was it found that the fuselage and tail surfaces of the X-15 research airplane had to be reinforced. It was determined that the vibration problem exhibited by these surfaces was compounded by thermal stresses that were induced simultaneously by other factors (ref.9-1).

Flight tests are also extremely useful in uncovering unrelated but significant phenomena. On the GTV program, which was primarily aimed at evaluation of ablative materials characteristics in re-entry environments, the phenomenon of roll resonance was observed. This unpredicted phenomenon, it was found, can seriously affect the total performance of the re-entry system unless special precautions are taken.

SLAMAST flight tests, aimed at simulating as closely as possible the actual flight conditions and environments of the prototype manned vehicle could well reveal phenomena heretofore unknown since experimental investigation of the flight regime associated with lifting re-entry vehicles and resultant vehicle behaviors are still in the early stages.

REFERENCE

9-1. I. E. Garrick, "A Survey of Aerothermoelasticity", Aerospace Engineering, January, 1963.